MAX-PLANCK-INSTITUT
FÜR METEOROLOGIE

IMPRS-ESM

International Max Planck Research School on Earth System Modelling

Influence of the representation of convection on the mid-Holocene West African Monsoon

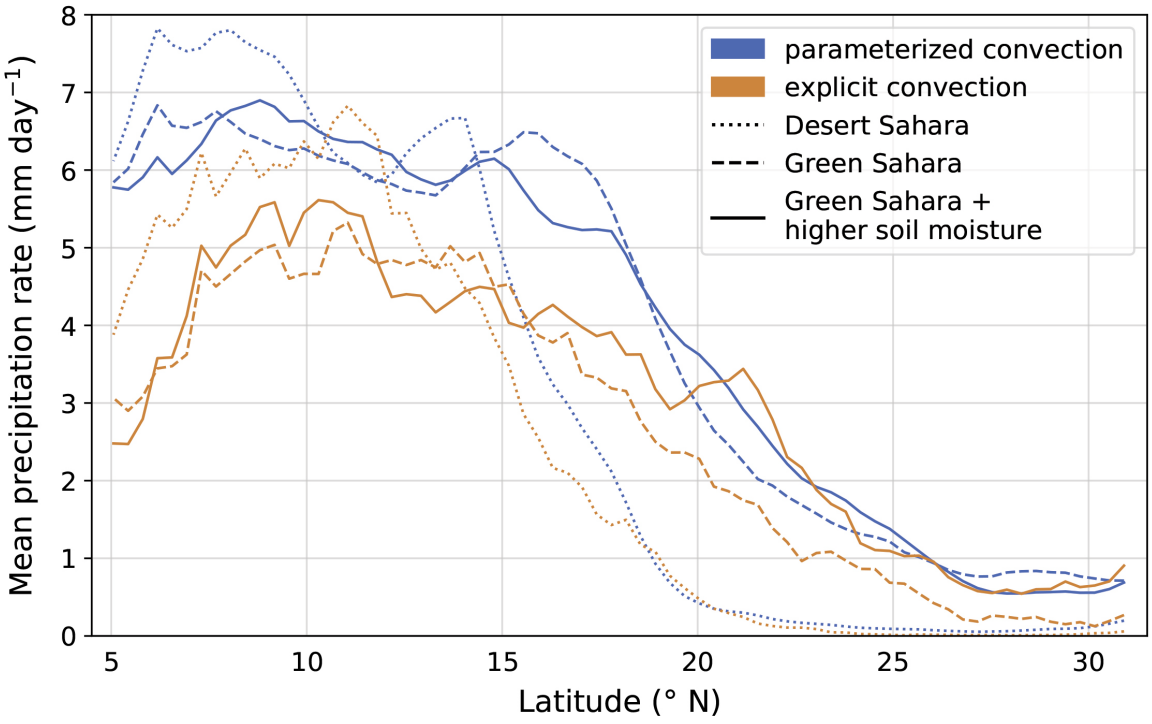

Leonore Jungandreas

Hamburg 2021

Berichte zur Erdsystemforschung
Reports on Earth System Science

247
2021

Hinweis

Die Berichte zur Erdsystemforschung werden vom Max-Planck-Institut für Meteorologie in Hamburg in unregelmäßiger Abfolge herausgegeben.

Sie enthalten wissenschaftliche und technische Beiträge, inklusive Dissertationen.

Die Beiträge geben nicht notwendigerweise die Auffassung des Instituts wieder.

Die "Berichte zur Erdsystemforschung" führen die vorherigen Reihen "Reports" und "Examensarbeiten" weiter.

Anschrift / Address

Max-Planck-Institut für Meteorologie
Bundesstrasse 53
20146 Hamburg
Deutschland

Tel./Phone: +49 (0)40 4 11 73 - 0
Fax: +49 (0)40 4 11 73 - 298

name.surname@mpimet.mpg.de
www.mpimet.mpg.de

Notice

The Reports on Earth System Science are published by the Max Planck Institute for Meteorology in Hamburg. They appear in irregular intervals.

They contain scientific and technical contributions, including PhD theses.

The Reports do not necessarily reflect the opinion of the Institute.

The "Reports on Earth System Science" continue the former "Reports" and "Examensarbeiten" of the Max Planck Institute.

Layout

Bettina Diallo and Norbert P. Noreiks
Communication

Copyright

Influence of the representation of convection on the mid-Holocene West African Monsoon

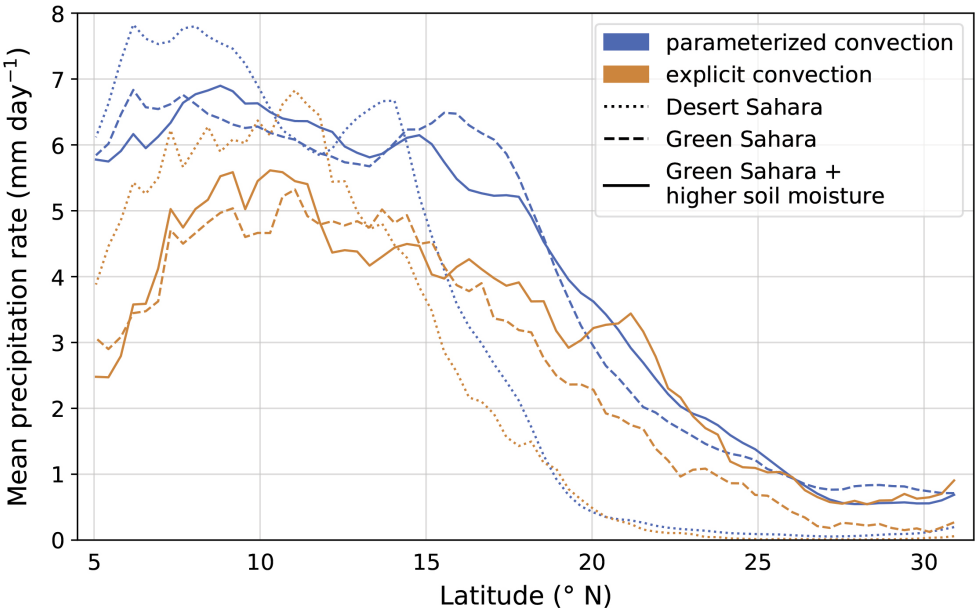

Leonore Jungandreas

Hamburg 2021

Leonore Jungandreas
aus Dresden, Deutschland

Max-Planck-Institut für Meteorologie
The International Max Planck Research School on Earth System Modelling
(IMPRS-ESM)
Bundesstrasse 53
20146 Hamburg

Tag der Disputation: 24. November 2021

Folgende Gutachter empfehlen die Annahme der Dissertation:
Prof. Dr. Martin Claussen
Dr. Cathy Hohenegger

Vorsitzender des Promotionsausschusses:
Prof. Dr. Hermann Held

Dekan der MIN-Fakultät:
Prof. Dr. Heinrich Graener

ISSN 1614-1199

Leonore Jungandreas

Influence of the representation of convection on the mid-Holocene West African Monsoon

ABSTRACT

The focus of this dissertation is whether and how explicitly resolved convection simulations, compared to parameterized convection simulations, modify the West African monsoon and the precipitation distribution over mid-Holocene North Africa. Previous models could not reproduce the northern extent of the West African monsoon during the mid-Holocene because they used a too coarse horizontal resolution and therefore had to parameterize convective processes. For present-day conditions, Marsham et al. (2013) show that explicitly resolved convection shifts monsoonal precipitation much farther north and is able to better represent several key characteristics of precipitation compared to observations and compared to parameterized convection.

Motivated by the results of Marsham et al. (2013), in the first part of this dissertation I investigate whether the use of explicitly resolved convection simulations shifts the monsoonal precipitation further north than parameterized convection simulations during the mid-Holocene. Unexpectedly, I find that the northern extent of monsoonal precipitation remains further south when convection is resolved. I argue that the absence of a northward shift is caused mainly by fundamentally different precipitation characteristics, and by the response of surface hydrology to them when convection is explicitly resolved. As a result, precipitation in parameterized convection simulations is generally higher and extends further north than in explicitly resolved convection simulations. This result demonstrates the importance of soil moisture and surface conditions in regulating precipitation in mid-Holocene North Africa.

Therefore, the second part of the thesis focuses on how land surface and soil moisture modify precipitation over North Africa in simulations with parameterized and explicitly resolved convection. For this purpose, I extend the simulations from the first part, which uses present-day land surface conditions, and prescribe a higher, idealized vegetation gradient over mid-Holocene North Africa that is closer to proxy data. First, prescribing a higher vegetation density over North Africa induces a positive land-atmosphere feedback with enhanced precipitation and a further northward extent of monsoonal precipitation, regardless of the representation of convection. However, parameterized convection leads to stronger land-atmosphere feedback and thus higher sensitivity of precipitation to land surface changes compared to explicitly resolved convection. I hypothesize that this greater sensitivity is due to the generally higher soil moisture in the simulations with parameterized convection, which results from more but less intense precipitation and lower runoff - a similar mechanism as in part 1. In contrast, increased runoff prevents the formation of a strong soil moisture-precipitation feedback in simulation with explicitly resolved convection. Based on these results, I emphasize that it is critical how the soil responds to precipitation, not just how precipitation is affected by soil moisture. The importance of soil hydrology to the strength of land-atmosphere coupling in models has not yet been considered.

To test the hypothesis, I run another set of simulations for explicit and parameterized convection with high vegetation density but with the same constant soil

moisture field. The results show that for the same land surface conditions, monsoonal precipitation extends as far north with explicit convection as with parameterized convection. However, precipitation rates are still higher near the Guinea coast and over most of the Sahel in simulations with parameterized convection. Nevertheless, these results show a strong influence of soil moisture on the West African monsoon and highlight the importance of a reliable representation of soil hydrology in models.

ZUSAMMENFASSUNG

Der Fokus dieser Dissertation liegt darauf zu untersuchen, ob und wie explizit aufgelöste Konvektionssimulationen, im Vergleich zu parametrisierten Konvektionssimulationen, den westafrikanischen Monsun und die Niederschlagsverteilung über Nordafrika während des mittleren Holozäns modifizieren. Bisherige Modelle konnten die nördliche Ausdehnung des westafrikanischen Monsuns während des mittleren Holozäns nicht korrekt abbilden, da sie eine zu grobe horizontale Auflösung verwendeten und konvektive Prozesse daher parametrisieren werden müssen. Für heutige Bedingungen zeigt Marsham u. a. (2013), dass explizit aufgelöste Konvektion den Monsunniederschlag viel weiter nach Norden verschiebt und mehrere Schlüsseleigenschaften des Niederschlags im Vergleich zu Beobachtungen und im Vergleich zu parametrisierter Konvektion besser darstellen kann.

Motiviert durch diese Ergebnisse von Marsham u. a. (2013) untersuche ich im ersten Teil dieser Dissertation, ob die Verwendung von explizit aufgelösten Konvektionssimulationen den Monsunniederschlag im mittleren Holozän weiter nach Norden verschiebt als parametrisierte Konvektionssimulationen. Unerwarteterweise zeigen die Ergebnisse, dass sich die nördliche Ausdehnung der Monsunniederschläge nicht weiter nach Norden erstreckt, wenn die Konvektion explizit aufgelöst wird. Ich argumentiere, dass die geringere Nordverschiebung hauptsächlich durch grundlegend unterschiedliche Niederschlagseigenschaften und durch die Reaktion der Bodenhydrologie auf diese spezifischen Niederschlagseigenschaften verursacht wird, wenn Konvektion explizit aufgelöst wird. Dadurch ist der Niederschlag in parametrisierten Konvektionssimulationen im Allgemeinen höher und reicht weiter nach Norden als in explizit aufgelösten Konvektionssimulationen. Dieses Ergebnis weist auf die wichtige Bedeutung der Bodenfeuchte und der Oberflächenbedingungen für die Regulierung des Niederschlags in Nordafrika hin.

Der zweite Teil der Dissertation konzentriert sich daher darauf, wie die Landoberfläche und die Bodenfeuchte den Niederschlag über Nordafrika in Simulationen mit parametrisierter und explizit aufgelöster Konvektion beeinflussen. Zu diesem Zweck erweitere ich die Simulationen aus dem ersten Teil der Dissertation, in dem heutige Landoberflächenbedingungen verwendet werden, und schreibe einen höheren, idealisierten Vegetationsgradienten über Nordafrika vor, der näher an Proxydaten ist. Das Vorschreiben einer höheren Vegetationsdichte über Nordafrika verursacht unabhängig von der Darstellung von Konvektion eine positive Land-Atmosphäre-Rückkopplung mit höheren Niederschlägen und einer weiter nördlichen Ausdehnung der Monsunniederschläge. Allerdings zeigen parametrisierte Konvektionssimulationen eine stärkere Land-Atmosphäre-Rückkopplung und damit eine höhere Empfindlichkeit des Niederschlags auf Veränderungen der Landoberfläche im Vergleich zu explizit aufgelöster Konvektionsimulationen. Ich stelle die Hypothese auf, dass diese höhere Sensitivität auf die allgemein höhere Bodenfeuchte in Simulationen mit parametrisierter Konvektion zurückzuführen ist, welche aus häufigeren, aber weniger intensiven Niederschlägen und geringerem Abfluss resultiert – ein ähnlicher Mechanismus wie im ersten Teil der Dissertation beschrieben. Im Gegensatz dazu verhindert ein höherer Abfluss die Herausbildung

einer starken Bodenfeuchte-Niederschlags-Rückkopplung in Simulation mit explizit aufgelöster Konvektion. Aufgrund dieser Ergebnisse betone ich, dass es entscheidend ist, wie der Boden auf Niederschlag reagiert, und nicht nur, wie Niederschlag durch die Bodenfeuchte beeinflusst wird. Die Bedeutung der Bodenhydrologie für die Stärke der Land-Atmosphäre-Kopplung in Modellen wurde so bisher noch nicht berücksichtigt.

Um die Hypothese zu überprüfen, führe ich weitere Simulationen mit expliziter und parametrisierter Konvektion und mit hoher Vegetationsdichte durch, in denen ich jedoch das gleiche, konstante Bodenfeuchtefeld vorschreibe. Die Ergebnisse dieser Simulationen zeigen, dass sich der Monsunniederschlag bei gleichen Landoberflächenbedingungen mit expliziter Konvektion genauso weit nach Norden ausbreitet wie mit parametrisierter Konvektion. Allerdings sind die Niederschlagsraten in der Nähe der Küste Guineas und über dem größten Teil der Sahelzone in Simulationen mit parametrisierter Konvektion weiterhin höher. Dennoch zeigen diese Ergebnisse den starken Einfluss der Bodenfeuchte auf den westafrikanischen Monsun und unterstreichen die Bedeutung einer zuverlässigen Darstellung der Bodenhydrologie in Modellen.

PUBLICATIONS RELATED TO THIS DISSERTATION

Teilveröffentlichungen dieser Dissertation

Jungandreas, Leonore, Hohenegger, Cathy, Claussen, Martin (2021). "Influence of the representation of convection on the mid-Holocene West African Monsoon." *Climate of the Past* 17, pp.1665-1684. DOI: 10.5194/cp-17-1665-2021

Jungandreas, Leonore, Hohenegger, Cathy, Claussen, Martin (to be submitted). "Effect of a vegetated Sahara on the West African monsoon rainbelt in mid-Holocene storm-resolving simulations."

Challenges are gifts, opportunities to learn.

— Andy Andrews

ACKNOWLEDGMENTS

Doing your Ph.D. is not easy - everyone knows this. This goes to everyone who supported and believed in me during this time.

The first I want to acknowledge is Martin Claussen. Over three years ago, you gave me this opportunity to work with you, and with the amazing community of the Max Planck Institute for Meteorology. Like probably every Ph.D., I fought against several difficulties and you stayed patient, friendly, and encouraging.

As my second supervisor, I want to thank you, Cathy Hohenegger, for the amazing job you did. You taught me valuable lessons in how to think, write and work scientifically. You put a lot of effort into reviewing my work and gave me a lot of input to think about.

Next, thanks to the best colleagues: I want to acknowledge Anne Dallmeyer. Whenever I felt insecure or lost my motivation, you helped me out of it, motivated, and encouraged me. Thank you very much for your ideas, thoughts, and help. Thank you for reading my texts from time to time, for giving me new input, and open up new perspectives.
Thank you to my nearest colleagues, Laura, Jule, and Theresa. Thank you for this amazing time with you, for "suffering" together, encouraging each other, talking, and laughing.
Thank you Reiner Schnur for your help to set up my simulations, for explaining to me technical things, and for your patience. Without your tremendous effort at the beginning of my Ph.D., I'd probably still try to run my simulations.
A special thanks to Jule, Theresa, Oliver Gutjahr, Alex Winkler, Geet George, Zoé Rehder, and Samantha Bicknell for reading parts of this dissertation and for your indispensable, inspiring feedback.
Thanks to Michaela Born, Cornelia Kampmann, and Antje Weitz for your support in all PhD-related questions and your organization that made all events and the time as a Ph.D. so uncomplicated.
Thanks to all colleagues at the MPI for making it so easy to ask questions without feeling stupid. I rarely experienced such a warm environment, full of helpfulness, kindness, and support.

I want to express my special gratitude to my family, and my dearest partner in life, Krystian. One cannot ask for more support, sympathy, or love as you showed me. Without your motivation, energy, love, and contentment I would have had a much harder time. Thank you for helping me to overcome all smaller and bigger obstacles in the past. Because of you, I look into the future curious and full of joy.

CONTENTS

LIST OF FIGURES

LIST OF TABLES

ACRONYMS

AHP	African humid period
AEJ	African easterly jet
AWJ	African westerly jet
CONV	Convergence
DIV	Divergence
DS	"Desert Sahara"
GS	"Green Sahara"
GS-cSM	"Green Sahara with constant soil moisture"
ICON-NWP	Icosahedral Nonhydrostatic - Numerical Weather Prediction
ITF	Innertropical front
JAS	June, July August
MAP	Mean annual precipiation
MPI-ESM	Max Planck Institute - Earth System Model
PMIP	Paleoclimate Modelling Intercomparison Project
SHL	Saharan heat low
SST	Sea surface temperatures
TEJ	Tropical easterly jet

UNIFYING ESSAY

Humid mid-Holocene conditions

During the mid-Holocene, some 11700 to 4200 yBP (years before present), the today widely uninhabitable North African continent experienced more humid conditions. Its landscape was characterized by widespread savanna-like vegetation such as grass- and shrublands (Jolly et al., 1998) with variable tree cover, permanent lakes and wetlands (Tierney et al., 2017). This period is commonly referred to as the "African Humid Period" (AHP) and is the most recent of several periodically evolving wet periods during the last 86 million years. The most recent AHP is a well-documented (e.g. Prentice et al. (2000), Bartlein et al. (2011), and Larrasoaña et al. (2013)), intensively investigated example of past climate change (Claussen et al., 2017) that can help us to better understand the processes and the response of the West African monsoon to external forcings and its representation in climate models.

Mechanisms of origin of the AHP

The more humid conditions during the AHP were triggered by steady variations in orbital parameters (Berger, 1978) and intensified by ocean-atmosphere (e.g. Kutzbach and Liu (1997), Hewitt and Mitchell (1998), Braconnot et al. (1999), Liu et al. (2004), Zhao et al. (2005), Braconnot et al. (2007), and Braconnot et al. (2012)) and land-atmosphere feedbacks (e.g. Claussen and Gayler (1997), Kutzbach and Liu (1997), Braconnot et al. (1999), Braconnot et al. (2012), and Claussen et al. (2017)) (Sec. 1.3). Most climate models, however, are not able to reproduce the precipitation distribution and/or the precipitation amount needed to allow for the extensive vegetation cover over mid-Holocene North Africa as indicated by paleobotanical data (Harrison et al., 1998; Joussaume et al., 1999). Especially the meridional precipitation gradient between the coastal region and the Sahara is often too steep in model simulations as compared to proxy data, with too much precipitation over the Sahel and too less north of it (Joussaume et al., 1999; Braconnot et al., 2012; Harrison et al., 2015; Brierley, 2020). Climate models therefore appear to misrepresent important mechanisms for the West African monsoon and may miss processes and feedbacks altogether.

AHP Modelling difficulties with global climate models

One of the often poorly captured processes in climate models is the representation of atmospheric convection (Sec. 1.4). With the representation of convection, I refer to whether convective processes are parameterized or explicitly resolved in model simulations. Since global climate models use horizontal grids that are too coarse ($\sim$ 100 km) to explicitly resolve convection, it must be parameterized, i.e., calculated as a function of resolved quantities. However, convective parameterizations are subject to numerous uncertainties and may not properly capture many key properties of precipitation, such as intensity, frequency, or diurnal cycle of convection (Yang and Slingo, 2001; Randall et al., 2003; Stephens et al., 2010; Dirmeyer et al., 2012; Fiedler et al., 2020). The representation of the West African monsoon in climate models seems to be particularly problematic in this regard (Bock et al., 2011; Pohl and Douville, 2011).

Storm-resolving simulations as the solution?

Investigating how the representation of convection affects the West African monsoon in climate models is, therefore, necessary to better understand the controls of convection and precipitation over North Africa. For present-day conditions, Marsham et al. (2013) examined the influence of the representation of convection on the West African monsoon. In their study, explicitly resolved convection simulations lead to a more realistic representation of several key properties of precipitation compared

to observations. With explicitly resolved convection, the monsoonal precipitation extends further north and peaks between 10 °N to 12 °N. In contrast, parameterized convection features a monotonically decreasing precipitation rate from the equator to the subtropics.

Introduction of my studies

Deep convective systems are a key feature of precipitation over North Africa during the monsoon season (Mathon et al., 2002). The encouraging results of Marsham et al. (2013) raises the question of whether resolving convection explicitly can improve the representation of precipitation, particularly the meridional distribution, also over mid-Holocene North Africa - a long-standing problem of global climate models. I investigate the different effects of the representation of convection on the mid-Holocene West African monsoon under different land-surface conditions by performing the first regional, storm-resolving simulations (horizontal scales from 2 to 5 km) of mid-Holocene North Africa.

In the first part, I focus on the "pure" influence of the representation of convection on the northward extent of monsoonal precipitation, without considering the amplifying land-atmosphere feedback mechanisms (Appendix 1; summarized in Sec 1.5). I first analyze simulations with prescribed present-day vegetation cover - the Sahara remains a desert. In the second part, I perform simulations with a prescribed, more realistic mid-Holocene vegetation cover. I compare these simulations to those from the first part and examine how the feedbacks between land and atmosphere change depending on whether convection is parameterized or explicitly resolved.

Outline of the Unifying essay

This essay will help the reader to understand the research context of the two studies presented in Appendix A and B and how they fit into and contribute to the current scientific knowledge. First, I briefly describe the principles of the highly complex West African monsoon system based on present-day studies (Sec. 1.2). I then explain how the West African monsoon during the mid-Holocene was enhanced by feedbacks between the ocean and atmosphere and, more importantly, between the land and atmosphere (Sec. 1.3). I will elaborate in more detail the importance of convective processes (and the need to resolve them explicitly) for the West African monsoon in Sec. 1.4. Afterwards, I introduce and summarize the two studies I conducted during the course of my dissertation in Sec. 1.5 and 1.6 and conclude in Sec. 1.7.

Although the following description of the West African monsoon system is based on present-day studies, the main mechanisms are assumed to hold for the past as well. A basic schematic illustration is shown in Fig. 1.1. In the following, the numbers in brackets relate the processes and features explained in the text to the ones illustrated and numbered in this schematic.

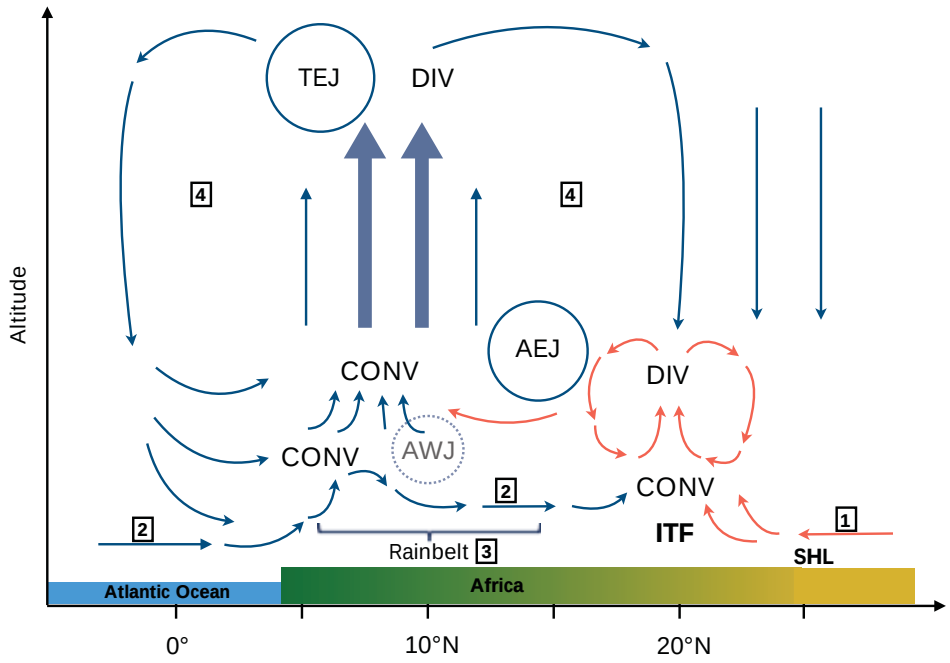

Figure 1.1: Schematic illustration of the West African monsoon system, adapted from Nicholson (2009a). The abbreviations term the following features: TEJ - Tropical easterly jet, AEJ - AEJ, AWJ - African westerly jet, ITF - Innertropical Front, SHL - Saharan heat low, DIV - divergence, CONV - convergence. The numbers in brackets refer to the processes described in the text (also marked), respectively.

The West African monsoon system is a highly complex system of many features, driven and influenced by interactions between land, atmosphere, and ocean. It determines the annual precipitation amount over North Africa, which peaks in the Sahel region between July and September. The West African monsoon system is associated with a pronounced seasonal shift of the low-level winds and the occurrence of the mid-level African easterly jet (AEJ) and the high-level Tropical easterly jet (TEJ). Moreover, the meso- and large-scale circulation in the tropics strongly interacts with the deep convective systems that are responsible for most of the precipitation (Holton, 2004; Hall and Peyrillé, 2006). Therefore, convective rainfall is not only a consequence of the West African monsoon circulation but also, in turn, strongly influences the monsoon circulation.

The Saharan heat low

The main driver of the West African monsoon circulation is the differential heating of the North African continent and the adjacent tropical Atlantic. During boreal

summer, the continent warms rapidly relative to the Atlantic Ocean, and a temperature maximum develops over the Western Sahara. The temperature maximum yields upward vertical motion and an intense, thermally-induced low-level low pressure system, the Saharan heat low (SHL), develops. The cyclonic flow around the Saharan heat low includes the northeasterly Harmattan winds [1], originating in the eastern Sahara and advect warm, dry air southward.

The southwesterly monsoon flow

As a result of the temperature contrast between the warm Sahara and the cool sea surface temperatures in the Atlantic ocean, a pressure gradient force develops and drives the southwesterly monsoon flow [2] (Thorncroft et al., 2011; Nicholson, 2013). With this southwesterly monsoon flow, moisture from the Gulf of Guinea is transported deep into the North African continent where it provides moisture for the formation of convection and precipitation. In addition, a significant amount of moisture is transported into the western Sahel by the African westerly jet (Pu and Cook, 2010), a low-level jet at about 10°N over the tropical Atlantic at 850hPa altitude (because it is not located over the continent but the Atlantic, it is only indicated in Fig. 1.1). The moisture is transported north up to the position of the Innertropical Front (ITF), where the low-level, southwesterly monsoon winds converge with the hot and dry northeasterly Harmattan winds.

The African easterly jet

Above the Saharan heat low, at about 600hPa, a high pressure system develops. As the pressure in the warm and dry air above the Saharan heat low decreases less than in the more humid and colder air southward, the meridional pressure gradient reverses with height, and a high pressure system with its core at approximately 600hPa is formed. This negative meridional gradient in geopotential and moisture induces a strong easterly wind, the African easterly jet (AEJ; (Cook, 1999))). The jet maximum is located at about 14°N and about 700-600 hPa above the southwesterly monsoon flow. The occurrence of dry convection north over the Sahara and moist convection to the south is assumed to maintain the AEJ (Thorncroft and Blackburn, 1999; Nicholson, 2013). The AEJ is associated with the mid-level export of moisture from the continent towards the Atlantic ocean. Hence, the stronger the jet the more moisture is transported westward (Cook, 1999). Consistently, several studies associate a weaker and further north located AEJ with wetter conditions over the Sahel (Cook, 1999; Nicholson and Grist, 2003; Sultan et al., 2003; Yeshanew and Jury, 2007).

The African easterly waves

A second, probably more important feature associated with the AEJ is the development of westward propagating, synoptic-scale systems that arise from baroclinic-barotropic instabilities associated with the horizontal and vertical shear of the AEJ (Burpee, 1972; Grist, 2002), the commonly-called African easterly waves. The lifting right ahead of the African easterly wave troughs are assumed to be a source of convection, leading to squall lines and organized mesoscale convective systems (e.g. Rennick (1976), Simmons (1977), Kwon (1989), and Thorncroft and Hoskins (1994a,b)). Additionally, the vertical wind shear in the vicinity of the AEJ supports the development of these mesoscale convective systems. These highly organized cloud clusters produce most (about 90%) of the Sahel rainfall (Lare and Nicholson, 1994; Mathon et al., 2002). The track of the African easterly waves and therefore of the rain-producing cloud clusters coincide with the maximum monsoonal rainfall [3] and is confined in a relatively narrow latitudinal band south of the AEJ.

The Tropical easterly jet and the region of upward vertical motion

The narrow band of the rainfall maximum is located between the axes of the AEJ and the Tropical easterly jet (TEJ) at about 14°N and 7°N (Nicholson, 2009b),

respectively. This region is characterized by strong vertical motion, high relative humidity (between 60-80% throughout the troposphere; Nicholson (2009b,c)) and is associated with a deep meridional overturning circulation [4] (Thorncroft et al., 2011). Besides the influence of the African easterly waves, the strong vertical motion between the two jets is assumed to be driven by latent heat release and the dynamics of the jets. At the right jet entrance and the left jet exit (in the flow direction of each jet), deviations from the geostrophic wind balance result in a divergent wind pattern. Owing to mass continuity, diverging air masses in the upper levels yield convergence at the surface and induced vertical upward motion, and thereby favor convection and precipitation. The specific locations of the AEJ and the TEJ over North Africa and the horizontal offset to each other yield the narrow band of upward vertical motion over the North African continent. However, deep moist convection between the jet axes itself induces uplifting by the latent heat release, hence, is not necessarily only a consequence but also drives and/or maintains the monsoon circulation. However, it is still under debate, how exactly the TEJ dynamics influence monsoonal rainfall (Nicholson and Klotter, 2021) or how the TEJ interacts with moist convection (Nicholson et al., 2007; Nicholson, 2009a; Lemburg et al., 2019). To my knowledge, there are no sensitivity experiments that try to disentangle the specific roles of the different components (for example the contribution of convective uplifting) interacting in the West African monsoon system.

1.3 THE WEST AFRICAN MONSOON AND ITS AMPLIFYING MECHANISMS DURING THE MID-HOLOCENE

The African humid period

As briefly mentioned in the introduction, more humid conditions prevailed in North Africa during the recent mid-Holocene AHP, due to an intensification of the West African monsoon system. Compared to today, precipitation over North Africa was higher and more uniformly distributed, with equally high precipitation amounts between 10 °N to 30 °N (Bartlein et al., 2011), ranging from 200 to 700 mm year^{-1} based on pollen reconstructions (Peyron et al., 2006; Bartlein et al., 2011). Estimates from the PMIP1 and 2 (Paleomodeling Intercomparison Project Phase 1 and 2) (Joussaume et al., 1999; Braconnot et al., 2007) suggest a precipitation increase during the mid-Holocene of around 200–300 mm year^{1}, the transition threshold for deserts to transform into a steppe biome type under present-day CO_2 concentrations. Considering the lower mid-Holocene CO_2 concentrations, which decreased the water use efficiency of plants, the precipitation estimate from the PMIP-models would have been higher and approximately match the paleobotanical records.

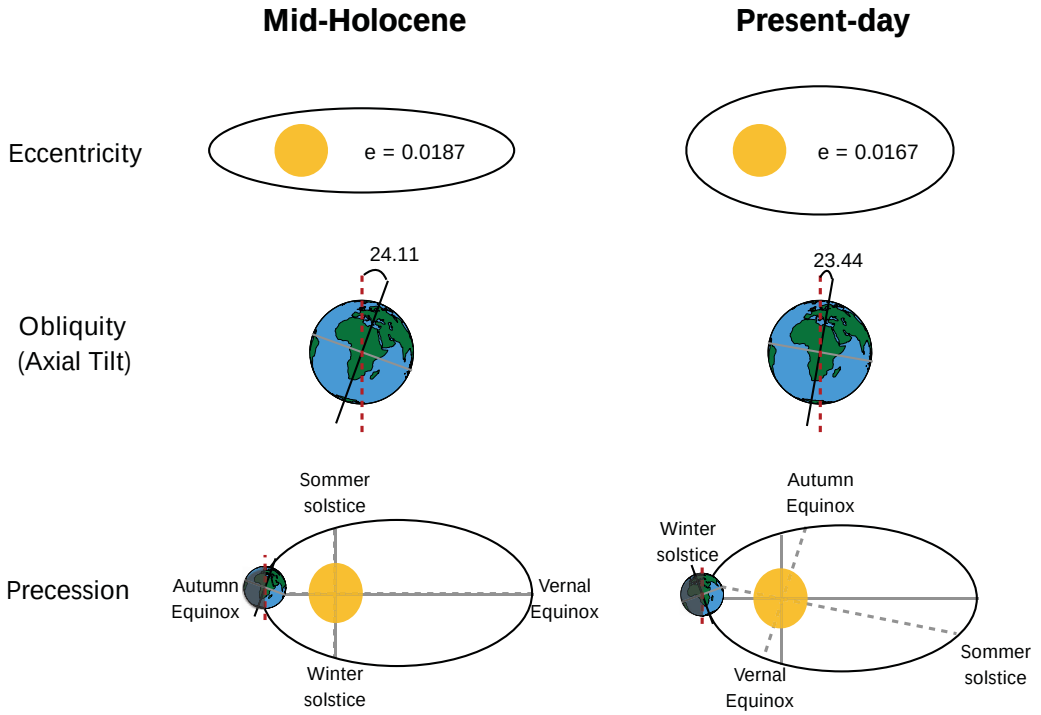

Figure 1.2: Schematic illustration of the orbital parameters for present-day conditions and how they differed during the mid-Holocene.

Orbital forcing - the pacemaker of the African humid period

The intensification of the West African monsoon was triggered by steady variations in orbital parameters (Berger, 1978). Besides an increased eccentricity and obliquity (axial tilt of the earth), the precessional cycle was the dominant pacemaker, shifting the perihelion to occur during boreal summer (Fig. 1.2) (Kutzbach and Guetter, 1986; Street-Perrott et al., 1990). In other words, during the early to mid-Holocene, the earth reached its sun-nearest point during northern hemispheric summer rather than during northern hemispheric winter than nowadays. A comparison of present-day

	present-day	mid-Holocene
Eccentricity of orbit	0.0167	0.0187
Axial tilt of earth (degree)	23.44	24.11
Position of perihelion* (degree)	78	179.1

* Position of perihelion (degrees of celestial longitude) measured clockwise from the vernal equinox

Table 1.1: Orbital parameters for present-day and mid-Holocene conditions (Kutzbach and Guetter (1986); Table 2).

and mid-Holocene orbital parameters are provided in Table 1.1. These changes in orbital parameters during the mid-Holocene increased the summer insolation and decreased the winter insolation over the northern hemisphere. Thus, the insolation seasonality was enhanced and therefore the land-sea temperature contrast was intensified. The stronger land-sea temperature gradient enhanced the West African monsoon circulation (Kutzbach, 1981; Kutzbach and Otto-Bliesner, 1982; Kutzbach and Guetter, 1986; Hall and Valdes, 1997; Kutzbach and Liu, 1997; Hewitt and Mitchell, 1998; Braconnot et al., 2000).

Necessary, amplifying mechanisms of the orbital forcing

This intensification of the West African monsoon was captured in early model attempts using mid-Holocene orbital parameters (see Fig. 1.3). However, they all underestimate or misrepresent the increase in precipitation and its meridional distribution across North Africa in the mid-Holocene (e.g. Joussaume et al. (1999) and Braconnot et al. (2012)), to sustain an extensive greening, as shown by paleobotanical data (Harrison et al., 1998; Joussaume et al., 1999). The initially induced changes of monsoonal rainfall likely required multiple amplifying feedback mechanisms to sustain the extensive vegetation cover, which can be reasonably well reproduced by climate models (e.g. Claussen and Gayler (1997) and Texier et al. (1997)). Several model experiments demonstrate the important amplifying mechanisms of ocean-atmosphere (e.g. Kutzbach and Liu (1997), Hewitt and Mitchell (1998), Braconnot et al. (1999), Liu et al. (2004), Zhao et al. (2005), Braconnot et al. (2007), and Braconnot et al. (2012)) and land-atmosphere feedbacks (e.g. Claussen and Gayler (1997), Kutzbach and Liu (1997), Braconnot et al. (1999), Braconnot et al. (2012), and Claussen et al. (2017)) to the initial orbital forcing.

1.3.1 *Ocean-atmosphere feedbacks*

Ocean feedbacks

The main influence of the ocean on the West African monsoon system is thought to be due to enhanced land-sea temperature contrast, resulting in a strengthened moisture advection towards the African continent (Zhao et al., 2005). The temperature gradient in the Atlantic ocean, however, also plays an important role for the precipitation over the Sahel. The temperature gradient in the Atlantic Ocean was weakened in

response to the insolation changes during the mid-Holocene. North of 5°N sea surface temperatures increased due to higher insolation, while it decreased south of 5°N due to less insolation on the southern hemisphere. The induced stronger warming of the Atlantic was further amplified by a wind-evaporation feedback (Kutzbach and Liu, 1997; Zhao et al., 2005). As a result, the ITF shift further north and thereby enhanced the monsoon circulation. The dipole warming in the Atlantic Ocean prolonged the monsoon season by the delayed response of the sea surface temperatures to the insolation changes (Kutzbach and Liu, 1997; Hewitt and Mitchell, 1998; Zhao et al., 2005) and favors late-summer precipitation located further north over Africa (Hewitt and Mitchell, 1998). The increased moisture transport formed a vertically deeper wedge of moist air feeding the West African monsoon, increased vertical upward motion and latent heating, and hence, enhanced the triggering of convection and the occurrence of precipitation over North Africa (Kutzbach and Liu, 1997).

1.3.2 *Land-atmosphere feedbacks*

Importance of the land-surface for the West African monsoon

Additionally to ocean-atmosphere feedbacks, various modeling studies focused on land-atmosphere coupling mechanisms and their amplifying influence on the mid-Holocene West African monsoon. Land surface processes have important effects on the regional climate over the North African continent, both in the present and in the past, as found by several studies (e.g. Charney et al. (1975), Charney (1975), Cunnington and Rowntree (1986), Sud and Molod (1988), Rowell and Blondin (1990), Kutzbach et al. (1996), Taylor and Ellis (2006), and Taylor et al. (2007)). The Sahel has been identified as a "hot spot" region of strong land-atmosphere coupling, supporting the ability of land-atmosphere feedbacks to induce strong changes in hydrology, vegetation, and, consequently, on the West African monsoon (Guo et al., 2006; Koster et al., 2006; Dirmeyer et al., 2009; Dirmeyer, 2011; Taylor et al., 2012).

Enhanced soil moisture in the Sahel has been identified as the main driver of enhanced monsoonal precipitation during the mid-Holocene. In a positive feedback loop, more precipitation increases soil moisture, which increases the vegetation cover and thereby reduces the soil albedo (wet soils and with higher vegetation cover are darker; e.g. Claussen and Gayler (1997), Kutzbach and Liu (1997), Texier et al. (1997), Broström et al. (1998), Braconnot et al. (2000), Doherty et al. (2000), and Vamborg et al. (2011)). Wetter soils and denser vegetation cover favors convective rainfall because of enhanced evapotranspiration that increases latent heat flux and therefore lower-tropospheric humidity in the atmosphere (e.g.Kutzbach et al. (1996) and Doherty et al. (2000)).

Intensification of the West African monsoon via enhanced land-sea temperature contrast

However, Levis et al. (2004) suggests that the change in soil albedo induced a stronger signal on the West African monsoon than the changes in evapotranspiration resulting from a higher vegetation cover. During the mid-Holocene, the reduction of the albedo due to wetter, i.e. darker soils and higher vegetation cover, resulted in a net increase of energy at the surface. In their simulations, the increase in net surface energy raised the surface temperature over the continent and enhanced the land-sea temperature gradient. Consequently, the monsoon circulation and precipitation over mid-Holocene North Africa was intensified (Street-Perrott et al., 1990; Ganopolski et al., 1998).

In contrast, Ripley et al. (1976) and Claussen and Gayler (1997) found a decrease in surface temperature over North Africa in response to increased evapotranspiration and higher cloud cover, which weakens the West African monsoon. However, Claussen and Gayler (1997) argues that the surplus of surface energy is dominantly transformed into latent heat flux (due to higher surface moisture availability) rather than into sensible heat flux. In response to the increased Bowen ratio, the vertical gradient of moist static energy increases within the boundary layer that destabilizes the atmosphere and favors convection and precipitation (Schär et al., 1999). The conclusions of Claussen and Gayler (1997) built upon the theory of the albedo-vegetation feedback, postulated already in the 1970s by Charney et al. (1975).

Intensification of the West African monsoon via increased boundary-layer moist static energy

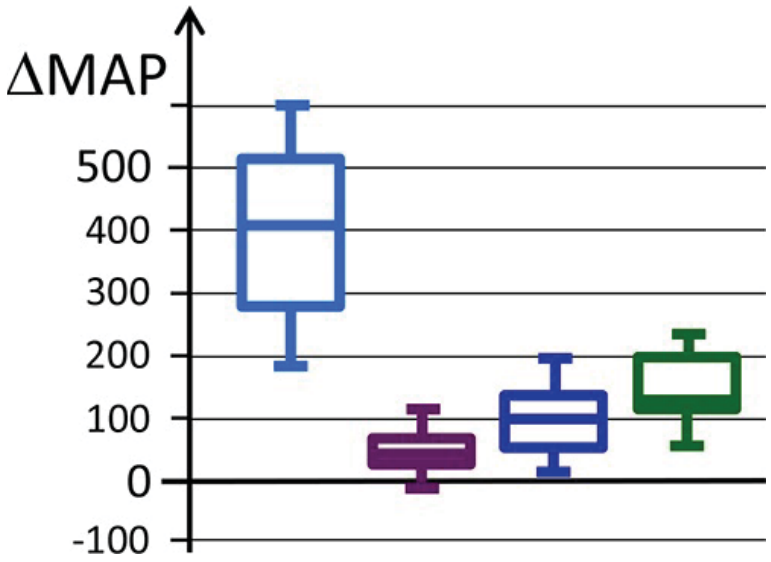

Figure 1.3: Differences between mid-Holocene and present-day mean annual precipitation (MAP) [mm yr^{-1}] in North Africa. The box displays the 25 to 75-percentile range, the line in each box represents the median value, and the whiskers depict the full range of values. The light blue box indicates reconstructed MAP differences. The purple, dark-blue, and green boxes shows simulated MAP differences from atmosphere-only models in which present-day SST were prescribed, from atmosphere-ocean models, and from atmosphere-ocean-vegetation models, respectively. (from Claussen et al. (2017), redrawn from Braconnot et al. (2012)).

Patricola and Cook (2007) and Rachmayani et al. (2015) emphasized another important dynamic feedback driven by decreased surface temperature (via enhanced latent heat flux; in contrast to Levis et al. (2004)) over North Africa that reduced the meridional temperature gradient. In response, the African easterly jet slows down due to the thermal wind balance (Cook, 1999; Wu et al., 2009). On the one hand, the weakening of the African easterly jet decreased the mid-level moisture export out of North Africa and therefore further increased the available moisture (additionally to enhanced evapotranspiration) for convection and precipitation (Cook, 1999). On the other hand, the African easterly jet shifted northward, as a result of a northward shifted temperature gradient maximum. This northward shift of the African easterly jet broadens the region of deep ascending motion, supporting the occurrence of

Dynamic intensification of the West African monsoon via a weakened African easterly jet

more vigorous convection further north in the Sahel-Sahara region (Xue and Shukla, 1993, 1996; Cook, 1999; Grist and Nicholson, 2001; Nicholson and Grist, 2001).

Climate models still underestimate the meridional precipitation gradient

Figure. 1.3 illustrates that climate models are able to simulate an amplification of the West African monsoon due to changes in orbital parameters (purple box). When ocean feedbacks (dark-blue box) and/or the synergistic effects between ocean, land, and atmosphere (green box) are included, monsoonal precipitation is further amplified (Ganopolski et al., 1998; Braconnot et al., 1999). However, the figure and several studies (Joussaume et al., 1999; Braconnot et al., 2012; Harrison et al., 2015; Brierley, 2020)) show that climate models generally underestimate the reconstructed amount and/or the meridional rainfall distribution. Although the inclusion of land-ocean-atmosphere feedbacks reduces this discrepancy, the model error remains substantial. Therefore, it is very likely that feedbacks and/or processes are still misrepresented or completely missed in climate models.

1.4 THE IMPORTANCE OF CONVECTIVE PROCESSES AND THEIR REPRESENTATION IN CLIMATE MODELS

Atmospheric convection acts on scales ranging from meters to kilometers and is hence a subgrid-scale process for global climate models that currently operate on horizontal resolutions of about 100 km. However, including convection in models is important because it is a key process for weather and climate. It provides source terms in the dynamic equations for heat, moisture, and momentum, thereby affecting the formation of clouds and precipitation and hence radiation (Rio et al., 2019). Convection is therefore parameterized in climate models, i.e., the mean effect of convection is calculated from large-scale quantities. However, convective parameterizations are known to be a key source of uncertainty in climate models. They are known to produce too much and too light rainfall and struggle to capture many key characteristics of precipitation such as the diurnal cycle, the location of the Innertropical front (ITF), or the northward propagation of the monsoons (Yang and Slingo, 2001; Randall et al., 2003; Stephens et al., 2010; Dirmeyer et al., 2012; Fiedler et al., 2020).

The importance of convective processes for the West African monsoon

The West African monsoon is strongly associated with deep convective systems that are responsible for most of the precipitation over North Africa. Mathon et al. (2002), for example, found that the precipitation over the present-day Sahel originates predominantly from mesoscale convective systems. Mesoscale convective systems are organized clusters of tropical convective clouds (Houze, 1993). These mesoscale convective systems are, on the one hand, driven by convective processes and therefore are hardly captured by convective parameterization schemes (Moncrieff, 1992). On the other hand, they are, even in their organized state, still too small to be resolved by the coarse horizontal resolution of the climate models. This indicates that processes associated with the West African monsoon, as well as precipitation itself, over North Africa are very likely influenced by the representation of convection in climate models.

Interaction between large and small scales

On smaller domains, e.g. over domains as large as Germany, storm-resolving simulations and/or for short periods, which allow for the explicit treatment of convection, have been performed and analyzed for several years already (e.g. Mass et al. (2002), Colle et al. (2005), Jankov et al. (2005), Hohenegger and Schar (2007), and Richard et al. (2007)). The West African monsoon, however, is a large-scale phenomenon. Hence, it needs large enough domains and sufficiently high resolution to properly capture the interaction between the monsoon circulation and the small-scale convective processes (Diongue et al., 2002; Redelsperger et al., 2002; Zhang et al., 2008). Due to the high computational effort, there are only a few simulation studies so far that have been carried out on storm-resolving resolution and over a large domain. For the same reason, storm-resolving simulations on larger domains have also only been run over short integration times. Today, however, the steady increase in computational power allows longer storm-resolving simulations on large enough domains.

Explicitly resolved convection simulations improve the meridional precipitation gradient over North Africa

For present-day conditions, Marsham et al. (2013) examined the influence of the representation of convection on the West African monsoon. They conducted a 10-day case study with the UK Met Office model, comparing simulations with explicitly resolved and parameterized convection over a regional domain in northwest Africa. In comparison to observations, simulations with explicitly resolved convection were

able to improve several key properties of precipitation. In addition, in comparison to simulations with parameterized convection, the maximum in monsoonal precipitation shifted further north and peaked between 10°N to 12°N. In contrast, precipitation peaks near the equator when convection was parameterized and its rate decreased toward the subtropics. They ascribe the stronger northward propagation of monsoonal precipitation in explicitly resolved convection simulations to a better representation of the diurnal cycle of moist convection. In explicitly resolved convection simulations condensational heating occurs in the evening/night when the monsoonal winds maximize (Parker et al., 2005). The condensational heating over the Sahel generates relatively low pressure and thereby enhances the monsoonal flow from the coast into the Sahel (and hampers a further northward transport into the Sahara). As a result, convection and monsoonal rainfall are supported further north over the Sahel. In parameterized convection simulations, condensational heating occurs midday. Because during the day monsoonal winds are weak due to dry convection, the transport of moist air into the Sahel is inhibited. Consequently, rainfall is mainly triggered near the equator and the coastal regions of North Africa. Based on this study, one would expect an improvement of the meridional precipitation distribution over mid-Holocene North Africa, which is hardly captured by state-of-the-art climate models. In the first study, related to this dissertation, I investigate the influence of the representation of convection on the West African monsoon during the mid-Holocene and examine whether the use of explicitly resolved convection extends the monsoonal precipitation further north as compared to parameterized convection (Sec. 1.5).

Convective processes at the core of land-atmosphere feedbacks

Different representations of convective processes are not only important for the West African monsoon itself, but they also affect the interactions between the land surface and the atmosphere (i.e. the West African monsoon) over North Africa, because convective processes are often at the core of these interactions (Hohenegger et al., 2009). Hohenegger et al. (2009) and Taylor et al. (2013) for example found, that parameterized and explicitly resolved convection produce fundamentally different soil moisture-precipitation feedbacks. While parameterized convection favors precipitation over moist soil via a positive soil moisture-precipitation feedback, explicitly resolved convection results in a negative feedback. In contrast, Leutwyler et al. (2021) found a positive feedback for both parameterized and explicit convection, but with differences in precipitation properties. While soil moisture anomalies in parameterized convection simulations result in an increased precipitation frequency, explicitly resolved convection simulations display increased precipitation intensity. Therefore, it is likely and reasonable to assume that the representation of convective processes also influences the sign, strength, and characteristics of land-atmosphere feedbacks in simulations of mid-Holocene North Africa. Whether the use of explicitly resolved convection also yields different feedback signs and/or strength as compared to parameterized convection over mid-Holocene North Africa is the main focus of the second study related to this dissertation (Sec. 1.6).

1.5 The influence of the representation of convection on the mid-Holocene West African monsoon (paper 1)

Our current scientific knowledge of the mid-Holocene West African monsoon and the previously described study of Marsham et al. (2013) raises the question, whether high-resolution simulations with explicitly resolved convection can improve the representation of the West African monsoon during the mid-Holocene. Therefore, the guiding research question of the first study is:

1. Does the explicit treatment of convection lead to a further northward propagation of monsoonal precipitation over mid-Holocene North Africa? *1. Research Question*

I analyze this question based on the first storm-resolving simulations of mid-Holocene North Africa, which I perform with the ICON (ICOsahedral Nonhydrostatic) model framework version 2.5.0 (Zängl et al., 2015) in its operational Numerical Weather Prediction (NWP) mode. In this first set of simulations, I followed the idea of the PMIP1 experiments and simulate with present-day land surface cover. As a first step, I thereby avoid the amplifying land-atmosphere feedbacks, which potentially additionally induce differences between parameterized and explicitly resolved convection simulations. Only orbital parameters, sea surface temperatures, initial and boundary conditions reflect mid-Holocene conditions and originate from the transient MPI-ESM Holocene simulations.

Proceeding from a 30-year spinup simulation, I conduct explicitly resolved as well as parameterized convection simulations of the summer monsoon season from June to October (JJASO). With a nesting strategy, the simulation domain is reduced from 40km horizontal grid spacing to 20km, 10km, and 5km. In the 40km-, 20km- and 10km-domain the convective parameterization is switched on. In the main paper, I refer to the simulations with 40km grid spacing and parameterized convection as 40km-P simulation. The 5km domain uses explicitly resolved convection and is labeled with 5km-E.

Results

Figure 1.4 shows the latitudinal distribution of precipitation for simulations with parameterized ("40km-P" and "10km-P") and explicitly resolved convection ("5km-E" and "10km-E"). In contrast to expectations, there is no northward extension of precipitation when convection is resolved explicitly. Parameterized convection simulations show higher amounts of precipitation and propagate slightly further north. Besides more supportive thermodynamic and dynamic atmospheric conditions for convection and precipitation, I demonstrate that especially the different interaction between precipitation intensity and runoff/soil moisture fundamentally affects the precipitation amount and its northward extension between parameterized and explicitly resolved convection simulations. In simulations with parameterized convection, light, permanent and large-scale precipitation moistens the soil steadily. The soil can store enough moisture to support evapotranspiration. Higher evapotranspiration increases the humidity in the lower atmosphere that favors the local formation of precipitation. Simulations with explicitly resolved convection produce more locally confined, strong precipitation events which produce larger amounts of runoff. Precipitation that feeds surface runoff no longer contributes to soil moisture and evaporation. The resulting drier soil substantially reduces the amount of moisture in the overlying atmosphere and hence prevents the formation of precipitation.

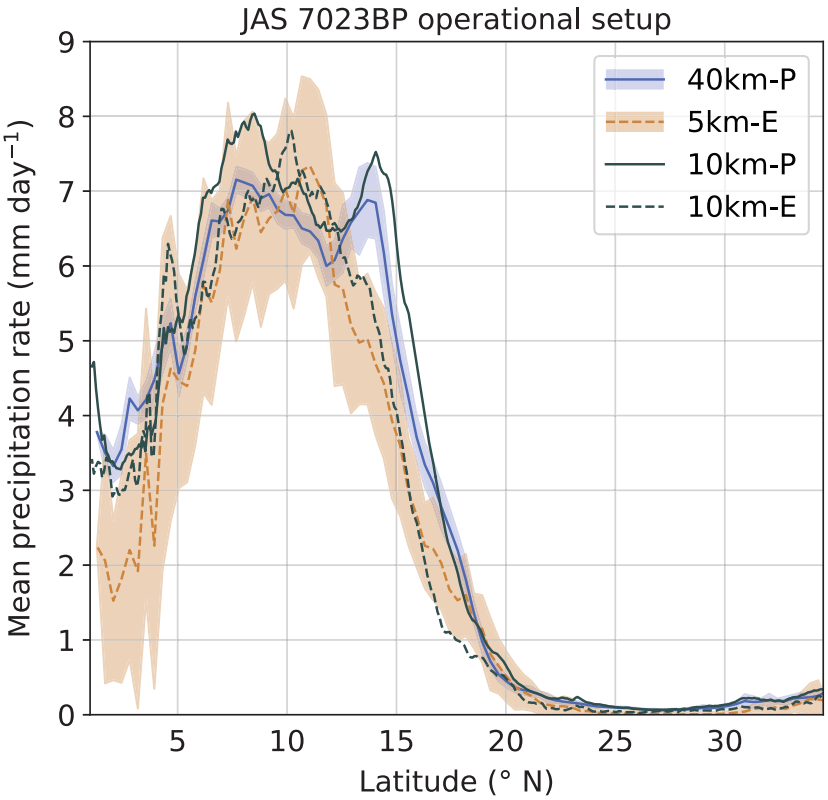

Figure 1.4: Meridional distribution of monsoonal precipitation for the operational simulations for the 40 km-P (blue-solid), the 5 km-E (orange-dashed), the 10 km-P (black-solid) and the 10 km-E (black-dashed) simulation. The shading displays the daily longitudinal mean standard deviation from the longitudinal mean JAS cycle for the 40 km-P and the 5 km-E simulation. The longitudinal mean is taken over the land points of domain spanning from 0°N-40°N and from 20°W-15°E.

So far, two factors were changed simultaneously in the 5km-E simulation, resolution and convection parameterization. Since there is no improvement concerning the northward extension of the monsoon in the 5km-E simulation, a separate examination of the horizontal resolution is needed. This motivates the second research question:

2. Research Question

2. Does the horizontal model resolution modifies the precipitation amount and distribution of the West African monsoon?

Results

To separate the effect of the representation of convection from the effect of different horizontal grid spacing, I analyze explicitly resolved and parameterized convection simulations with the same grid spacing of 10km. These simulations are labeled 10km-E and 10km-P simulation, respectively. The results indicate that simulations with the same representation of convection (40km-P and 10km-P or 10km-E and 5km-E) show more similar results (also visible in Fig. 1.4). The thermodynamic and dynamic atmospheric conditions are more supportive for the development of convection

and precipitation in the 10km-P simulations. Moreover, I find the same runoff/soil moisture-mechanism in the 10km simulations as in the 40km and 5km simulations. The 10km-E simulations generate higher amounts of runoff and consequently exhibit drier soils as a result of more local and intense precipitation events as compared to the 10km-P simulations. I conclude that the horizontal resolution has only minor quantitative effects on the results.

Marsham et al. (2013) identified differences in the diurnal cycle of convection between parameterized and explicitly resolved convection simulations as a key mechanism for the further northward shifted monsoonal precipitation in their simulations. Related to their findings, I pose a third research question:

3. Research Question

3. Does the diurnal cycle of convection influences the northward extension of precipitation over mid-Holocene North Africa?

Results

In our model framework and simulation setup, the diurnal cycle of convection does not substantially influence the northward extension of precipitation over mid-Holocene North Africa. I argue that the strong differences, i.e. the northward extension and amount of monsoonal precipitation in explicitly resolved compared to parameterized convection simulation, between Marsham et al. (2013) and my study originate mainly from fundamentally different convective parameterization schemes, which are very likely to influence and modulate the results.

This first study reveals two main results.

Key findings of the first study

1. Explicitly resolved convection does not necessarily shift the monsoonal precipitation further north as compared to parameterized convection in simulations with the ICON-NWP model.

2. Whether convection is parameterized or explicitly resolved alters the precipitation intensity and its spatial distribution (widespread or local), which has significant implications for the hydrological cycle in simulations.

These results suggest that soil hydrology controls precipitation through runoff and soil moisture. For models, this means that the representation of the soil and its hydrology can significantly influence the precipitation. This study indicates that the representation of the soil hydrology in models, especially the treatment of water runoff, potentially controls the amount of rainfall in explicitly resolved convection simulations via the soil moisture. Hence, climate models which aim for improved land-atmosphere interaction need both, explicitly resolved convection and reliable land surface schemes.

1.6 Effect of a vegetated Sahara on the West African monsoon rainbelt in mid-Holocene storm-resolving simulations (paper 2)

The results of the first study demonstrate the important role of the land surface for the monsoonal precipitation over (mid-Holocene) North Africa. Soil moisture in our simulations is strongly controlled by runoff, which, in turn, is determined whether convection is explicitly resolved or parameterized. Hence, it shows that different representations of convection can yield crucial consequences for the hydrological cycle.

Therefore, it stands to reason to investigate the influence of different land surface conditions on the West African monsoon and for the different representations of convection in more detail. I prescribing a higher mid-Holocene vegetation cover, closer to proxy data, which is assumed to amplify the monsoonal rainfall and therefore to increase soil moisture (compare to Sec. 1.3), hence to yield a positive land-atmosphere feedback. Based on the findings of the first study and the current scientific knowledge about land-atmosphere feedbacks (Sec. 1.3), the guiding research questions I pursue are:

1. and 2. Research Question

1. Is the land-atmosphere feedback different in sign and strength in explicitly resolved and parameterized convection simulations?
2. Can the vegetation-precipitation feedback overcome the limiting influence of runoff on soil moisture and now extend the monsoonal precipitation equally far north in explicitly resolved as in parameterized convection simulations?

To answer these research questions, I extend the simulations introduced in Sec. 1.5 in two ways. As a first step, I prescribe an idealized vegetation gradient over North Africa based on the modeled vegetation gradient in the dynamic-vegetation MPI-ESM Holocene simulations. I refer to these simulations as GS (for "Green Sahara") simulations. Similar to the approach in paper 1, I first perform a 30-year spinup simulation and proceed with explicitly resolved and parameterized convection simulations of a summer monsoon season (JJASO). The model and the modeling setup (domains, the nesting strategy, boundary conditions, orbital and atmospheric parameters) remain the same as in the "Desert Sahara" (DS) simulations in paper 1.

Results

Overall, I find positive land-atmosphere feedbacks in the simulation with a denser vegetation cover for the mid-Holocene (GS), regardless of the representation of convection. The higher vegetation cover results in an increase in the surface latent heat flux and therefore in low-level atmospheric moisture. The atmospheric stability decreases leading to more favorable conditions for convection and precipitation. Moreover, the increase in surface latent heat flux (and increased cloud cover) leads to a decrease in the temperature gradient over the North African continent. Hence, the denser vegetation cover does not directly strengthen the monsoonal flow as for example shown by Street-Perrott et al. (1990) or Ganopolski et al. (1998). The decrease in the temperature gradient induces changes in atmospheric dynamics, i.e. mainly in the African easterly jet, thus influencing the West African monsoon circulation. The African easterly jet weakens and shifts further north. These changes support a further northward expansion of the monsoonal rainbelt similar to the results of

Patricola and Cook (2007) and Rachmayani et al. (2015). Thus, the precipitation gradient between the coastal region and the Sahara decreases in the vegetated Sahara state in both representations of convection.

However, I demonstrate that the differences between the DS and the GS simulation are generally more pronounced in the parameterized convection simulations compared to the explicitly resolved convection simulations. Additionally, precipitation is still higher and shows a stronger northward extent compared to explicitly resolved convection simulations. The stronger differences in parameterized convection simulations indicate a higher sensitivity of precipitation to changes in the land surface. This higher sensitivity in parameterized convection simulations agrees with previous present-day studies (e.g. Hohenegger et al. (2009)). I hypothesize that the higher sensitivity of parameterized convection simulations dominantly originates from higher soil moisture which is governed by high precipitation rates and, simultaneously, lower runoff - a similar precipitation-runoff/soil moisture mechanism as revealed in the first study.

Therefore, we need to rethink how studies approach the land-atmosphere coupling as they mainly relate changes in precipitation to changes in the land surface. This study, however, emphasizes that it is not only important how precipitation reacts to a certain change in the land surface but how the land surface reacts to precipitation. The results indicate that the limitation of soil moisture, due to higher amounts of runoff, in explicitly resolved convection simulations impedes the formation of a strong positive soil moisture-precipitation feedback in the GS simulations. In contrast, in parameterized convection simulations, low-intense precipitation is more frequent and widespread, allowing for a consistent re-moistening of the soil and sustains a strong positive land-atmosphere feedback.

This raises a new hypothesis which I pose as a third interesting research question:

3. Does lower soil moisture in the explicitly resolved convection simulations lead to a less northward extent of monsoonal precipitation? *3. Research Question*

I perform two additional simulations of vegetated North Africa in which soil moisture is initialized from the same field and kept constant over time in both explicitly resolved and parameterized convection simulations. These simulations are labeled with GS-cSM ("Green Sahara with constant soil moisture"). In these simulations, the feedback between the type and amount of precipitation, the resulting runoff (which both fundamentally depend on the representation of convection), and soil moisture are eliminated.

Results

When the impact of the representation of convection (via the precipitation intensity) on runoff/soil moisture is eliminated, soil moisture strongly increases in explicitly resolved convection simulations. As a result, evapotranspiration and precipitation are enhanced, especially over the Sahel-Sahara region. In contrast, no substantial differences appear in parameterized convection simulations. Consequently, the monsoonal precipitation in these constant-soil moisture simulations extends equally strong north in explicitly resolved and parameterized convection simulations (Fig. 1.5). However, precipitation over the coastal and southern Sahel region (up to about 20°N) remains much higher in the parameterized convection than in explicitly resolved convection simulations (Fig. 1.5). I suggest that especially

the influence of soil moisture on the atmospheric dynamics, i.e., the AEJ, increases precipitation over the northern Sahel and Sahara region.

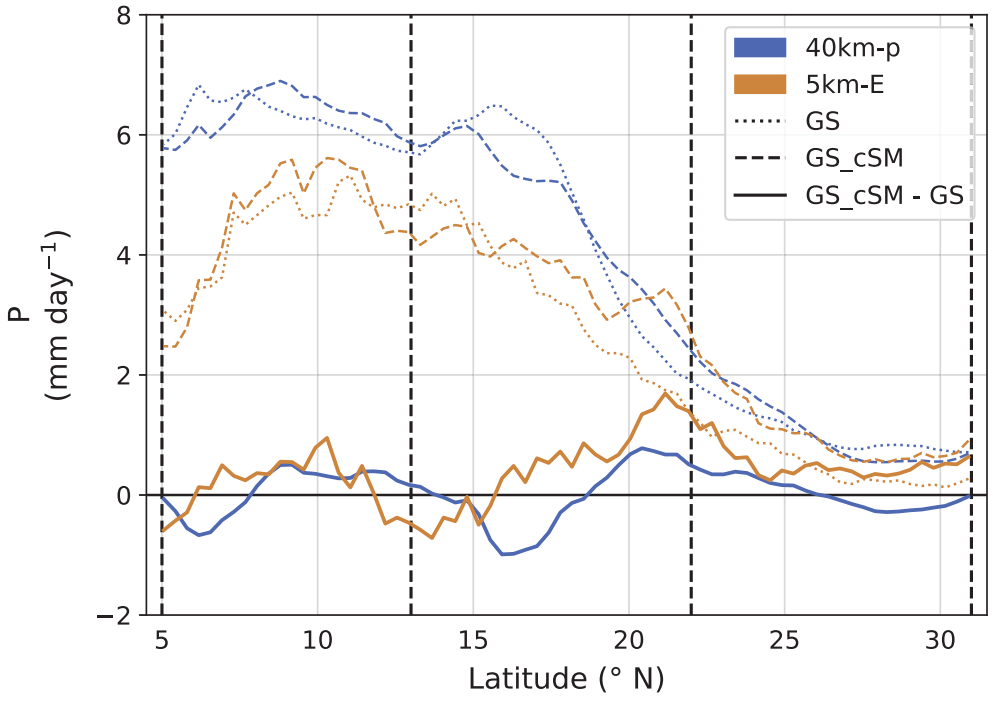

Figure 1.5: Meridional distribution of monsoonal precipitation for GS (dotted), the GS_cSM (dashed) and the difference between the GS_cSM and the GS simulation (solid) for the 40 km-P (blue) and the 5 km-E (orange) simulations. The longitudinal mean is taken over the domain spanning from 5°N-31°N and from 18°W-15°E. The vertical dashed lines indicate the boarders of the "coastal" region spanning from 5°N-13°N and from 18°W-15°E, for the "Sahel" region spanning from 13°N-22°N and from 18°W-15°E and for the "Sahara" region spanning from 22°N-31°N and from 18°W-15°E.

The main findings of this second study are:

Key findings of the second study

1. Both representations of convection generate a positive land-atmosphere feedback if a denser vegetation cover is prescribed over North Africa, but parameterized convection simulations show a higher sensitivity of precipitation to these changes in the vegetation cover than explicitly resolved convection simulations.

2. While previous studies focused on how precipitation is determined by a change in soil moisture, here I state that it is particularly important how soil moisture (via runoff) reacts to changes (or differences) in precipitation.

1.7 CONCLUSION AND OUTLOOK

The presented results in this dissertation implicate important mechanisms to improve the modeling of the most recent AHP. The use of storm-resolving simulations plays a major role in this attempt. This dissertation emphasizes that especially two related mechanisms should be considered for a reliable precipitation response:

1. Whether convection is explicitly resolved or parameterized significantly influences the precipitation characteristics such as intensity, frequency, and spatial distribution and can have far-reaching consequences on the hydrological cycle.

and hence,

2. Land surface processes need more attention, especially runoff because it regulates the soil moisture that in turn controls the evapotranspiration and hence the available moisture for the formation of precipitation in the atmosphere.

Therefore, the representation of the AHP will benefit from improved land surface processes in storm-resolving models. The representation of land surface processes is a major limitation of the ICON-NWP model framework. Important land surface processes to further improve the modeling of the AHP (and which are not sufficiently included in the ICON-NWP model) are for example:

1. **The representation of runoff**: models need to be able to redistribute an excess of precipitation in one location via runoff to regions that experience (too) less precipitation (unlike the ICON-NWP model).

2. **The development/retreat of lakes, wetlands, and rivers:** Connected to the representation of runoff is the ability of models to store excessive precipitation water overground and to generate extended wetlands, lakes or enlarge existing river networks, as experienced over mid-Holocene North Africa. The generation of these overground moisture reservoirs involves strong positive feedbacks and further enhance precipitation as shown by Krinner et al. (2012) and in a new study of Specht et al. (in peer-review). Based on the presented results, I hypothesize that the precipitation characteristics in explicitly resolved convection simulations are more likely to produce such extended lakes and wetlands if runoff is treated properly and if the model would be able to generate lakes and wetlands dynamically.

Besides interactive land-atmosphere coupling and dynamic vegetation, the ICON-NWP model lags ocean-atmosphere interactions. But ocean-atmosphere interactions also influenced the climate over North Africa in the past (Kutzbach and Liu, 1997; Hewitt and Mitchell, 1998; Braconnot et al., 1999; Liu et al., 2004; Zhao et al., 2005; Braconnot et al., 2007; Braconnot et al., 2012), present and future climate (e.g. Bader and Latif (2003), Giannini et al. (2003, 2005), Biasutti et al. (2008), and Park et al. (2015)). Therefore, I argue that including a coupled ocean scheme and an improved land component would be beneficial for simulations of the most recent AHP, but also for simulations of present and future climate. Additionally, the increasing ability to run longer storm-resolving simulations on a global scale and with fully coupled climate models will allow us to study land-ocean-atmosphere feedbacks (and other processes) under the important aspect of the representation of convection.

Such simulations of past climate changes can potentially improve projections of a warming future climate (Braconnot et al., 2012; Hopcroft et al., 2021). Especially for such a vulnerable and troubled society as in the Sahel region, more reliable statements about the future are urgently needed. The reasons for future and past climate changes are different and therefore mechanisms that drove droughts and wet phases over the Sahel in the past could be different in the future (Held et al., 2005; Biasutti et al., 2008; Cook, 2008). To provide better future climate projections, the mechanisms and feedbacks introduced above, need to be included, better understood, and evaluated in global climate models for past and present-day climate. We need to understand the mechanisms, strength, and sign as well as interactions between these land-ocean-atmosphere processes to estimate the response of the climate system to any forcing.

APPENDICES

A

INFLUENCE OF THE REPRESENTATION OF CONVECTION ON THE MID-HOLOCENE WEST AFRICAN MONSOON

The work in this appendix has been published as:

Jungandreas, Leonore, Hohenegger, Cathy, Claussen, Martin (2021). "Influence of the representation of convection on the mid-Holocene West African Monsoon." *Climate of the Past* 17, pp.1665-1684. DOI: 10.5194/cp-17-1665-2021

Influence of the representation of convection on the mid-Holocene West African Monsoon

Leonore Jungandreas[1], Cathy Hohenegger[1], Martin Claussen[1,2]

[1] Max Planck Institute for Meteorology, Bundesstraße 53, 20146 Hamburg
[2] Center for Earth System Research and Sustainability, Universität Hamburg, Bundesstraße 53, 20146 Hamburg

Abstract

Global climate models experience difficulties in simulating the northward extension of the monsoonal precipitation over north Africa during the mid-Holocene as revealed by proxy data. A common feature of these models is that they usually operate on grids that are too coarse to explicitly resolve convection, but convection is the most essential mechanism leading to precipitation in the West African Monsoon region. Here, we investigate how the representation of tropical deep convection in the ICOsahedral Nonhydrostatic (ICON) climate model affects the meridional distribution of monsoonal precipitation during the mid-Holocene by comparing regional simulations of the summer monsoon season (July to September; JAS) with parameterized and explicitly resolved convection.

In the explicitly resolved convection simulation, the more localized nature of precipitation and the absence of permanent light precipitation as compared to the parameterized convection simulation is closer to expectations. However, in the JAS mean, the parameterized convection simulation produces more precipitation and extends further north than the explicitly resolved convection simulation, especially between 12 and 17 °N. The higher precipitation rates in the parameterized convection simulation are consistent with a stronger monsoonal circulation over land. Furthermore, the atmosphere in the parameterized convection simulation is less stably stratified and notably moister. The differences in atmospheric water vapor are the result of substantial differences in the probability distribution function of precipitation and its resulting interactions with the land surface. The parametrization of convection produces light and large-scale precipitation, keeping the soils moist and supporting the development of convection. In contrast, less frequent but locally intense precipitation events lead to high amounts of runoff in the explicitly resolved convection simulations. The stronger runoff inhibits the moistening of the soil during the monsoon season and limits the amount of water available to evaporation in the explicitly resolved convection simulation.

A.1 INTRODUCTION

During the mid-Holocene, around 9000 to 6000 years before present (BP), the landscape of the today's extremely arid Sahara was transformed into a widespread savannah-like landscape characterized by grass- and shrublands (Jolly et al., 1998), variable tree cover and permanent lakes and wetlands (Tierney et al., 2017). This remarkable transformation of the Sahara, which is commonly called "Green Sahara", can be attributed to an intensified West African Monsoon (WAM) (Kutzbach and Otto-Bliesner, 1982; Kutzbach and Liu, 1997). The intensification of the WAM circulation was driven by a higher summer insolation in the Northern Hemisphere during the mid-Holocene (Kutzbach and Guetter, 1986; Street-Perrott et al., 1990). Reconstructions of precipitation from proxy data (Peyron et al., 2006; Bartlein et al., 2011) indicate around 200 to 700 mm yr^1 more precipitation over the Sahel–Saharan region during this humid period. However, global general circulation models (GCMs) capture neither the reconstructed mean precipitation (Yu and Harrison, 1996; Braconnot et al., 2012) nor the change in precipitation between the coastal regions of Africa and the arid Sahel–Sahara for the mid-Holocene (Joussaume et al., 1999; Braconnot et al., 2012; Harrison et al., 2015; Brierley, 2020). Compared to reconstructions, most climate models (e.g., used in PMIP3 and PMIP4) are able to reproduce the precipitation amount over the Sahel but produce too little precipitation north of 15 °N, resulting in an overly strong meridional precipitation gradient.

The reasons for the mismatch between climate models and reconstructions are still debated. Feedback mechanisms between the land/vegetation (e.g. Claussen and Gayler (1997), Kutzbach and Liu (1997), Braconnot et al. (1999), Braconnot et al. (2012), and Claussen et al. (2017)), ocean (e.g. Kutzbach and Liu (1997), Hewitt and Mitchell (1998), Braconnot et al. (1999), and Braconnot et al. (2012)) and the atmosphere are known to enhance the orbitally induced increase in mid-Holocene monsoonal precipitation (Joussaume et al., 1999; Braconnot et al., 2012). A better representation of the land surface in GCMs may be necessary to substantially increase precipitation levels (e.g. Levis et al. (2004) and Vamborg et al. (2010)). As another factor, changes in dust fluxes between present-day and mid-Holocene conditions have been mentioned and are a subject of controversy (Pausata et al., 2016; Thompson et al., 2019). Finally, by adding an artificial heating source within the atmospheric boundary layer over the Sahara, Dixit et al. (2018) were able to increase the magnitude and northward extent of precipitation comparable to what is seen in proxy data. They argued that GCMs miss an important local diabatic heating source over the Sahel–Saharan region.

The parameterization of convection poses another limitation for GCMs. For most, if not all, paleosimulations, GCMs usually operate on relatively coarse horizontal resolution ($\sim$ 200 km), where convection is not explicitly resolved. Several studies (Yang and Slingo, 2001; Randall et al., 2003; Stephens et al., 2010; Dirmeyer et al., 2012; Fiedler et al., 2020) have shown that simulations with parameterized convection are not able to reproduce many key characteristics of the present-day precipitation distribution, such as the location of the Intertropical Convergence Zone (ITCZ), the propagation of the monsoon or the diurnal cycle of precipitation. Also, they produce rainfall that is both too much and too light.

This raises the question as to whether convection-permitting simulations can improve the representation of the WAM and the precipitation distribution for mid-

Holocene climate conditions. Support for this hypothesis comes from the study by Marsham et al. (2013). For present-day conditions, they conducted short (covering only 10 days) simulations with explicitly resolved convection and parameterized convection for a regional domain located in northwest Africa. In their study, the monsoonal precipitation propagated further northward and peaked between 10 to 12 °N in their simulation with explicit convection, in better agreement with observations. They ascribed the improvement of the precipitation pattern to the better representation of the diurnal cycle of convection.

Using the ICON-NWP model (ICOsahedral Nonhydrostatic model framework for numerical weather prediction), we investigate how the representation of convection impacts the mid-Holocene WAM. We perform parameterized and explicitly resolved convection simulations with prescribed mid-Holocene atmospheric initial and boundary conditions for two entire monsoon seasons. The main aim of the study is to test whether explicitly resolving convection leads to a stronger northward propagation of the WAM during the mid-Holocene.

The paper is structured as follows: We describe the model and different simulation setups in section 2. In section 3, we present and explain the simulated precipitation patterns. A summary and conclusion follows in section 4.

A.2 METHODS

A.2.1 *Model*

We use the ICON model framework version 2.5.0 (Zängl et al., 2015) in its operational NWP mode. ICON was developed through a collaboration between the Max Planck Institute for Meteorology and the German Weather Service. The model has already been used and evaluated with respect to tropical convection and circulation by several studies (e.g. Klocke et al. (2017), Stevens et al. (2019), and Hohenegger et al. (2020)). Zängl et al. (2015) lists the physical parameterizations of the model framework. The parameterization of convection is based on the bulk mass-flux approach introduced by Tiedtke (1989) with modifications by Bechtold et al. (2014). We will switch the convective parameterization on or off, depending on the grid spacing. Our limited-area simulations are forced with initial and boundary data from a transient global Holocene simulation, previously conducted with the Max Planck Institute Earth System Model (MPI-ESM) and covering the years from 8000 BP (before present, where the year 2000 is used as the reference) to 150 BP. Dallmeyer et al. (2020) describes the performance of the transient MPI-ESM Holocene simulations in detail. Furthermore, we prescribe 6-hourly sea surface temperature (SST) and sea ice (SIC) fields originating from the transient Holocene simulations. The orbital parameters and the tracer gases, carbon dioxide (CO_2), methane (CH_4) and nitrogen oxide (N_2O), reflect mid-Holocene conditions, as in the MPI-ESM Holocene simulation. Concerning the description of the land surface and vegetation, we take the external parameters from reanalysis data of the Integrated Forecast System (IFS) of the European Centre for Medium-Range Weather Forecasts (ECMWF). Similar to the setup of the simulations in the first Paleoclimate Modelling Intercomparison Project (PMIP; i.e., Joussaume et al. (1999), Braconnot et al. (2000), and Braconnot et al. (2004)), the external data reflect present-day conditions. By using present-day surface conditions in this study, we, for a first step, ignore the enhancement of precipitation

due to extended vegetation and wetter soil moisture conditions. Furthermore, with a higher vegetation cover, the atmosphere–soil hydrology interactions are also likely to change substantially. Plants enhance the infiltration of water into the soil and increase the interception storage of water. Therefore, they increase evapotranspiration into the atmosphere from interception and by transpiration of water from deeper soil layers.

A.2.2 *Simulation Setup*

Firstly, we perform a 30-year "spinup" simulation on a regional domain (see Fig. A.1) with 40 km horizontal grid spacing and 75 vertical levels. The spinup simulation runs for the period 7039 to 7010 BP. The convective parameterization is active in this simulation. After around 15 years, the soil moisture equilibrates to a stable state. We choose 2 years after the 15-year spinup phase and perform several nesting experiments for the boreal summer monsoon season. The nesting experiments are initialized for 30 May and run for 5 months (June to October; JJASO). The parent domain of the nested simulation is identical to the domain of the spinup simulation with the same horizontal and vertical resolution. The nesting configuration then reduces the horizontal grid spacing by a factor of 2 down to the 5 km horizontal resolution (Fig. 1). The nested simulations with 40, 20 and 10 km grid spacing are run with parameterized convection. In the following, we refer to these simulations as the 40, the 20 and the 10 km-P simulations. The 5 km simulations resolve convection explicitly and are referred to as the 5 km-E simulations. We simulate with a one-way nesting strategy. The nested simulations are initialized 1 h after another. Lateral boundary conditions for the nested simulations are obtained from their parent simulation and updated every 6 h.

For each nesting suite, we perform two simulations, one for the year 7023 BP and one for the year 7019 BP. We selected these two years from the spinup simulations based on the simulated mean precipitation (Fig. A.2 a) and the mean meridional distribution of precipitation (Fig. A.2 b) within each year from June to October and over land points of the 5 km-domain (Fig. A.1). We chose the year 7023 BP as it displays a combination of generally higher precipitation amounts and slightly higher precipitation rates at latitudes north of 15 ° N relative to the other simulated spinup years. The year 7019 BP, in contrast, gives the combination of slightly weaker precipitation amounts and weaker precipitation rates north of 15 ° N compared to most of the other years of the spinup simulation.

For each nesting suite, we perform two simulations: one for the year 7023 BP and one for the year 7019 BP. We selected these 2 years from the spinup simulation based on the simulated mean precipitation (Fig. A.2 a) and the mean meridional distribution of precipitation (Fig. A.2 b) within each year from June to October and over land points of the 5 km domain (Fig. A.1). We chose the year 7023 BP as it displays a combination of generally higher precipitation amounts and slightly higher precipitation rates at latitudes north of 15 °N relative to the other simulated spinup years. The year 7019 BP, in contrast, gives the combination of slightly weaker precipitation amounts and weaker precipitation rates north of 15 °N compared to most of the other years of the spinup simulation.

Marsham et al. (2013) identified the difference in the simulated precipitation diurnal cycle between explicitly resolved and parameterized convection as the main

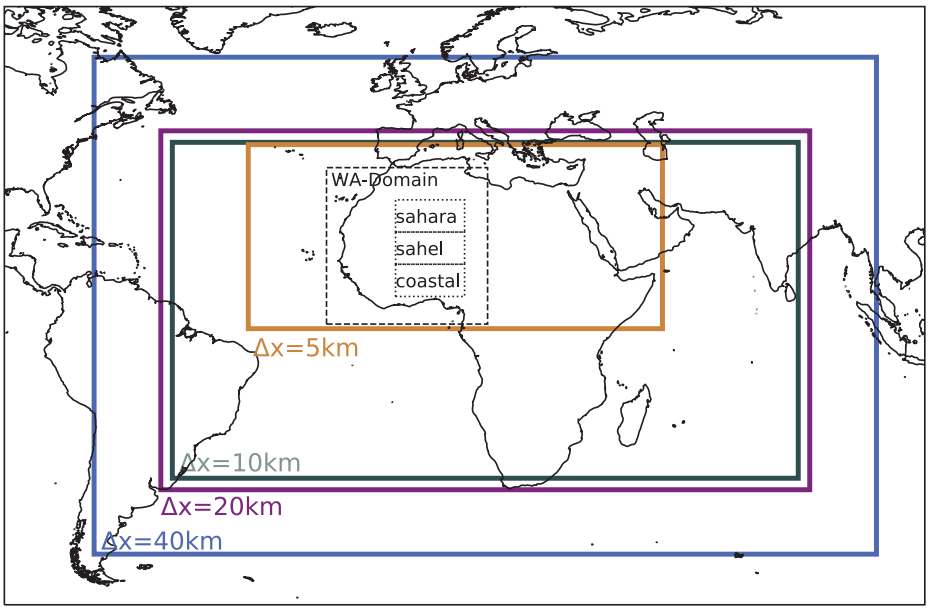

Figure A.1: Colored domains display the nesting domains of the simulations for the various grid spacings (as indicated). The dashed black domain with the label "WA domain" (west Africa) shows the analysis domain for Figs. 3, 4, 6, 8, and 10 and spans the area from 1–35 °N and from 20 E–15 °W. The three dotted black domains over north Africa are used to calculate the skew-T diagrams for the coastal African region ("coastal"), the Sahel region ("Sahel") and the Saharan region ("Sahara") in Fig. 7. The coastal region spans from 6–14 °N and from 5 °E–10 °W. The Sahel region spans from 14–21 °N and from 5 °E–10 °W and the Sahara region from 21–28 °N and from 5 °E–10 °W.

reason for the different meridional distributions of precipitation for their simulations under present-day conditions. In contrast to Marsham et al. (2013) and to GCMs used in PMIP, the convective parameterization used in the operational setup of ICON-NWP simulates the peak of diurnal convection in the late afternoon instead of noon in agreement with observations, due to modifications introduced by Bechtold et al. (2014). Thus, the timing of the precipitation diurnal cycle in simulations with explicit and parameterized convection is similar in our case (Fig. A.3 a). To test the importance of the timing of the diurnal cycle of precipitation for the representation of the monsoon propagation during the mid-Holocene, we perform a second set of nested simulations where we removed the modifications by Bechtold et al. (2014). In this simulation with the modified diurnal cycle, the convection peaks around noon, as expected (Fig. A.3 b). Even though the diurnal cycle of the 5 km-E simulation is not directly modified in this second set of nested simulations, comparing this simulation to our control simulation reveals small differences because the two 5 km-E simulations are driven by the 40 km-P simulations with different diurnal cycles, respectively. In the following, simulations with the modified diurnal cycle are labeled with "mod" (Sect. 3.6).

We perform a third suite of nested simulations to separate the impact of resolution on the WAM from the impact of the representation of convection. In these simulations, the 20 and 10 km simulations are run with explicitly resolved convection. These simulations are referred to as the 20 and 10 km-E simulations. We compare these with the 20 and 10 km-P simulations.

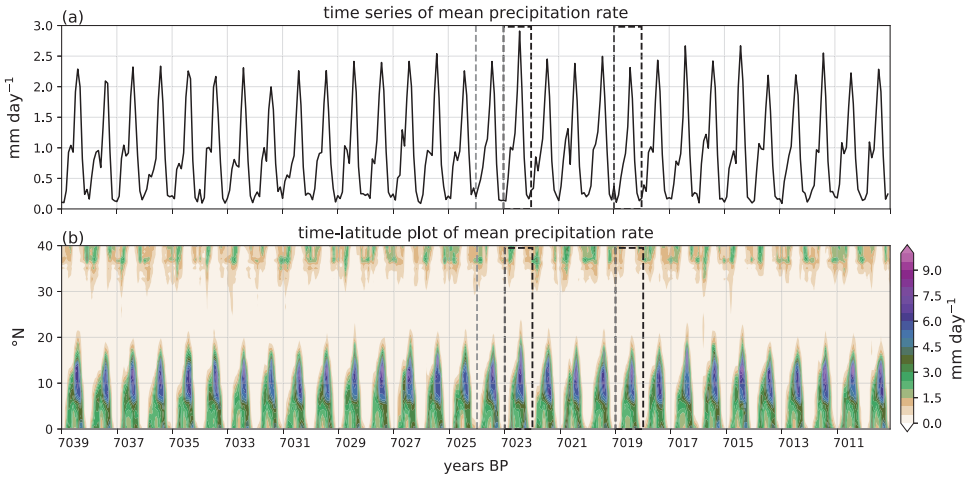

Figure A.2: The 30-year time series of the mean precipitation rate (a) and the latitude–time plot of the mean precipitation rate over land (b) indicating the northward extension of the WAM every year for the whole 5 km domain spanning the area from 0–40° N and from 37° E–53° W. The dashed light-gray line indicates the end of the spinup phase when soil moisture is on a constant level. The dashed rectangles show the years we chose for our analysis: 7023 BP (strong) and 7019 BP (weak).

A.3 Results and Discussion

A.3.1 *Precipitation distribution*

During the mid-Holocene, the northward propagation of precipitation constitutes the main difference to today's precipitation pattern. As described in the introduction, reconstructions point towards less precipitation over equatorial Africa and the Sahel region but substantially more precipitation over the Sahara. Therefore, we are mainly interested in the meridional precipitation gradient which modulates the landscape and vegetation cover of the north African continent.

In the JJASO simulations with ICON-NWP, we identify July to September (JAS) as the strongest monsoon months. Therefore, we mainly focus our analysis on these 3 months. Furthermore, as the simulations for the two years (7023 BP and 7019 BP) reveal similar results, we only show the results for 7023 BP.

Figure A.4 a clearly shows that the 40 km-P simulation produces more precipitation and precipitation that reaches further north than the 5 km-E simulation. On average and from 12 to 17 °N, it rains 0.8 mm day^{-}1 more in the 40 km-P simulation than in the 5 km-E simulation at each latitude. Over 5 months, this sums up to over 120 mm per latitude which could already impact the vegetation cover. A secondary precipitation peak is also visible around 15° N in the 40 km-P simulation, a peak that is absent in the 5 km-E simulation. The fact that the parameterized simulation produces more precipitation is not only true for the 40 km-P simulation but also for all grid spacings where parameterized convection is used.

Figure A.4 a also shows that the mean meridional distribution of monsoonal precipitation is predominantly determined by the representation of convection rather than the resolution. This becomes visible by comparing the 10 km-P and

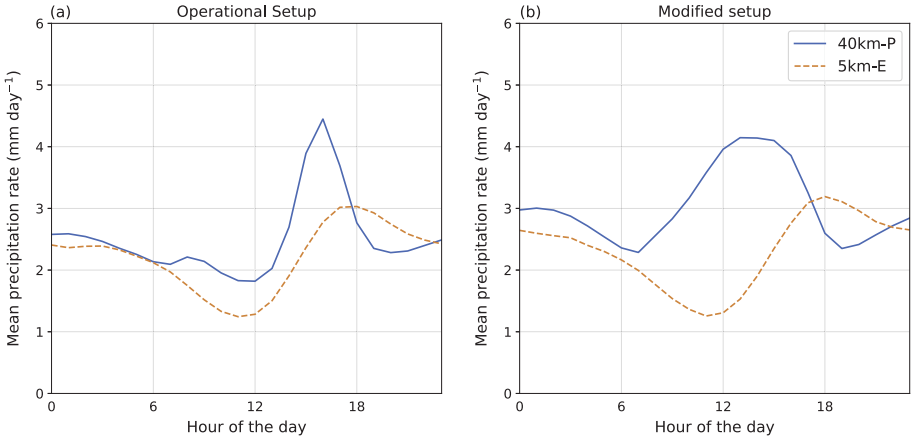

Figure A.3: Mean diurnal cycle of precipitation for the 40 km-P (solid blue) and the 5 km-E (dashed orange) simulation for July to September (JAS). (a) The diurnal cycle for the operational ICON-NWP model; (b) the diurnal cycle of the modified ICON-NWP setup used in Sec. A.3.6. The diurnal cycle is calculated over the dashed "WA domain" outlined in Fig. A.1.

the 10 km-E simulations. The 10 km-P simulation is more similar to the 40 km-P simulation than to the 10 km-E simulation. Conversely, the 10 km-E simulation is more similar to the 5 km-E simulation than to 10 km-P. This is also valid for the 20 km-P and 20 km-E simulations (not shown). Given these similarities and the fact that grid spacings finer than 5 km are typically employed when conducting convection-permitting simulations, we focus our analysis on the 40 km-P and 5 km-E simulations. The analysis was repeated for the 10 km-P and 10 km-E simulations and can be found in Appendix A.5.

In the following, we begin by analyzing the large-scale mean state of the atmosphere by examining the pressure field and the large-scale dynamics of the WAM circulation to understand the precipitation differences (Sec. A.3.2). We then investigate whether and how the thermodynamic structure of the atmosphere supports the development of convection and precipitation in the 40 km-P and 5 km-E simulations (Sec. A.3.3). As this analysis points to strong differences in the moisture field between the 40 km-P and the 5 km-E simulations, we examine in the following two sections differences in moisture transport (Sec. A.3.4) and differences in evapotranspiration (Sec. A.3.5), the two moisture sources for precipitation. Finally, we test whether the diurnal cycle of convection impacts the propagation of the WAM over north Africa as suggested by Marsham et al. (2013) (Sect. A.3.6).

A.3.2 *Large - Scale Circulation*

To understand the unexpectedly stronger precipitation in the 40 km-P simulation compared to the 5 km-E simulation, we start with the analysis of the large-scale circulation characteristics. The WAM winds are predominantly driven by the near-surface pressure gradient between the heat low over the warm African continent and the high pressure system over the colder Gulf of Guinea (Thorncroft et al., 2011; Nicholson, 2013).

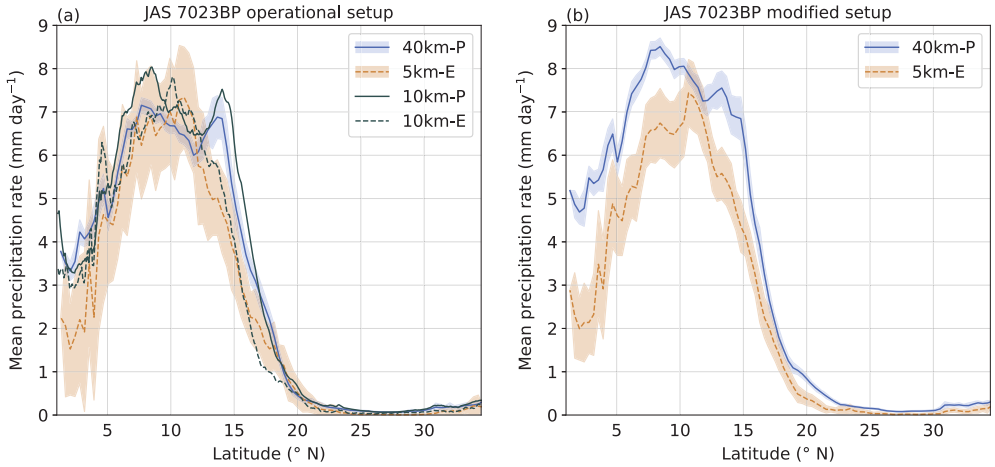

Figure A.4: Meridional distribution of monsoonal precipitation for (a) the operational simulations and (b) the setup with modified diurnal cycle (analyzed in Sec. A.3.6) for the 40 km-P (solid blue), the 5 km-E (dashed orange), the 10 km-P (solid black) and the 10 km-E (dashed black) simulations. The shading displays the daily longitudinal mean standard deviation from the longitudinal mean JAS cycle for the 40 km-P and the 5 km-E simulation. The longitudinal mean is taken over the land points of the WA domain outlined in Fig. A.1.

The pressure gradient between the Saharan heat low (SHL) and the high pressure system over the Gulf of Guinea is stronger in the 5 km-E simulation. This can be seen in Figure A.5, which shows the mean 925 hPa geopotential height and the mean wind field at 925 hPa for the 40 km-P and 5 km-E simulations, respectively. The stronger high pressure system over the tropical Atlantic in the 5 km-E simulation compared to the 40 km-P simulation leads to a stronger pressure gradient in the Gulf of Guinea and to stronger winds in the Gulf of Guinea (Fig. A.5 c). These winds in the Gulf of Guinea modulate the moisture transport into central Africa and support a stronger monsoon in the 5 km-E simulation, which cannot directly explain our previous findings of a weaker monsoon propagation in the 5 km-E simulation.

In contrast, the pressure gradient between the subtropical east Atlantic and the SHL are stronger in the 40 km-P simulation. In the latter simulation, the SHL and the high pressure system in the subtropical east Atlantic are stronger compared to the 5 km-E simulation. In addition to the stronger pressure systems, the SHL extends further west in the 40 km-P than in 5 km-E simulation, leading to an even stronger pressure gradient along the coast of Morocco and in the subtropical east Atlantic. The stronger pressure gradient accelerates the wind along the coast of Morocco and Western Sahara in the 40 km-P simulation (Fig. A.5 c) and results in a stronger wind convergence in the tropical Atlantic along 10° N. This wind convergence is important for the moisture transport into the Western Sahara. The stronger winds along 10° N indicate a stronger moisture transport into this region in the 40 km-P than in the 5 km-E simulation.

The northward propagation of precipitation during the West African Monsoon depends not only on the strength of the southwesterly low-level monsoon flow but also on the strength of the Harmattan and the vertical lifting of air masses throughout the troposphere. The northerlies associated with the hot and dry Harmattan

winds are stronger in the 5 km-E than in the 40 km-P simulation and counteract more strongly against the southerly monsoon flow. This surface convergence zone between the southerly monsoon flow and the northerly Harmattan is known as the Intertropical Front (ITF). In the 5 km-E simulation, the ITF is located further south at around 17 to 18 °N, while in the 40 km-P simulation it is located at around 20° N (Fig. A.6). The more northerly location of the ITF, as well as the generally weaker northward component against and above the surface monsoon winds, support the development of convection and therefore the higher precipitation rates further north in the 40 km-P than in the 5 km-E simulation (Fig. A.4 a).

In the JAS mean, the vertical wind is stronger in the 40 km-P simulation compared to the 5 km-E simulation (Fig. A.6). Additionally, the ascent region is broader in the 40 km-P simulation compared to the 5 km-E simulation. This, on average, stronger and broader ascent region is consistent with stronger precipitation in the 40 km-P simulation as opposed to the 5 km-E simulation.

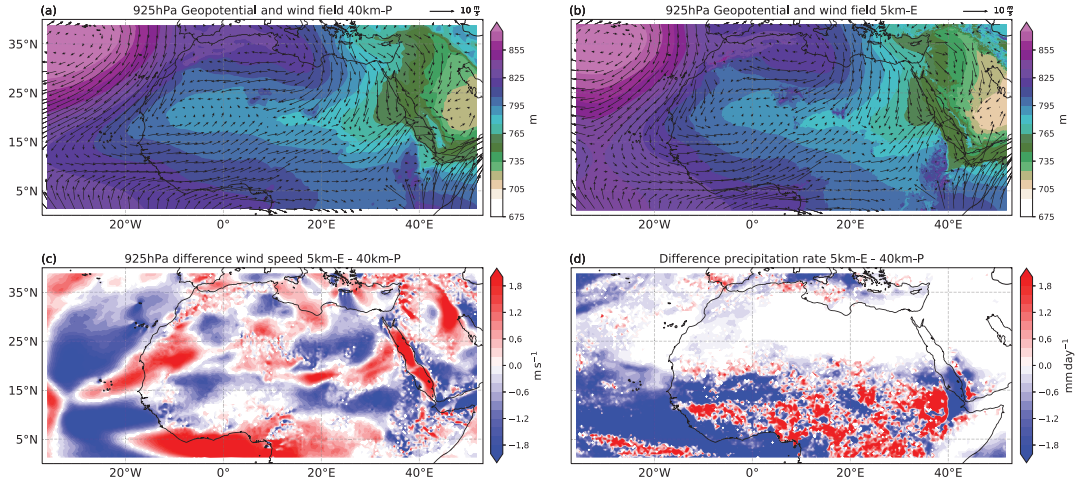

Figure A.5: JAS mean geopotential height (shading) and mean wind field (vectors; m s^{-}1) at 925 hPa for the 40 km-P (a) and the 5 km-E simulations (b), the difference in JAS mean wind speed at 925 hPa (c) and the difference in JAS mean precipitation rate (d) between the 5 km-E and 40 km-P simulations, respectively. White colors in panels (c, d) display difference values between 0.1 and 0.1.

The strongest vertical velocities are located between 5 and 15° N in the 40 km-P simulation and between 8 and 15° N in the 5 km-E simulation. They are associated with the lifting between the tropical easterly jet at around 5° N and at 200 hPa height and the African easterly jet (AEJ) at around 16° N and at 600 hPa height. A second weaker updraft region is located between 17 and 20° N and is associated with the lifting of air masses at the ITF. We want to comment on the fact that we find a slightly weaker AEJ in the 5 km-E simulation compared to the 40 km-P simulation. For example, Cook (1999) and Nicholson and Grist (2001) associated a weaker AEJ with wetter conditions over Africa in present-day conditions, which is contradictory to our results. Grist and Nicholson (2001) and Nicholson and Grist (2001) suggest that the location of the AEJ is more important than its intensity. They link a more northern location of the AEJ core with higher rainfall and rainfall further north. Fig. A.6 shows that the AEJ core in our simulations is located slightly further north in the 40 km-P than in the 5 km-E simulation. This is consistent with the higher

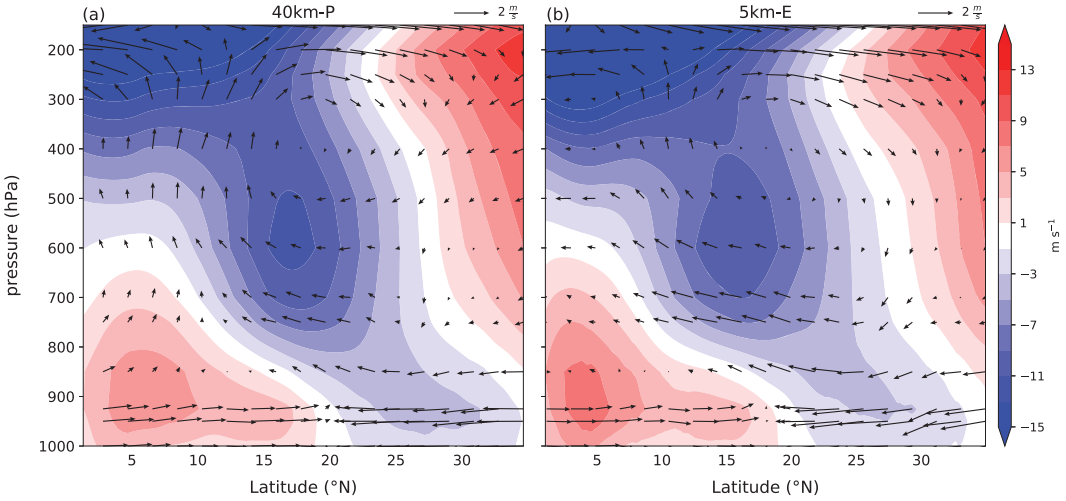

Figure A.6: JAS mean cross section of the zonally averaged wind field for the 40 km-P (a) and for the 5 km-E simulation (b). The shading shows the zonal wind in $m\,s^1$. The vectors show the meridional and vertical wind field ($m\,s^1$), where the vertical wind component is multiplied with 100 to make the vectors better visible. The mean is taken over all points of the dashed "WA domain" outlined in Fig. A.1.

precipitation rates and the slightly stronger northward extension of monsoonal rainfall in the 40 km-P compared to the 5 km-E simulation and with the findings from Grist and Nicholson (2001) and Nicholson and Grist (2001).

In conclusion, the stronger horizontal monsoon circulation (southwesterlies), the more northward location of the ITF, as well as the stronger and broader ascent region in the 40 km-P simulation as compared to the 5 km-E simulation, are all consistent with a stronger monsoon and a more northward propagation, in agreement with Fig. A.4. Only the pressure gradient between the Gulf of Guinea and the SHL is stronger in the 5 km-E simulation. As will be shown later, the stronger pressure gradient between the Gulf of Guinea and the SHL does transport more moisture onto the African continent in the 5 km-E simulation, an effect nevertheless overcompensated by an excessively strong local drying of the African continent due to high amounts of runoff (see Sec. A.3.4 and Sec. A.3.5).

A.3.3 *Thermodynamics*

The large-scale monsoon circulation supports the higher precipitation rates in the 40 km-P simulation than in the 5 km-E simulation. However, if and how the prevailing atmospheric conditions lead to the development of convection and precipitation are essentially determined by the thermodynamic structure of the atmosphere. To investigate this, we examine the thermodynamical profiles for both representations of convection. We look at thermodynamical profiles for three different regions of north Africa as outlined in Fig. A.1: the "coastal" region, the "Sahel" region and the "Sahara" region. Fig. A.7 shows the corresponding thermodynamical profiles for 8 September 7023 BP at 12:00 UTC. We choose 8 September as being representative of the prevalent state of the atmosphere for both representations of convection during JAS, as confirmed with Table A.2.

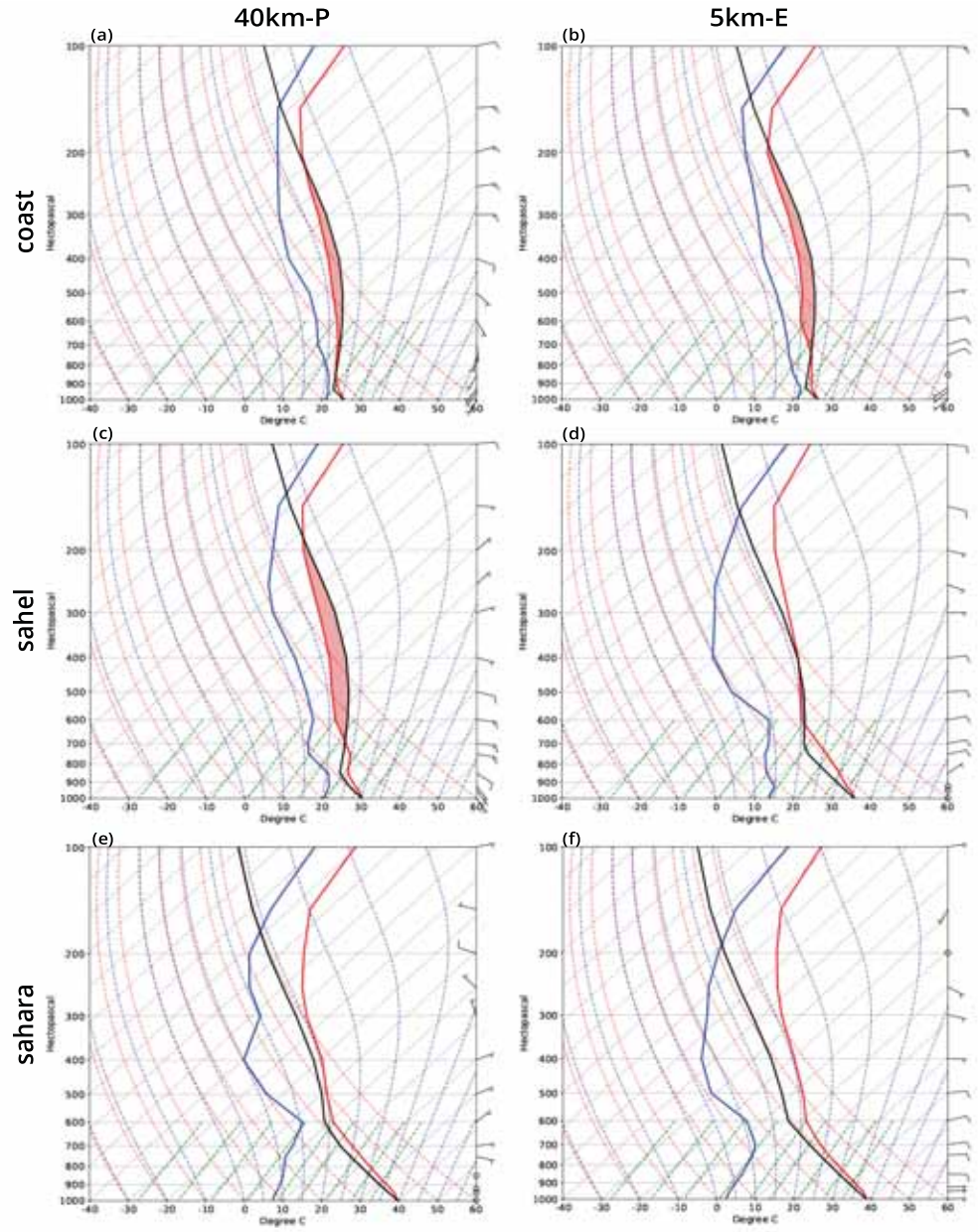

Figure A.7: Skew-T diagrams for 8 September 7023 BP 12:00 UTC for the 40 km-P (a, c, e) and the 5 km-E (b, d, f) simulations. The red line depicts the temperature profile, the blue line the dew point and the black line the path an air parcel would take through the atmosphere. The profiles are averaged over the three domains outlined in Fig. A.1 labeled with "coast", "Sahel" and "Sahara". The red-shaded area displays the CAPE. The lines in the background refer to the dry adiabats (dashed red), moist adiabats (dashed blue), isotherms (solid gray tilted) and isobars (solid gray horizontal).

		40 km-P	5 km-E
coastal	CAPE ($J\,kg^{-1}$)	877.9	869.6
	CIN ($J\,kg^{-1}$)	-27.1	-43.6
	T - T_d (°C)	5.1	6.1
sahel	CAPE ($J\,kg^{-1}$)	868.8	431.3
	CIN ($J\,kg^{-1}$)	-172.0	-221.5
	T - T_d (°C)	13.4	17.3
sahara	CAPE ($J\,kg^{-1}$)	46.8	11.9
	CIN ($J\,kg^{-1}$)	-120.8	-65.8
	T - T_d (°C)	30.6	32.8

Table A.1: JAS-mean values of CAPE, CIN and dew point depression for the coastal, Sahel and Sahara region (Fig. A.1).

The thermodynamic profiles over the coastal region show a higher level of convective inhibition (CIN) in the 5 km-E simulation compared to the 40 km-P simulation. As both the 40 km-P and the 5 km-E simulation have similar mean surface temperatures around 26 °C and mean dew-point temperatures of around 21 °C, the higher CIN in the 5 km-E simulation is a result of a more stably stratified atmosphere between 900 and 700 hPa. Combined with the weaker prevailing vertical velocity in the 5 km-E simulation (see Sec. A.3.2), we conclude that convection can be less easily triggered in the 5 km-E simulation.

The atmospheric conditions get even less supportive of convection in the 5 km-E simulation, when approaching the Sahara region. Over the Sahel, the 5 km-E simulation becomes even drier, consistent with a much higher surface temperature and low dew point. The combination of a warm temperature profile and a low dew-point temperature raises the lifting condensation level (LCL) and the level of free convection (LFC). Therefore, even if convection is triggered in the 5 km-E simulation, clouds will not deepen past 400 hPa height. From this, we would expect only little precipitation. The 40 km-P simulation stays moister in the Sahel region compared to the 5 km-E simulation. Moreover, the LCL in the 40 km-P simulation is lower and the convection, if triggered, can become very deep. The resulting precipitation is likely to be stronger than in the 5 km-E simulation.

Over the Sahara, both the 40 km-P and the 5 km-E simulations become even drier and surface temperatures rise. The lack of moisture and the stably stratified atmosphere in both simulations reveal that it becomes very unlikely that convection is triggered and precipitation develops in this region.

Table A.1 lists the mean values of CAPE, CIN and the dew-point depression for the three regions to emphasize that the results are valid over the whole JAS season. These findings emphasize that the moisture availability and the thermodynamical state of the atmosphere are much more supportive of the development of convection in the 40 km-P simulation than in the 5 km-E simulation. Together with the stronger vertical motion in the 40 km-P simulation (see Sec. A.3.2), this is consistent with the

higher precipitation rates in the 40 km-P simulation. Furthermore, this suggests that, besides the large-scale circulation and the stability of the atmosphere, the availability of moisture in the two simulations also contributes to the differences in precipitation. We turn our attention to the availability of moisture in the 40 km-P and the 5 km-E simulations in the next two sections.

A.3.4 *Moisture Field and Moisture Transport*

The thermodynamical profiles revealed more humid conditions in the 40 km-P simulation compared to the 5 km-E simulation, especially in the semi-arid transition zone of the Sahel region. Now, we investigate the moisture field in more detail. The moisture field supports the findings from the previous section that the 40 km-P simulation is overall moister over the continent than the 5 km-E simulation (Fig. A.8). The vertical cross section of specific humidity in Fig. A.8a and b shows higher amounts of water vapor in the planetary boundary layer in the 40 km-P simulation compared to the 5 km-E simulation, especially between 15 and 25° N. This region coincides with the region where we found higher precipitation rates in the 40 km-P than in the 5 km-E simulation. Above 900 hPa, the specific humidity exhibits similar

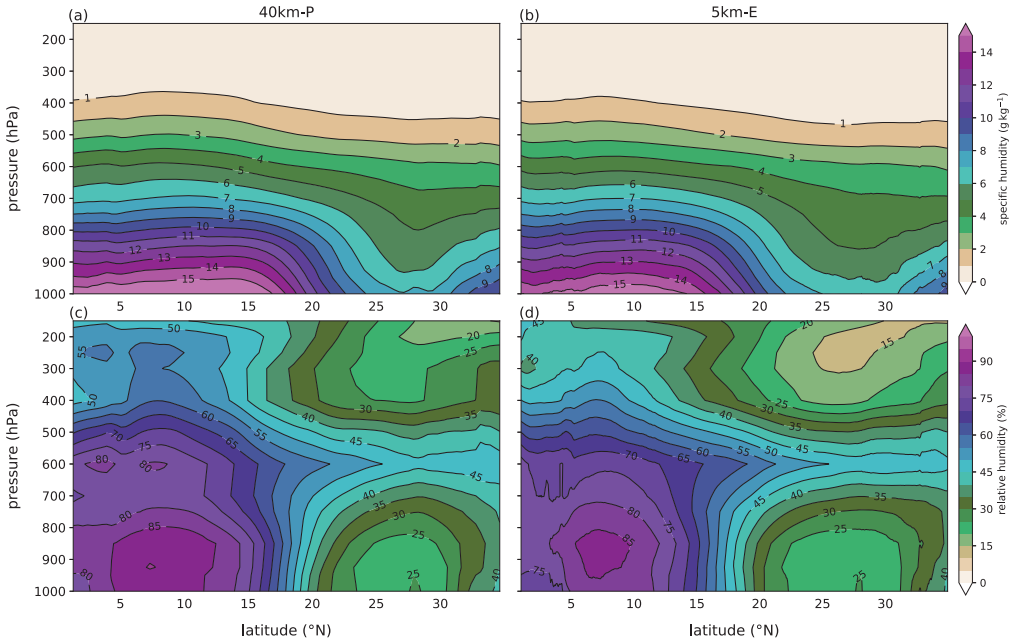

Figure A.8: JAS mean vertical cross section of specific humidity in g kg^1 in the two upper panels (a, b) and for relative humidity in % in the two bottom panels (c, d) for the 40 km-P (a, c) and the 5 km-E (b, d) simulations, respectively. The mean is taken over land of the "WA domain" (dashed domain) outlined in Fig. A.1.

The vertical cross section of relative humidity displays a deep core of moist air at around 8° N in both simulations, extending from the surface into the upper troposphere. This region coincides with the region of the strongest vertical velocities (Fig. A.6). Throughout the troposphere, the moisture in the deep core exceeds 50 %, whereas over the Sahara, the relative humidity is much lower. Comparing the two simulations, the 40 km-P simulation shows higher values of relative humidity

throughout the depth of the troposphere. This would tend to favor precipitation in the 40 km-P simulation.

There are two possible mechanisms for supplying moisture for precipitation over the continent: (1) advection of moisture from surrounding regions and (2) local evapo(transpi)ration (see Sect. A.3.5). This provides two possible explanations for the on-average wetter atmosphere in the 40 km-P simulation. The north African continent receives more moisture through the moisture transport from the ocean and/or moisture recycling over land is more effective in the 40 km-P than in the 5 km-E simulation.

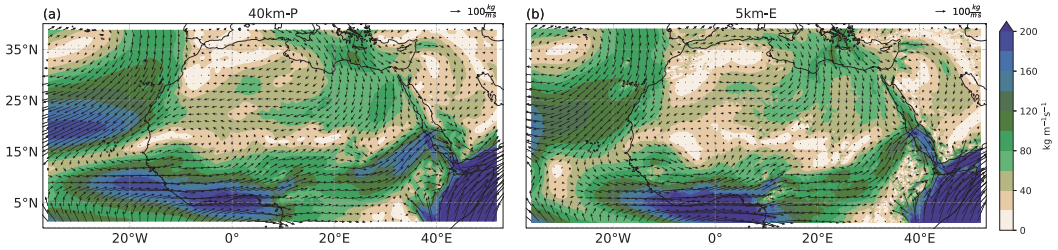

Figure A.9: JAS 1000 to 850 hPa vertically integrated moisture flux magnitude (shading) and mean vertically integrated moisture flux (vectors; kg m^{-1} s^{-1}) for the 40 km-P (a) and the 5 km-E (b) simulations.

First, we look at the moisture transport. Figure A.9 shows the JAS vertically integrated moisture flux magnitude and moisture flux for the 40 km-P and the 5 km-E simulations. We integrate the lower atmosphere levels from 1000 to 850 hPa. The stronger winds in the tropical Atlantic in the 40 km-P simulation (see Fig. A.5 c and section A.3.2), which are associated with the African westerly jet, result in a stronger moisture transport from this region into the west Sahel–Saharan region compared to the 5 km-E simulation. Furthermore, the moisture transport originating from the Mediterranean Sea towards the Sahara is stronger in the 40 km-P simulation compared to the 5 km-E simulation. However, and more importantly, the moisture transport from the Gulf of Guinea, which supplies moisture dominantly into central north Africa, is stronger in the 5 km-E simulation compared to the 40 km-P simulation due to the stronger winds in this region (compare to Fig. A.5 c and Sect. A.3.2). The result that the tropical Atlantic along 10° N and the Gulf of Guinea supply moisture for the west Sahel–Saharan region and central-north Africa, respectively, is consistent with the results from Druyan and Koster (1989) and Lélé et al. (2015) for present-day conditions. Over the WA domain, the domain-mean moisture flux is 84.2 and 81.8 kg m^{-1} s^{-1} for the 40 km-P and the 5 km-E simulations, respectively. Hence, in a mean sense, there is a slightly larger domain-mean moisture flux over the WA domain in the 40 km-P simulation compared to the 5 km-E simulation.

A.3.5 *Land-atmoshpere coupling*

Besides the moisture transport from the ocean and humid coastal regions into north Africa, the local source of moisture due to evapotranspiration needs to be considered as well. The evapotranspiration (Fig. A.10 a) coincides with the precipitation rates (Fig. A.4 a) in the 40 km-P and the 5 km-E simulations. In other words, between the Equator and 8° N, the evapotranspiration is higher in the 40 km-P simulation than in the 5 km-E simulation. Between 8 and 12° N, evapotranspiration is equally strong

in both simulations, and north of 12° N it becomes larger in the 40 km-P simulation again. The regions of higher evapotranspiration in the 40 km-P simulation reflect the higher precipitation rates in the 40 km-P simulation compared to the 5 km-E simulation.

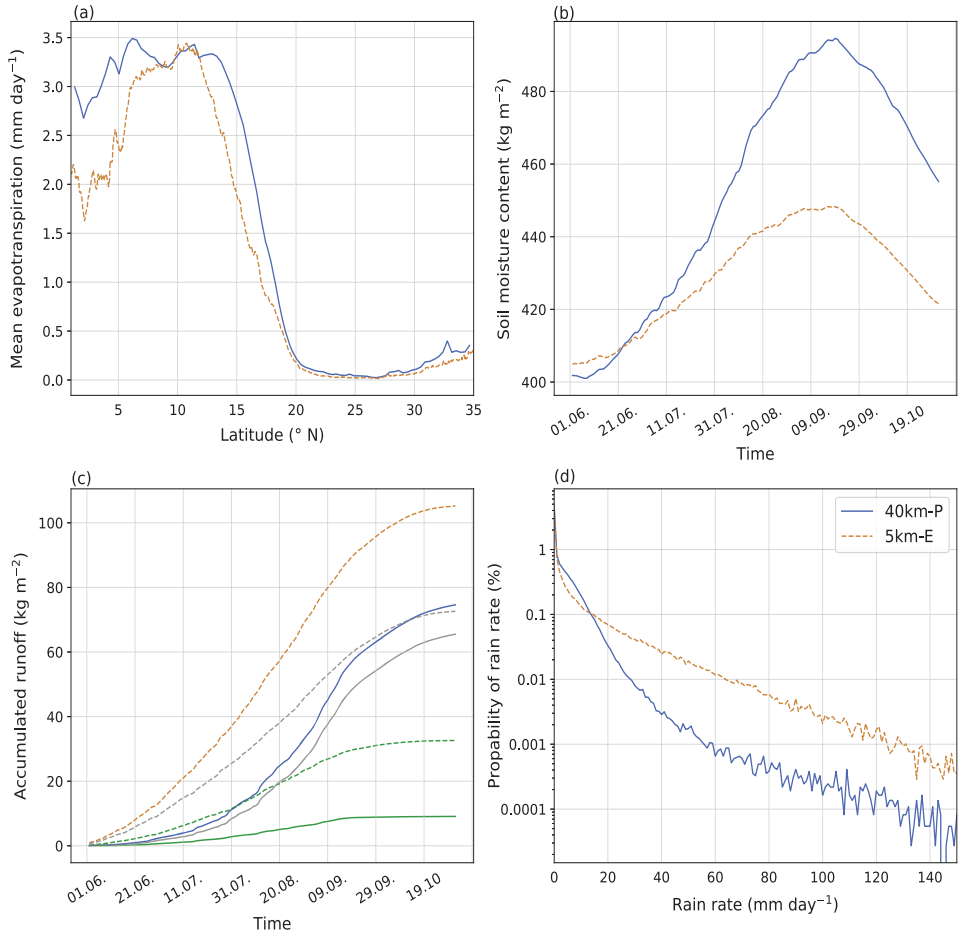

Figure A.10: (a) JAS mean meridional distribution of evaporation (b) time series of soil water content: sum over the first six layers (1.62 m), (c) JJASO time series of accumulated runoff, surface runoff (green lines) and groundwater runoff (gray lines), (d) probability density function (PDF) of JAS mean rain rate for the 40 km-P (solid blue) and the 5 km-E (dashed orange) simulation excluding days with rain rates equal to 0 mm day^{-}1. All calculations are performed over land of the dashed "WA domain" outlined in Fig. A.1.

The evaporation is strongly coupled to soil moisture, especially in regions with sparse or no vegetation. The soil moisture up to 1.62 m depth is much lower in the 5 km-E simulation compared to the 40 km-P simulation especially during our analysis period from July to September (Fig. A.10 b). The lower soil moisture in the 5 km-E simulation is due to higher amounts of total runoff (Fig. A.10 c) compared to the 40 km-P simulation. The higher runoff is due to both higher surface and higher groundwater runoff, where groundwater runoff refers to the subsurface runoff in all soil layers. The ratio between surface and groundwater runoff is higher in the 5 km-E compared to the 40 km-P simulation, as it is expected from the precipitation characteristics (see next paragraph). The high amount of runoff

in the 5 km-E simulation prevents the remoistening of the soil by precipitation, maintaining low levels of soil moisture and leading to an overly dry and warm atmosphere for convection to develop efficiently. Based on results from Savenije (1996), the runoff plays a key role for the recycling of water over semi-arid regions (i.e., the Sahel–Saharan region).

The differences in the amount of runoff in the 40 km-P and the 5 km-E simulation are driven by substantial differences in the characteristics of the precipitation distribution. Figure 10d displays the probability that a simulation produces dominantly light (low rain rates) or stronger precipitation events (high rain rates). The figure reveals that in the parameterized simulations it is much more likely to produce light rainfall ($<15\,\mathrm{mm\,day^{1}}$), while the simulation with explicitly resolved convection exhibits much more intense precipitation events ($>15\,\mathrm{mm\,day^{-1}}$). The light rainfall in the 40 km-P simulation is widespread over the whole domain, while the precipitation in the 5 km-E simulation occurs more locally (not shown). High amounts of precipitation in a short time interval and over a small area in the 5 km-E simulation lead to the high amounts of runoff, as the water uptake by the soil is limited. On the contrary, in the 40 km-P simulation, the constantly light and large-scale precipitation sufficiently moistens the soil throughout the simulation period.

A.3.6 *Diurnal cycle*

Marsham et al. (2013) identified the difference in the timing of the precipitation diurnal cycle between parameterized and explicit convection as the main driver for the differences in the meridional distribution of precipitation in their present-day simulations. We test whether this effect has an impact in our simulations. We find that the precipitation in the 40 km-P modified ("MOD") setup is neither weaker nor shifted further southward compared to the 5 km-E and the 40 km-P simulation (Fig. A.4 b). Moreover, the 40 km-P_{MOD} simulation exhibits even more precipitation, especially between the Equator and 15° N compared to the other simulations. We conclude that a later precipitation peak does not favor a more northward propagation of precipitation in our model framework, as was the case in Marsham et al. (2013).

The differences between our results and the results of Marsham et al. (2013) can be due to various aspects related to the model and simulation setup. Firstly, the model Marsham et al. (2013) used utilizes a different convective parameterization than ICON-NWP. ICON-NWP uses the same convection scheme as the IFS, a convection scheme that has been continuously developed and tuned to best match today's precipitation distribution.

Secondly, the analyzed period in our study is 3 months, while Marsham et al. (2013) focused on a 10 day period. They chose their simulation period during the peak of the monsoon season from the end of July until the beginning of August. We also find 15 day periods in our simulations where the 5 km-E simulation propagates further north than the 40 km-P simulation. This suggests that the northward extent of monsoonal precipitation is very variable on short timescales.

Thirdly, we simulate a much larger domain, covering the whole north African continent and parts of the Atlantic Ocean, while Marsham et al. (2013) focused on a smaller land-only domain from 10° E to 10° W and 5 to 25° N. The latter two facts imply that different characteristics and amounts of precipitation from different

regions in Africa, as well as the large-scale circulation and effects from the Atlantic ocean influence our analysis. These effects are not captured in the study of Marsham et al. (2013). Berthou et al. (2019) performed a 10-year study comparing simulations with explicit and parameterized convection performed with the Met Office Unified Model. This is the same model which was used in Marsham et al. (2013). In the 10-year mean, the simulations with explicitly resolved convection did not show a substantially stronger northward extent of precipitation than the parameterized ones, a result closer to our findings.

A.4 SUMMARY AND CONCLUSION

In this study, we investigated whether the representation of convection (parameterized versus explicit) impacts the meridional distribution of monsoonal rainfall under mid-Holocene atmospheric conditions (i.e., orbital parameters, tracer gases) over north Africa. For that purpose, we ran regional nested simulations with the atmospheric model, ICON-NWP. To analyze the meridional distribution of precipitation in both settings, we compared 40 km parameterized (40 km-P) with 5 km explicitly resolved convection (5 km-E) simulations. Furthermore, we isolated the impact of different resolutions from those of different representations of convection by comparing 10 km parameterized (10 km-P) and explicitly resolved convection (10 km-E) simulations. In agreement with the results of previous studies conducted for present-day conditions (Marsham et al. (2013) , Dirmeyer et al. (2012), Pearson et al. (2014)), the precipitation distributions across simulations with the same representation of convection are more similar than those simulations with the same grid spacing.

Marsham et al. (2013) found a stronger northward propagation of precipitation in explicit convection simulations compared to the parameterized simulation for present-day conditions. This motivated our study and raised the following question: does the representation of convection also impact the northward extent of the WAM during the mid-Holocene? In the JAS mean, our 40 km-P simulation produces around 0.8 mm day^{-}1 per latitude more precipitation north of 12° N than the 5 km-E simulation. As such, the representation of convection does impact the northward extent of the WAM but in an opposite way than initially thought, with a stronger propagation in the parameterized simulation. Compared to the results of Marsham et al. (2013), this is mainly because the parametrization of convection in ICON-NWP produces already a more realistic meridional distribution of precipitation than the Met Office Unified Model.

The differences in the meridional precipitation distribution between explicitly resolved convection and parameterized convection in our simulations is caused by thee factors:

- We identified a generally stronger monsoonal circulation over the north African continent in the 40 km-P than in the 5 km-E simulation. The near-surface southwesterly monsoon flow over land is stronger in the 40 km-P than in the 5 km-E simulation. Furthermore, in the 5 km-E simulation, the northerlies from the hot and dry Harmattan counteract more strongly the monsoonal winds. These northerlies push the ITF southward. We also found that the (positive) vertical component of the wind field is, in the JAS mean, stronger over all of the analyzed domain in the 40 km-P than in the 5 km-E simulation.

– The thermodynamic structure of the atmosphere in the 40 km-P simulation is more supportive of the development of clouds and precipitation. The convective inhibition is lower in the 40 km-P simulation compared to the 5 km-E simulation due to the atmosphere being less stable.

– The 40 km-P simulation is moister than the 5 km-E simulation. This is especially true for the region between 15 and 25° N, which coincides with the region of higher precipitation in the 40 km-P simulation compared to the 5 km-E simulation. The strength of moisture transport from the ocean to the African continent depends on the ocean region; over the Gulf of Guinea, the moisture transport is stronger in the 5 km-E simulation, but the moisture transport from the tropical east Atlantic is stronger in the 40 km-P simulation. More importantly, we found more evapotranspiration in the 40 km-P than in the 5 km-E simulation. The higher evapotranspiration rate is due to a higher soil moisture content throughout the whole simulation period. This is due to much weaker runoff in the 40 km-P than in the 5 km-E simulation. These differences in runoff result from substantially different precipitation characteristics. In the 40 km-P simulation, light precipitation can be stored by the soil more easily. The moister soils favor evapotranspiration, which then makes it easier to trigger convection and to produce precipitation. In contrast, the 5 km-E simulation exhibits much more intense precipitation events which occur less frequently and more locally, producing strong runoff and preventing the soil moisture from being refilled by precipitation. The drier conditions, especially in the transition zone of the Sahel region, hamper the development of convection and precipitation in the 5 km-E simulation compared to the 40 km-P simulation.

We conclude that using regional climate simulations using resolved, i.e., explicitly resolved, deep convection does not necessarily produce more precipitation in the mid-Holocene Sahara–Sahel region than simulations with parameterized deep convection. However, we have shown that the precipitation characteristics, in particular the absence of permanent light rainfall and more intense convective events in the simulations with resolved deep convection, are closer to what one would expect.

Our study pinpoints to the key role that soil hydrology may take in controlling the amount of rainfall in simulations with explicitly resolved convection. On the one hand, the used land-surface scheme might be limited to store large moisture amounts in the soil. On the other hand, it is not able to create overground lakes and wetlands in mid-Holocene climate simulations. However, these local moisture sources in the mid-Holocene Sahara–Sahel region might involve important local feedback mechanisms in simulations with explicitly resolved convection. To investigate these possible limitations of our simulations, the atmosphere–soil hydrology interaction will be subject to further numerical experiments in which we will also include the effect of a more vegetated "Green Sahara" on the difference between simulations with resolved and parameterized deep convection.

A.5 ANALYSIS OF 10 KM SIMULATIONS

Here, we present the figures that we analyzed in the main paper again for the parameterized and explicitly resolved convection simulation with 10 km horizontal resolution.

In Fig. A.4 (a) and in the corresponding section, we argued that the meridional distribution of precipitation in the WA domain (Fig. A.1) is more similar between the 40 and 10 km-P simulations and between the 5 and 10 km-E simulations, respectively, than between the 10 km-P and 10 km-E simulations. Here, we want to analyze the 10 km simulations a bit more carefully. The 10 km-P simulation produces more precipitation than the 10 km-E simulation. Especially interesting for us is the higher precipitation north of around 13° N. Similar to the 40 km-P simulation, the 10 km-P simulation exhibits a double precipitation peak, which is absent in the 10 km-E simulation. In the following, we show that the mechanisms described in the main paper also hold for the 10 km-P and 10 km-E simulations.

A.5.1 *Large-scale circulation*

Fig. A.11 shows that the SHL is stronger and extends further west in the 10 km-P than in the 10 km-E simulation. In contrast to the 40 km-P and 5 km-E, the pressure gradient between the SHL and the high pressure system over the Gulf of Guinea is stronger in the 10 km-P than in the 10 km-E simulation (Fig. A.11 a and b). This drives stronger winds in the Gulf of Guinea in the 10 km-P simulation.

In contrast, the pressure gradient between the SHL and the high pressure system in the east subtropical Atlantic is slightly stronger in the 10 km-E simulation, accelerating the wind along the west African coast and in the Atlantic between 10° N to around 24° N. However, the African westerly jet (at around 5 to 10° N) is stronger in the 10 km-P compared to the 10 km-E simulation, similar to the results in the 40 km-P and 5 km-E simulations. The differences in the wind speed (Fig. A.11 c) and in precipitation (Fig. A.11 d) are very similar to those in Fig. A.11c and d. Fig. A.12 shows that the low-level monsoon winds are equally strong or only slightly stronger in the 10 km-P compared to the 10 km-E simulation. The dry Harmattan, antagonizing the monsoon flow, is slightly stronger in the 10 km-E, pushing the ITF further south (to around 17° N) in the 10 km-E simulation compared to the 10 km-P simulation (ITF at around 20° N).

Strongly similar to Fig. A.6 is the difference in the strength of the vertical ascent between the 10 km simulations. In the 10 km-P simulation, the vertical upward wind is substantially stronger in the mean than in the 10 km-E simulation, consistent with the results we find in the 40 km-P and the 5 km-E simulations. The stronger upward motion and the further northward-located ITF are supportive of convection and precipitation in the parameterized simulation.

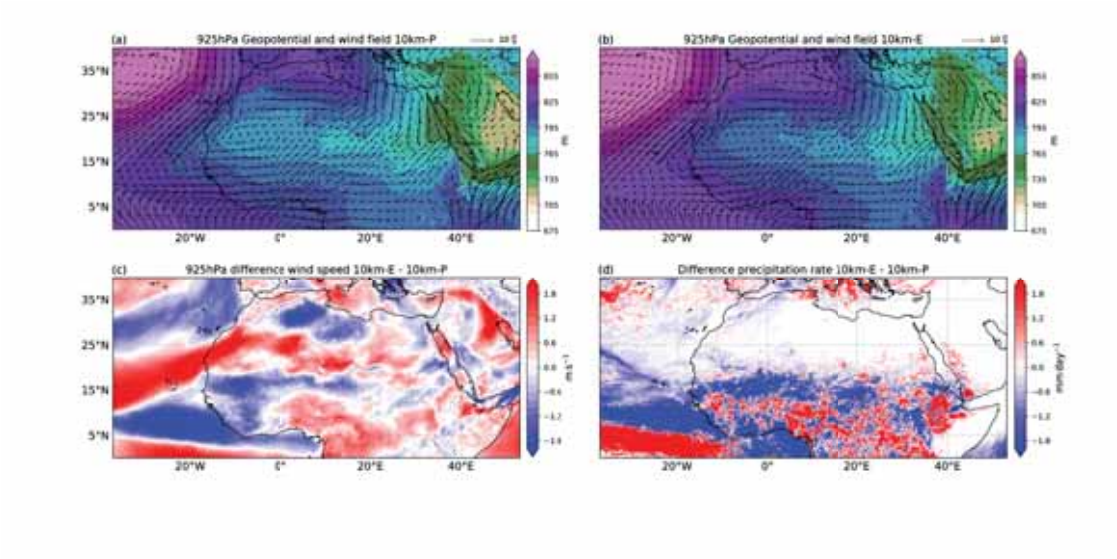

Figure A.11: The same as Fig. A.5 but for the 10km-P and 10 km-E simulation.

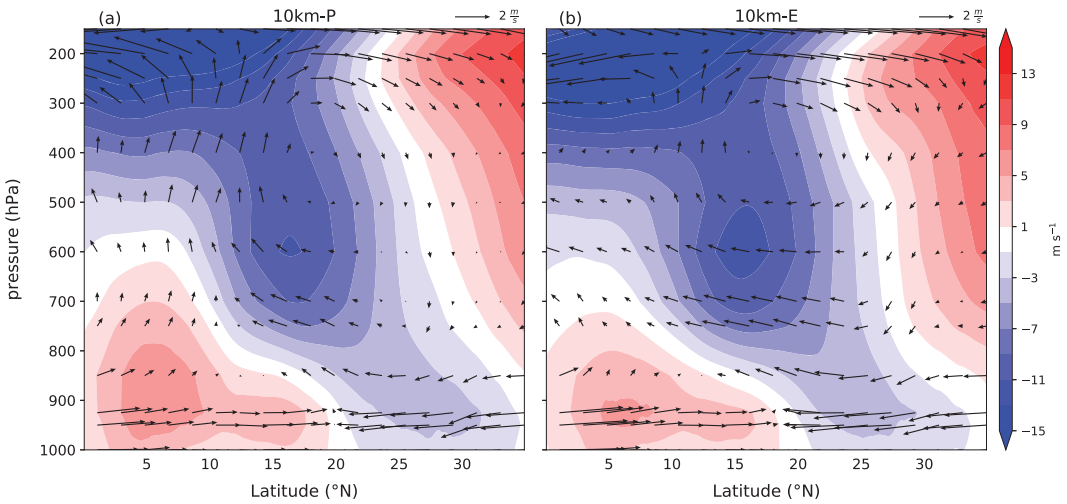

Figure A.12: The same as Fig. A.6 but for the 10km-P and 10 km-E simulation.

A.5.2 *Thermodynamics*

We present the mean CAPE and CIN values in Table A.2, similar to Table A.1 in Sec. A.3.3. We show that the thermodynamic structure of the atmosphere in the 10 km-P and the 10 km-E simulations is similar to that in the 40 km-P and 5 km-E simulations, respectively (Sec. A.3.3). In particular, the differences between explicit and parameterized convection over the Sahel, with a larger dew-point depression and an atmosphere less conductive to convection, are also clearly visible when comparing the 10 km-P to the 10 km-E simulation.

		10 km-P	10 km-E
coastal	CAPE (J kg^{-1})	771.5	942.6
	CIN (J kg^{-1})	-29.7	-35.9
	T - T$_d$ (°C)	5.3	5.8
sahel	CAPE (J kg^{-1})	772.3	381.2
	CIN (J kg^{-1})	-187.6	-227.5
	T - T$_d$ (°C)	13.6	17.6
sahara	CAPE (J kg^{-1})	60.8	5.7
	CIN (J kg^{-1})	-121.9	-31.4
	T - T$_d$ (°C)	29.9	32.9

Table A.2: The same as table A.1 but for the 10 km-P and 10 km-E simulation.

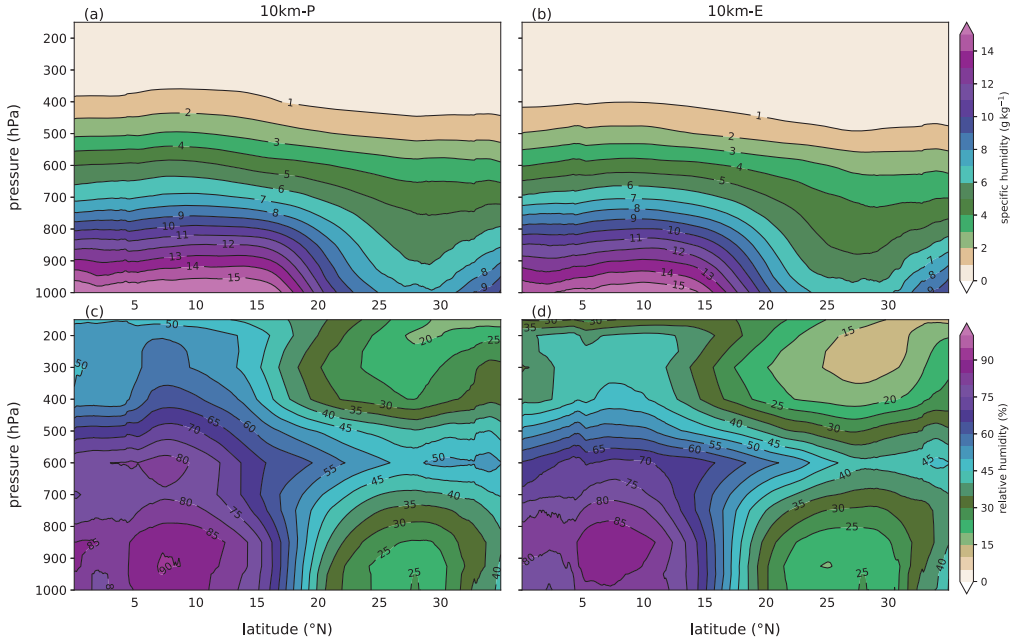

Figure A.13: The same as Fig. A.8 but for the 10km-P and 10 km-E simulation.

A.5.3 *Moisture field and moisture transport*

The more humid conditions revealed by the thermodynamics are confirmed by the vertical moisture cross section (Fig. A.13) of specific ((Fig. A.13a and b) and relative humidity ((Fig. A.13c and d). In the lowest atmosphere levels, the 10 km-P simulation is more humid than the 10 km-E simulation, especially north of 15° N – the transition region where we also find the higher precipitation rates (Fig. A.4).

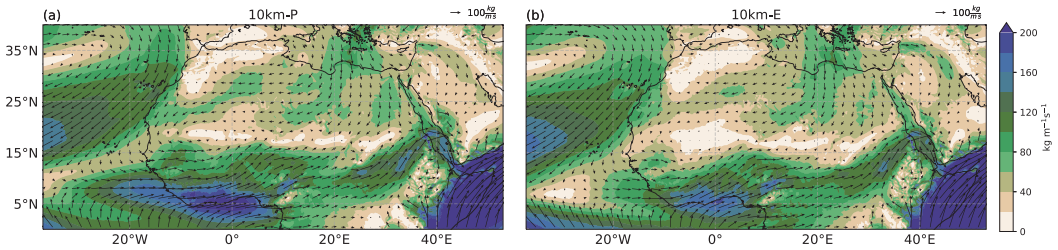

Figure A.14: The same as Fig. A.9 but for the 10km-P and 10 km-E simulation.

The horizontal transport of moisture from the Atlantic and the Gulf of Guinea region towards the African continent is higher in the 10 km-P than in the 10 km-E simulation, consistent with the moisture cross section (Fig. A.13). The moisture import from the Mediterranean Sea is similar in both simulations. The mean moisture transport in the WA domain is 84.5 and 69.6 $\mathrm{kg\,m^{-1}\,s^{-1}}$ in the 10 km-P and 10 km-E simulations, respectively. Therefore, the higher moisture transport supports the generally moister conditions revealed by Fig. A.13.

A.5.4 *Land-Atmosphere Coupling*

The coupling of the atmosphere and the surface is very similar, as described in Sec. A.3.5. Figure Fig. A.15 (a) shows higher evapotranspiration over land at all latitudes in the 10 km-P compared to the 10 km-E simulation. The higher evaporation is consistent with the higher soil moisture values shown in Fig. A.15 (b). The higher evapotranspiration rates in the 10 km-P simulation are consistent with weaker surface and groundwater runoff compared to the 10 km-E simulation. With other words, the soil loses less water into runoff and stays moister. This is forced by differences in the precipitation intensity and its spatial distribution. Figure Fig. A.15 (d) shows that the 10 km-P simulation produces more often (higher probability values) light and widespread precipitation compared to the 10 km-E simulation.

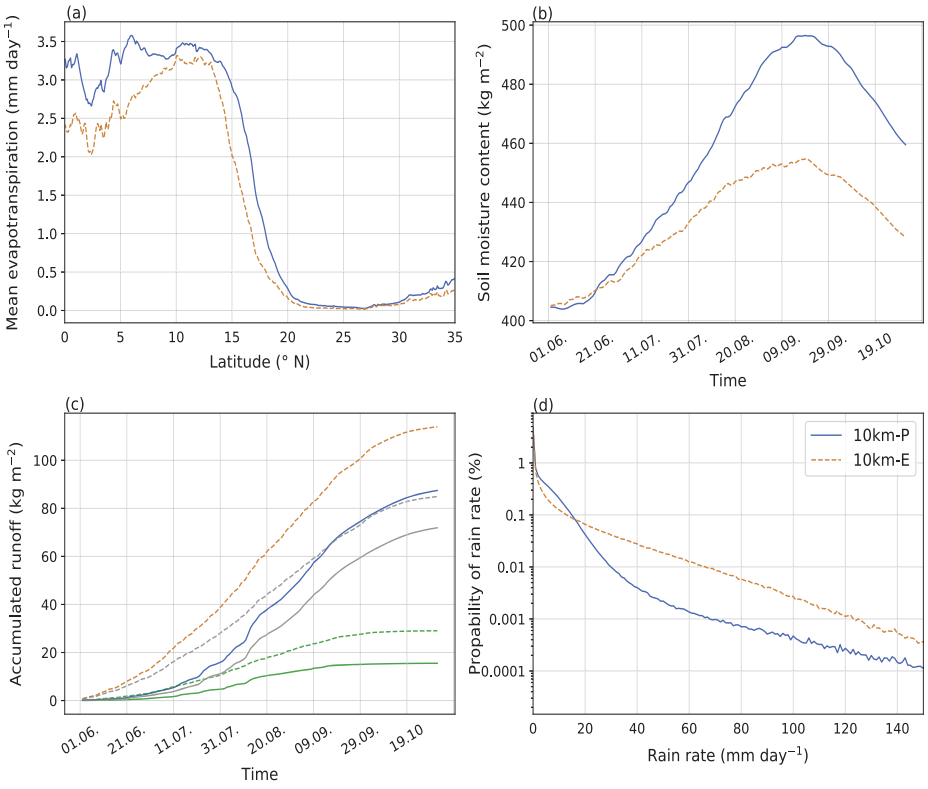

Figure A.15: The same as Fig. A.10 but for the 10km-P and 10 km-E simulation.

B

EFFECT OF A VEGETATED SAHARA ON THE WEST AFRICAN MONSOON RAINBELT IN MID-HOLOCENE STORM-RESOLVING SIMULATIONS

The work in this appendix will be submitted as:

Jungandreas, Leonore, Hohenegger, Cathy, Claussen, Martin (to be submitted). "Effect of a vegetated Sahara on the West African monsoon rainbelt in mid-Holocene storm-resolving simulations."

LJ performed the simulations and analysis. CH and MC gave input, ideas and feedback to the analysis of the simulations. LJ prepared the manuscript with contributions from all co-authors.

I reserve that this work will be subject of further changes before it is submitted.

Effect of a vegetated Sahara on the West African monsoon rainbelt in mid-Holocene storm-resolving simulations

Leonore Jungandreas[1], Cathy Hohenegger[1], Martin Claussen[1,2]

[1] Max Planck Institute for Meteorology, Bundesstraße 53, 20146 Hamburg
[2] Center for Earth System Research and Sustainability, Universität Hamburg, Bundesstraße 53, 20146 Hamburg

Abstract

Several studies indicate that land-atmosphere processes are essential for the, still misrepresented, northward extent of monsoonal precipitation over North Africa during the mid-Holocene. Land-atmosphere feedbacks, however, can be fundamentally different depending on whether convection is explicitly resolved or parameterized in climate models. Therefore, we aim to investigate whether and how land-atmosphere feedbacks influence the monsoonal precipitation in both explicitly resolved and parameterized convection simulations over mid-Holocene North Africa.

Mid-Holocene simulations of North Africa with a higher vegetation cover, compared to mid-Holocene simulations with present-day land surface cover, show a positive land-atmosphere feedback regardless of the representation of convection. Both explicitly resolved and parameterized convection simulations, display a northward extension of monsoonal precipitation by about 4-5° and a decreased precipitation gradient between the Guinea coast and the Sahara, closer to proxy data. The northward extension of monsoonal precipitation is mainly caused by a combination of increased latent heating and the weakening and northward displacement of the African easterly jet.

Besides these similarities, precipitation characteristics such as intensity, spatial distribution, and frequency are different and strongly determined by the representation of convection. These different precipitation characteristics influence the hydrological cycle and the land-atmosphere coupling in our simulations of mid-Holocene North Africa. In explicitly resolved convection simulations, the land-atmosphere coupling is weaker than in parameterized convection simulations. In contrast to previous studies, this is not because the response of precipitation to a change in latent heat flux is weaker, but because the response of soil moisture to a change in precipitation is much smaller. Because of locally confined, intense precipitation events in explicitly resolved convection simulations, runoff is high and soil moisture is not refilled as in parameterized convection simulations. We argue that this limitation of the soil moisture in explicitly resolved convection simulations restrains the potential precipitation response to an increased vegetation cover compared to parameterized convection simulations.

We show that under the same constant soil moisture conditions, i.e. not influenced by the runoff, explicitly resolved convection simulations show a stronger increase in precipitation and extend precipitation further north compared to parameterized convection simulations.

During the middle Holocene, about 5000 to 11000 years ago, the climate of the North African continent was wetter than today and its landscape was characterized by a denser vegetation cover consisting of grass- and shrublands Jolly et al. (1998) and shaped by abundant lakes and wetlands (Tierney et al., 2017).

This so-called "African humid period" (AHP) was likely triggered by steady variations in the Earth's orbit (Kutzbach and Guetter, 1986; Street-Perrott et al., 1990). These variations lead to a higher northern hemispheric insolation and thereby to an intensified West African Monsoon circulation (Kutzbach and Otto-Bliesner, 1982; Kutzbach and Liu, 1997). It is widely accepted that the initial changes in the West African monsoon circulation were fundamentally amplified by ocean-atmosphere (Kutzbach and Liu, 1997) and land-atmosphere feedbacks (Claussen and Gayler, 1997; Braconnot et al., 1999; Braconnot et al., 2012; Krinner et al., 2012; Claussen et al., 2017; Gaetani et al., 2017)), causing strong changes in the hydrological cycle and vegetation, as indicated by numerous proxy data (e.g.Peyron et al. (2006) and Bartlein et al. (2011)).

Compared to these proxy data, climate models still struggle to reproduce the precipitation distribution (i.e the amplitude and/or the extension of the tropical rainbelt) to support the greening of the semi-arid and arid regions of the North African continent (e.g. Joussaume et al. (1999), Braconnot et al. (2012), Harrison et al. (2015), and Brierley (2020)). Besides the often-misrepresented precipitation distribution, Hopcroft et al. (2017) demonstrated that the coupled atmosphere-vegetation components of state-of-the-art earth system models are also sources of uncertainties and can be a reason for unrealistic simulations of past African humid periods. A possible explanation for diverging rainfall distributions could be the parameterization of convective rainfall, recently explored by Jungandreas et al. (2021), which is used in coarse-resolution climate models (e.g. Yang and Slingo (2001), Randall et al. (2003), Stephens et al. (2010), Dirmeyer et al. (2012), and Fiedler et al. (2020)). However, no substantial effect on meridional precipitation distribution over mid-Holocene North Africa was found by comparing simulations with parameterized and explicitly resolved convection (Jungandreas et al., 2021). Instead, feedbacks of the land surface and precipitation were identified as an important process for the hydrological cycle, which differs from how convection is represented in the model. Resolving convection explicitly leads to less frequent but more local and intense precipitation. As the soil is not able to absorb the high amount of rainfall, a large fraction is removed from the system as runoff and thus causes an overly strong drying of the soil. The lower soil moisture yields lower latent heat flux and consequently an extenuated convective activity. In contrast, parameterizing convection causes less intense but more frequent precipitation that steadily moistens the soil, generating less runoff and thus leads to higher latent heat fluxes and further supports convection.

In their simulation, Jungandreas et al. (2021) prescribed present-day conditions for the vegetation cover, like the simulation setup used in the Paleoclimate Modeling Intercomparison Project phase 1 (PMIP1). This in relation to early and mid-Holocene conditions unrealistic specification of land-surface conditions prompts the question of whether and how more realistic land-surface coverage and thus, higher

soil moisture and modified hydrological conditions, reflect into differences in the precipitation distribution in both representations of convection.

In the present study, we investigate this land-atmosphere coupling over mid-Holocene North Africa in simulations with explicitly resolved and parameterized convection. We extend the simulations of Jungandreas et al. (2021) in two ways. First, we prescribe a more realistic vegetation cover over mid-Holocene North Africa based on transient mid-Holocene simulations of the Max-Planck Institute Earth System Model (MPI-ESM) (Dallmeyer et al., 2020). Second, we want to isolate the effect of the representation of convection on runoff/soil moisture and therefore on precipitation from the response of precipitation to the increased vegetation cover. To demonstrate how strong the effect of the precipitation-runoff-soil moisture pathway in our simulations is, we conduct an experiment with the same constant soil moisture, implicitly removing the control of runoff on soil moisture.

B.2 METHODS

B.2.1 *Model*

The model and simulation setup used in this study is identical to the one used in Jungandreas et al. (2021). Nevertheless, we start to briefly recapitulate the most important features of the model. For more model details, see Jungandreas et al. (2021). Subsequently, we introduce two new experimental setups used in this study.

We use the ICON (ICOsahedral Nonhydrostatic) model framework version 2.5.0 (Zängl et al., 2015) in its operational Numerical Weather Prediction (NWP) mode. The ICON-NWP model framework supports the performance of nested experiments. The nesting allows us to run coarse horizontal resolution simulations with parameterized convection and high-resolution simulations using explicitly resolved convection, simultaneously. We simulate with a one-way nesting strategy. The convective parametrization used in our simulations is based on the bulk mass-flux approach introduced by Tiedtke (1989) with modifications by Bechtold et al. (2014). Zängl et al. (2015) lists the other physical parameterizations of the model framework. All simulations are limited-area simulations. The domains are outlined in Fig. B.1 as well as the main analysis domain we use in our investigations.

B.2.2 *Simulation Setup*

We perform a 30 - year spinup simulation that covers the period from 7039 BP (before present with the year 2000 used as a reference) to 7010 BP. The spinup simulation is conducted on a regional domain with 40 km horizontal grid spacing and 75 vertical levels (blue domain outlined in Fig. B.1) and simulates with parameterized convection. The soil moisture reaches a stable state after around 15 years (of the 30-year spinup period). We select two years after this 15-year soil moisture-spinup phase and start our nesting experiments for the boreal summer monsoon season. The nesting experiments are initialized for 30th May and run for five months (JJASO).

The parent domain of the nested simulation is identical to the domain of the spinup simulation with the same horizontal and vertical resolution. The nested domains have horizontal resolutions of 20 km, 10 km, and 5 km (Fig. B.1). While the simulations with 40 km, 20 km, and 10 km grid spacing simulate with parameterized

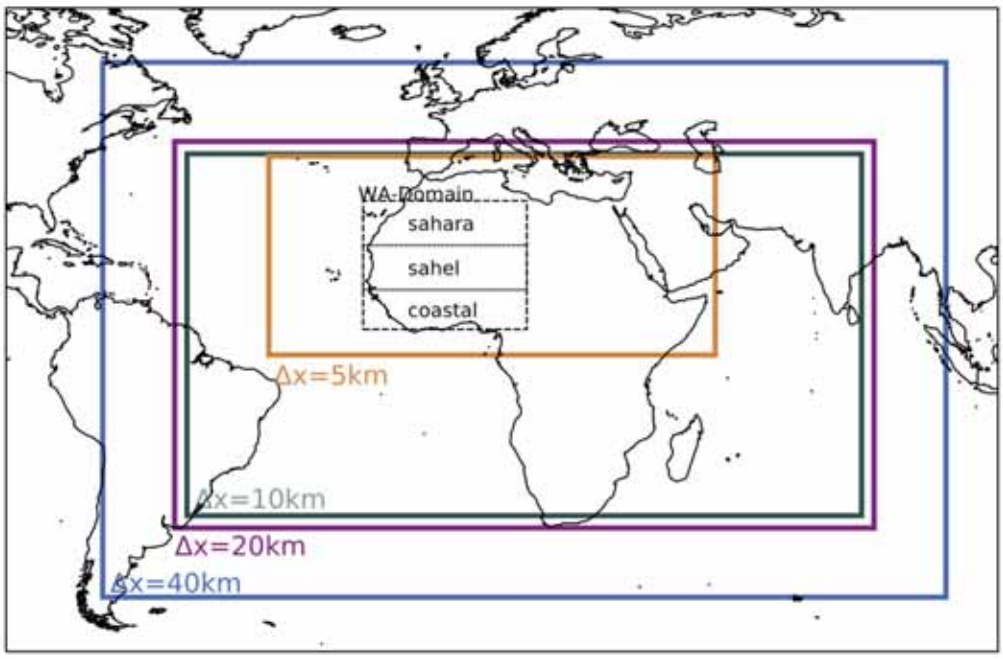

Figure B.1: Solid, colored domains outline the nesting domains of the simulations for the various grid spacings (as indicated). The dashed, black domain labeled with "WA-Domain" (West Africa) displays the main analysis. The WA-Domain spans the area from 5 °N-31 °N and from 18 °E-15 °W. The three dotted, black domains within the WA-Domain are used to distinguish the coastal African region ("coastal"), the Sahel region ("Sahel"), and the Saharan region ("Sahara") that are indicated in the longitudinal-mean plots. The coastal region spans from 5 °N-13 °N and from 18 °E-15 °W. The Sahel region spans from 13 °N-22 °N and from 18 °E-15 °W and the Sahara region from 22 °N-31 °N and from 18 °E-15 °W.

convection, the 5 km domain uses explicitly resolved convection. In the following, we refer to the simulations with 40 km horizontal grid spacing and parameterized convection as 40km-P simulations. Similarly, the 5km resolution simulation with explicitly resolved convection is labeled with 5km-E. The nested simulations are initialized one hour after another by their respective parent domain. Lateral boundary conditions for the nested simulations are obtained from their parent simulation and updated every 6 hours.

The initial and boundary data originate from the transient global Holocene simulation conducted with the MPI - Earth System Model (ESM).We further prescribe 6 - hourly sea surface temperature (SST) and sea ice (SIC) fields from this simulation, as well as the same orbital parameters and tracer gases carbon dioxide (CO_2), methane (CH_4) and nitrogen oxide (N_2O). More details about the transient MPI-ESM Holocene simulation are provided by Dallmeyer et al. (2020).

In our analysis (Sec. B.3), we focus our analysis on the three strongest monsoon months from July to September (JAS). Further, we investigate both, the 40 km parameterized convection and the 5 km explicitly resolved convection simulations, to analyze whether and how differently the atmosphere responds to the underlying surface conditions in both representations of convection. To address the influence of the horizontal resolution on our results, we redo our analysis but compare the 10km-P and 10km-E simulations. The results of this analysis are attached in Appendix B.5.

B.2.2.1 *The "Green Sahara" simulations (GS)*

To investigate the influence of the land surface on the monsoonal rainbelt in parameterized and explicitly resolved convection simulations, we compare simulations with present-day vegetation cover (Jungandreas et al. (2021), Fig.B.2a) to simulations with a higher, more realistic mid-Holocene-like vegetation cover (Fig.B.2b). Because the largest area of North Africa in the simulations with present-day vegetation cover is bare soil (desert) or sparse vegetation we refer to these simulations in the following as "DS"-simulations (for "Desert Sahara"). The simulations with a higher vegetation cover are introduced in this study.

We prescribe an idealized, denser vegetation cover over the whole simulation domain guided by the MPI-ESM Holocene simulations (see Dallmeyer et al. (2020)). (Note, prescribing values from the MPI-ESM mid-Holocene simulations directly, as we did for the boundary data, is not possible, because the MPI-ESM uses a different land module compared to the ICON-NWP. Therefore, the number of different vegetation types, as well as the types themselves, do not match between the models. This makes it difficult to translate the vegetation types or related variable values directly from the MPI-ESM to the ICON model.) We extend the evergreen tropical rainforest (Fig. B.2b, dark green) up to around 15°N. North of the rainforest we prescribe a decreasing vegetation gradient from closed to open shrubland (light yellow), to closed to open herbaceous vegetation (dark red), to sparse vegetation (lighter red). Bare soil (desert) prevails only over a small area over Egypt. In the following, we label these vegetated Sahara simulations with "GS" (for "Green Sahara").

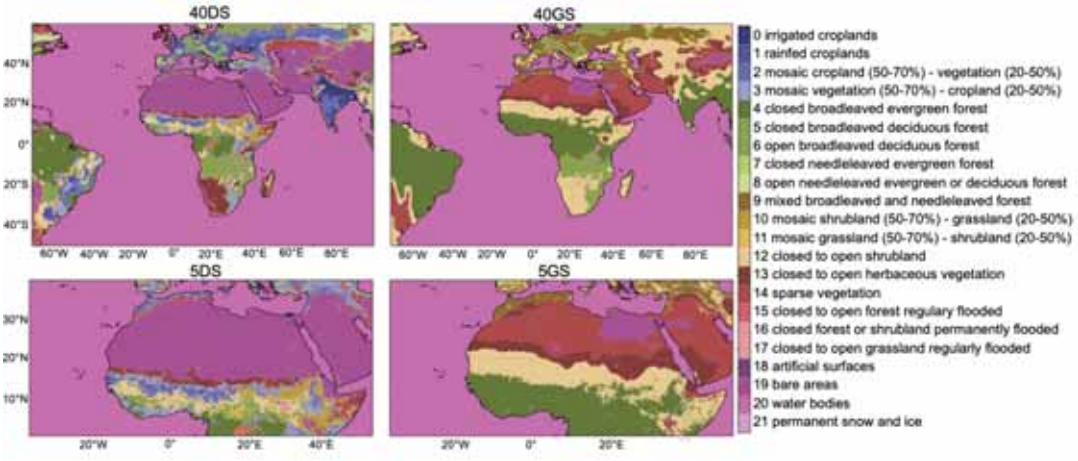

Figure B.2: Land surface cover for the "Desert Sahara" (a,c) and "Green Sahara" (b,d) simulations for the 40 km and the 5 km simulations, respectively.

Additionally, to the vegetation cover, we adjust all variables that are prescribed in our simulations and that depend on the vegetation type for example the leaf area index, surface albedo, root depth, minimal stomata resistance, and several others. Based on the present-day values, which originate from the ERA-reanalysis dataset, we prescribe spatially constant values and adjust them to be consistent for the respective vegetation type. We calculated these spatially constant values as follows:

1. we calculate the dominant land cover type (≡ vegetation type) for each grid cell of the present-day land cover distribution of the 40km-domain (see Fig. B.2).

2. these grid cells with the same dominant vegetation type are used to calculate the mean and either the 75th or the 85th percentile value for each variable.

3. we prescribe these mean or percentile values to the idealized mid-Holocene land-cover types, respectively.

ICON-NWP only calculates with one vegetation type per grid box, the dominant one, and not with fractions of several vegetation types as preset by the IFS. The surface variables calculated and preset by the IFS, for example, albedo or leaf area index, therefore, consider the presence of different vegetation types per grid box. By using only the dominant vegetation type for the calculations of the constant surface variables, the mean value sometimes underestimates the variable values as compared to the present-day values. In these cases, we use the 75th or the 85th percentile values.

B.2.2.2 *GS simulations with constant soil moisture GS-cSM*

Additionally to the GS simulations, we perform a second set of GS simulations but with a prescribed soil moisture field that we keep constant for the whole simulations period. We label these simulations with GS-cSM (for "Green Sahara with constant soil moisture"). We prescribe the soil moisture field of the 1st September 00 UTC of the 40km-P GS simulation to all four domains at all times. The soil moisture field from the 1st September displays relatively high soil moisture levels, compared to the soil moisture levels at the beginning of the GS-simulations (Sec. B.2.2.1), to provide enough soil moisture for evapotranspiration. These GS-cSM simulations allow us to test our hypothesis that differences in the 40km-P and the 5km-E DS and GS simulations, i.e., the response of precipitation to the underlying surface conditions, are dominantly induced by differences in runoff/soil moisture (see Sec. B.3.2). Apart from keeping the soil moisture constant, the simulation setup in the GS-cSM simulations is identical to the GS simulation setup.

B.3 RESULTS AND DISCUSSION

In the following two sections (Sec. B.3.1 and Sec. B.3.2), we start to compare simulations with present-day land surface cover (DS) introduced by Jungandreas et al. (2021) with the simulations with higher, mid-Holocene-like vegetation cover (GS, Sec, B.2.2.1) to first investigate the sign and strength of the evolving land-atmosphere feedback. In Sec. B.3.1 we first demonstrate that parameterized and explicitly resolved convection simulations generally both show a positive land-atmosphere coupling. Therefore, we do not distinguish between the 40km-P and the 5km-E simulations yet but describe the features that are similar in both representations of convection. Subsequently, in Sec. B.3.2 we highlight the differences between parameterized and explicitly resolved convection and the consequences of these differences.

If not further specified by "coastal", "Sahel" or "Sahara", all analyses are conducted over the WA-Domain outlined in Fig. B.1 and for the time period from July to September, the three strongest monsoon months.

B.3.1 *Land-atmosphere coupling - similar feedbacks in parameterized and explicitly resolved convection simulations*

B.3.1.1 *Changes in vegetation and the surface energy budget*

In our simulations, the main influence of the change in vegetation cover is, on the one hand, the influence on the energy partitioning into latent and sensible heat flux and, on the other hand, the change of the temperature gradient over the North African continent between the drier, warmer region of the Sahara and the cooler, moister regions near the coast. In the following, we will first describe changes in the vegetation cover and how they influence the surface energy budget over North Africa. Note that we use the terms latent heat flux (energy) and evapotranspiration (mass) interchangeable, as we calculated the evapotranspiration from the latent heat flux to better compare it to the precipitation rate.

In the GS simulations, prescribed vegetation shows a strong increase over the whole WA-domain with the strongest increase over the Sahel region compared to the DS simulations (Fig. B.3 a,b). Prescribing a higher vegetation cover strongly decreases the albedo by about 55% (see Table B.1). The decrease in albedo implies about 50% less reflection of solar incoming radiation at the surface, thus higher absorption of solar radiation. The increased absorption of solar energy at the surface compensates for the decrease in incoming solar radiation due to higher cloud cover.

The thermal outgoing radiation at the surface slightly decreases and the longwave, downward radiation increases due to higher cloud cover. Therefore, the net-thermal energy and the net radiation at the surface increases. This increase in net energy at the surface increases the total heat flux (sensible + latent heat flux) into the atmosphere. How much of the total energy is transformed into latent and sensible heat strongly depends on the water availability at the surface.

Especially over the Sahel (a region strongly controlled by the water availability) the increase in vegetation cover increases the interception storage of water and makes deeper soil water available for evapotranspiration. Therefore, the increase in the surface heat fluxes (Table. B.1) over the Sahel is dominated by the increase in latent heat flux. The strongest increase in latent heat flux coincides with the strongest increase in vegetation cover (Fig. B.3 a-d). Over the coastal region, latent heat flux is high and variations between the GS and the DS simulations are small. These small variations can be attributed to already high latent heat fluxes in the DS simulations due to dense vegetation and plentiful soil moisture (not shown). In contrast, over the Sahara, the increase in vegetation cover is as high as over the coastal region but differences in latent heat flux are comparatively small. The increase in sensible heat flux dominates the increase in the surface heat fluxes, due to generally low water availability over the Sahara.

Differences in the temperature field are dominantly determined by differences in the latent heat flux. Latent heat flux is more effective in transporting energy from the surface into the atmosphere and can cool the surface. As shown in Fig. B.3 e and f, near-surface, atmospheric temperature (here shown for 950hPa) decreases in

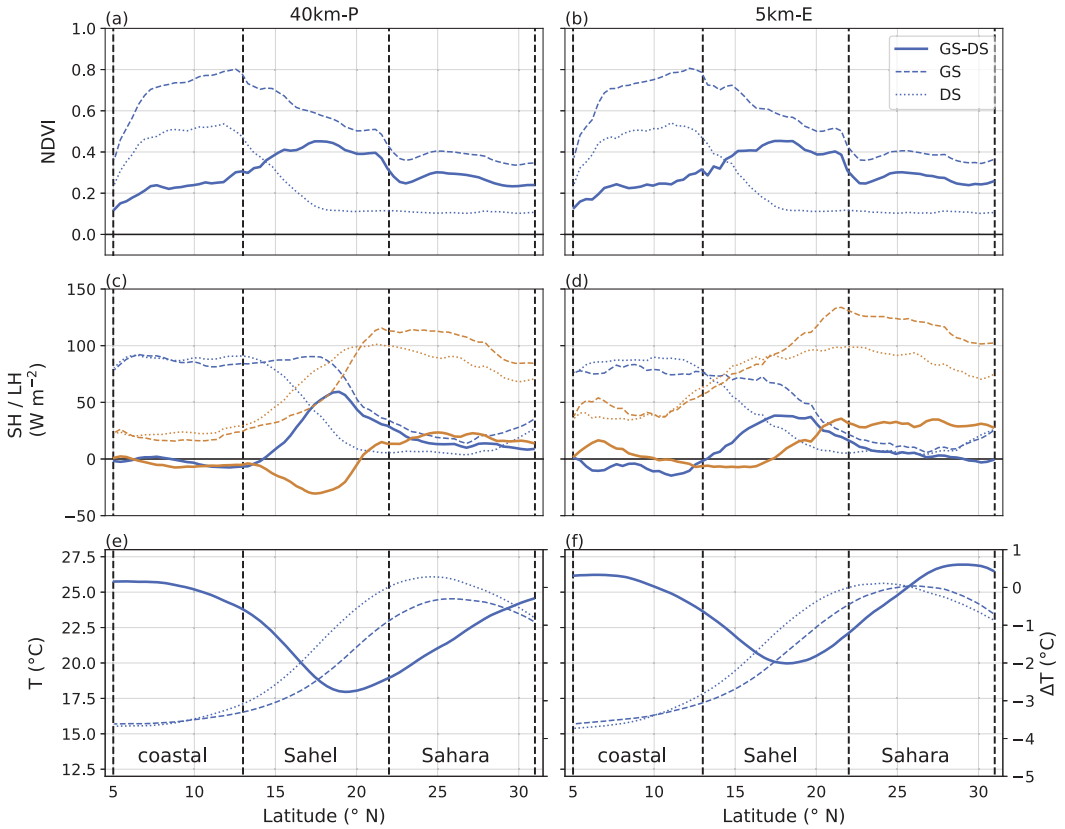

Figure B.3: JAS-mean meridional distribution of the normalized difference vegetation index (NDVI; a,b), the latent heat flux (blue) and sensible heat flux (orange) (c,d) and the 950hPa-temperature (e,f). Note the second y-axis in the panels e and f for the difference temperature (solid blue). The longitudinal mean is taken over the WA-Domain for the 40km (a,c,e) and the 5km (b,d,f) simulations, respectively. The lines indicate the distribution for the Desert Sahara-simulation (DS, blue dotted line), for the Green Sahara-simulation (GS, blue dashed line), and the difference between the GS and the DS simulation (blue (orange) solid line). The vertical black, dashed lines indicate the borders of the coastal, the Sahel, and the Sahara region outlined in Fig. B.1.

the GS compared to the DS simulations. The strongest decrease in temperature is located over the Sahel region and coincides with the region of the strongest increase in latent heat flux. The maximum temperature over the Sahara weakens and/or shifts northward where vegetation cover is less dense and thus, sensible heat flux is higher. Simultaneously, the temperature over the coastal region does not change substantially. Consequently, the temperature gradient between the Sahara and the humid coastal regions is decreased and its maximum shifts north by about 2-3°. This temperature coupling is especially important for the formation and the location of the African easterly jet over North Africa thus influences the dynamics of the atmosphere and will be further discussed in Section B.3.1.4.

B.3.1.2 *Changes in precipitation*

In this section, we first describe the changes in precipitation that evolve between the GS and DS simulations due to the higher vegetation cover. In the subsequent sections, we explain how the changes in the land surface described in Sec. B.3.1.1,

	40 km-P DS	40 km-P GS	5 km-E DS	5 km-E GS
SW↓ ($W\,m^{-2}$)	267.34	235.05	280.52	253.58
SW↑ ($W\,m^{-2}$)	64.80	31.44	67.87	34.15
SW_{net} ($W\,m^{-2}$)	202.54	203.61	212.65	219.43
LW↓ ($W\,m^{-2}$)	396.59	403.88	393.06	402.82
LW↑ ($W\,m^{-2}$)	475.09	464.99	476.29	470.84
LW_{net} ($W\,m^{-2}$)	-78.50	-61.11	-83.22	-68.01
R_{net} ($W\,m^{-2}$)	124.04	142.5	129.43	151.42
LH ($W\,m^{-2}$)	45.78	60.16	41.03	48.57
SH ($W\,m^{-2}$)	61.45	62.28	72.81	87.86
Res ($W\,m^{-2}$)	16.81	20.06	15.59	15.56

Table B.1: JAS-mean values of radiation components at the surface averaged over the WA-Domain (Fig. B.1) for the 40 km-P DS and GS simulation and for the 5 km-E DS and GS simulation. The abbreviations used are as follows: SW↓ - downward, shortwave radiation, SW↑ - upward, shortwave radiation, SW_{net} - net shortwave radiation, LW↓ - downward, longwave radiation, LW↑ - upward, longwave radiation, LW_{net} - net longwave radiation, R_{net} - net radiation, LH - latent heat flux, SH - sensible heat flux, Res - Residuum term.

induce these changes in precipitation by altering the thermodynamics and dynamics of the atmosphere.

Similar to the latent heat flux, the precipitation differences (Fig. 1.4) between the GS and the DS simulations show a strong meridional dependence with decreasing precipitation over the coastal region and increasing precipitation over the Sahel-Sahara region indicating a northward shift of the monsoonal rainbelt. The strongest increase of precipitation is simulated over the Sahel region and coincides with the region of the strongest increase in latent heat flux and with the strongest decrease in temperature. This higher precipitation over the Sahel-Sahara region results in a northward shift of monsoonal precipitation by about 4-5°. We estimate the significance of the difference between the GS and the DS simulations based on the daily longitudinal mean standard deviation from the longitudinal mean JAS cycle. We calculated the standard deviation only for the 40km-P simulation based on the last 15 years of the 40km-resolution spinup simulations (Sec. B.2.2). The standard deviation indicates that the differences in the meridional precipitation distribution between the GS and DS simulation are significant north of about 17°N. (We refrain from calculating the standard deviation for the 5km-E simulations due to the too-short simulation period to obtain robust results. However, based on the calculations for the 40km-P simulation we estimate that differences between the 5km-E GS and DS simulations are significant north of about 17°N, too.)

Subsequently, we explain the land-atmosphere feedbacks which induce these strong changes in the precipitation amount and distribution shown in Fig. B.4. We

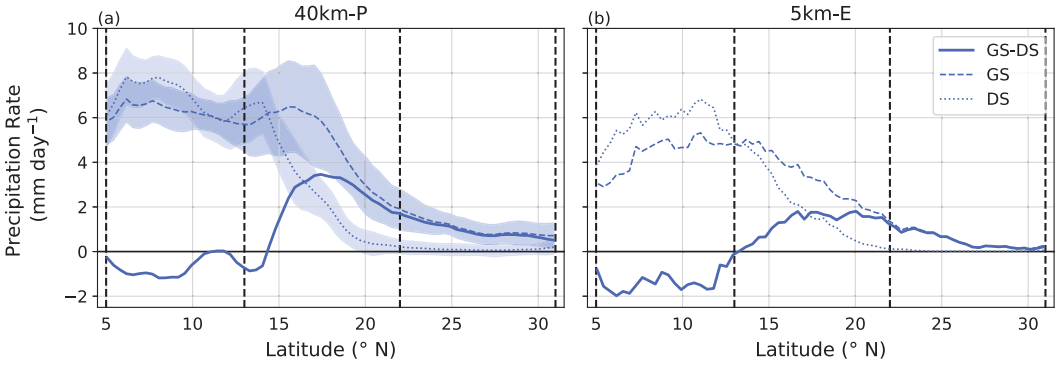

Figure B.4: JAS-mean meridional distribution of precipitation rate for the 40km-P (a) and the 5km-E (b) simulations, respectively. The longitudinal-mean is taken over the WA-Domain. The precipitation distribution for the DS-simulation (blue dotted line), for the GS-simulation (blue dashed line), and the difference between the GS and the DS simulations (blue solid line) is displayed. The blue shading indicates two times the daily longitudinal mean standard deviation from the longitudinal mean JAS cycle. The vertical black, dashed lines indicate the borders of the coastal, the Sahel, and the Sahara region outlined in Fig. B.1.

start with the influence of the increased latent heat flux on atmospheric thermodynamics. Afterward, we focus on the dynamics of the WAM which are altered by the changes in the temperature gradient over the continent.

B.3.1.3 *Changes in atmospheric thermodynamics*

The change in surface latent heat flux influences the moisture in the lower troposphere as shown in Fig. B.5. The increase in relative humidity in the lowest atmosphere layers over the Sahel and Sahara region can be linked to the increase in latent heat flux (Fig. B.3 c,d). This increase in boundary-layer relative humidity supports the triggering of convection over these regions. In turn, the increase in convective activity is likely the reason for the increase in the upper tropospheric humidity as it distributes boundary layer-moisture upwards.

Changes in the stability parameters, such as CAPE (Convective Available Potential Energy) or CIN (Convective Inhibition; i.e., the energy required to lift the air parcel to the level of free convection (LFC))) listed in Table B.2, confirm the more supportive conditions for the triggering of convection in the GS simulations over the Sahel-Sahara region. CAPE increases, CIN becomes less negative, hence, the LFC lowers.

B.3.1.4 *Changes in atmospheric dynamics*

Since Fig. B.4 indicates that precipitation shifts from the coastal into the Sahel region, rather than increasing over the whole domain, we suggest that the main cause for the further northward propagation of monsoonal precipitation in the GS simulations is of dynamical nature. In the following, we demonstrate the dynamic feedbacks that evolve in response to a higher prescribed vegetation cover.

Despite the decrease in temperature (Fig. B.3 e,f), the strength of the low pressure system (not shown) over the Sahara increases. This strengthening of the low pressure system is potentially caused by stronger uplift at the surface which in turn is caused by the increase in net energy (i.e. by increased latent and sensible heat flux; see

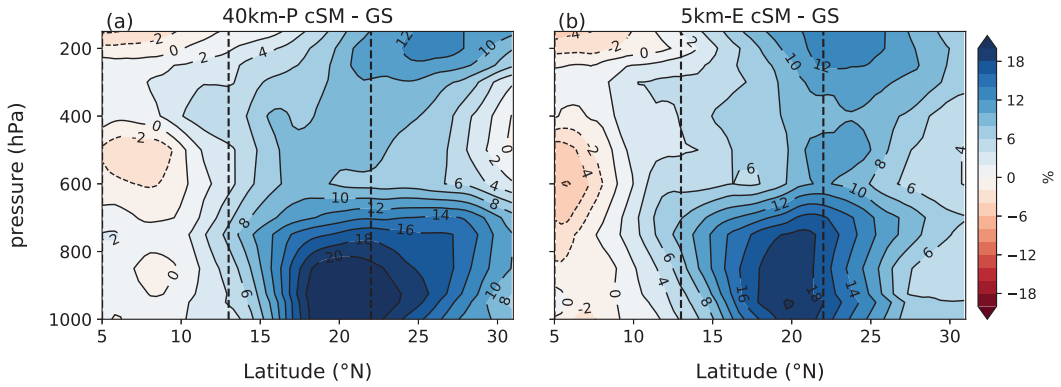

Figure B.5: Vertical cross section of the difference in relative humidity between the GS and the DS simulation for the 40 km-P (a) and for the 5 km-E simulation (b). The fields are averaged over the WA-Domain outlined in Fig. B.1. The vertical dashed lines display the borders of the coastal, the Sahel and the Sahara domain also outlined in Fig. B.1.

		40 km-P DS	40 km-P GS	5 km-E DS	5 km-E GS
coastal	CAPE (J kg^{-1})	737.2	561.1	706.7	505.6
	CIN (J kg^{-1})	-29.4	-25.7	-37.5	-34.1
	LFC (m)	724	651	1131	1236
	cloud cover (%)	87	89	77	79
sahel	CAPE (J kg^{-1})	382.1	500.7	159.8	220.6
	CIN (J kg^{-1})	-232.8	-131.9	-262.0	-211.5
	LFC (m)	2280	1482	2617	1940
	cloud cover (%)	44	68	36	58
sahara	CAPE (J kg^{-1})	0.0	12.1	0.0	2.1
	CIN (J kg^{-1})	0.0	-106.2	0.0	-102.9
	LFC (m)	3687	2804	3321	2974
	cloud cover (%)	17	34	20	36

Table B.2: JAS-mean values of 12 UTC CAPE and CIN and JAS-mean level of free convection (LFC) and total cloud cover for the coastal, Sahel and Sahara region (Fig. B.1) for the 40 km-P DS and GS simulation and for the 5 km-E DS and GS simulation, respectively.

Tabel. B.1) at the surface. Therefore, the surface pressure gradient between the Sahara and the tropical Atlantic Ocean increases and drives a stronger southwesterly monsoon circulation (Fig. B.6). The strengthened southwesterly winds transport cool and moist air deep into the African continent and provide more moisture for convection and precipitation. Additionally, the location of the Innertropical

Front (ITF, the location where the southwesterly monsoon flow converges with the northeasterly Harmattan winds) shifts about 2° further north. Therefore, the low and mid-level lifting over the northern Sahel and southern Sahara region that is associated with the lifting of air at the ITF (Nicholson, 2009a; Thorncroft et al., 2011) strengthens in the GS simulations and shift further north from about 20°N to 22°N. This change in the low-level dynamics supports the higher precipitation rates over the Sahel and Sahara region in the GS compared to the DS simulations.

The decrease in the temperature gradient (Fig. B.3) and its northward shift weakens the African easterly jet (AEJ; indicated by the local maximum of easterly wind speed (reddish color) at about 600hPa) and shift its core about 3° north in the GS compared to the DS simulations (Fig. B.6; (Cook, 1999; Wu et al., 2009). The weakening of the AEJ, on the one hand, causes less moisture export from the African continent at mid-levels. Hence, more moisture remains over North Africa as a source for clouds and precipitation. Several studies (e.g. Cook (1999), Grist and Nicholson (2001), and Nicholson and Grist (2001)) confirm that the northward displacement and a weakening of the AEJ are associated with more humid conditions over the Sahel.

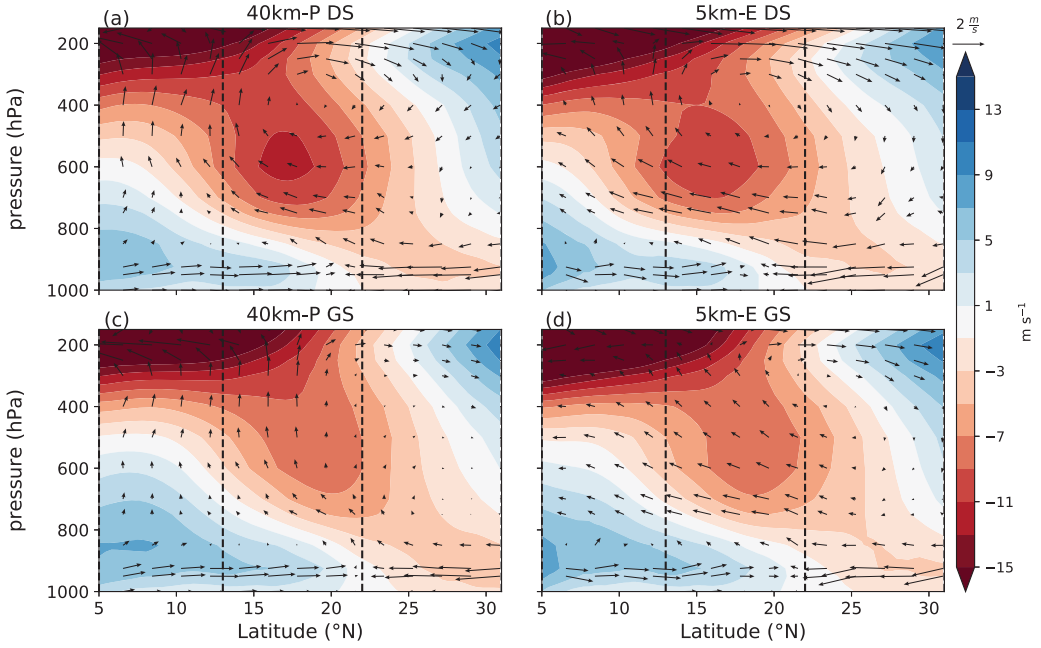

Figure B.6: Vertical cross-section of the wind field over the WA-domain (Fig. B.1). The shading displays the mean zonal wind, and the arrows the mean meridional and vertical wind for the 40km-P (a,c) and the 5km-E(b,d) and the DS (a,b) and the GS (c,d) simulations, respectively. Note that the vertical wind speed is multiplied by 100 to make arrows better visible. The dashed vertical lines indicate the borders of the coastal, Sahel, and Sahara domain also displayed in Fig. B.1

Additionally, with the northward shift of the AEJ, the region of strong ascent between the Tropical easterly jet (TEJ; maximum easterly winds at about 200hPa)

and the AEJ axes (e.g.Grist and Nicholson (2001) and Nicholson and Grist (2001)) broaden (and/or shifts northward), as confirmed by the difference in vertical upward motion between the GS and DS simulations (Fig. B.7). Fig. B.7 displays a decrease in vertical upward motion over the coastal region and an increase over the Sahel-Sahara region up to about 25°N. This increased vertical upward motion over the Sahel-Sahara region potentially also contributes to increased upper-tropospheric relative humidity (Fig. B.5). The ascending motion between the jet axes is part of a deep meridional overturning circulation (Thorncroft et al., 2011) that not only distributes moisture within the whole troposphere (Fig. B.5) but additionally forces the low-level inflow of fresh, moist monsoonal air from the south and southwest. Stronger upward motion and higher atmospheric humidity lead to more supportive conditions for convection and therefore support the higher precipitation rates (Fig. B.4). Vice versa, increased convection, in turn, moistens the atmosphere.

North of 25°N the reddish color in Fig. B.7 indicates that the descending motion over the Sahara (associated with the upper-level Saharan high) is weakened, as expected from the decrease in albedo based on the Charney-feedback (Charney et al., 1975). We argue that the increase in precipitation over the southern Sahara, despite unsupportive thermodynamical conditions (compare to Table A.1), is due to the stronger, further northward located dynamical uplift of air at the ITF, higher moisture from evapotranspiration, and weaker descending motion over the Sahara.

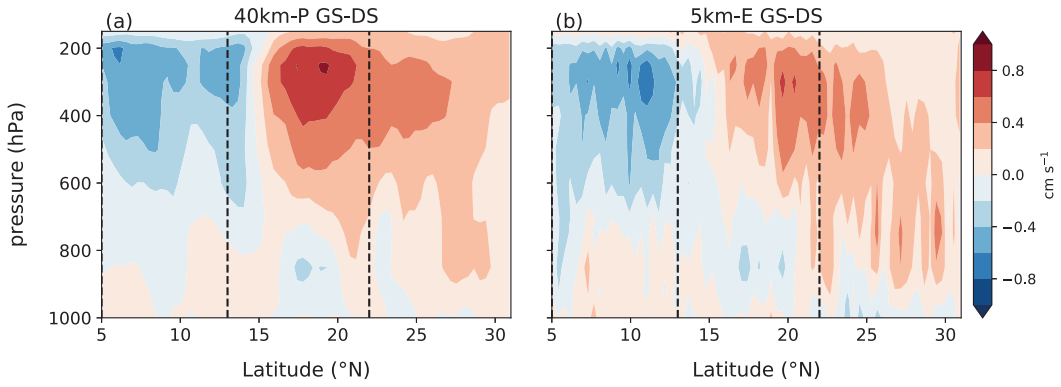

Figure B.7: Vertical cross section of the difference in the vertical wind component between the GS and the DS simulation (a,b) for the 40 km-P (a) and the 5 km-E simulation (b) averaged over the WA-Domain outlined in Fig. B.1. The dashed vertical lines again indicate the borders of the coastal, Sahel and Sahara domain also displayed in Fig. B.1.

We found that conditions for convection and precipitation become more supportive in the GS compared to the DS simulations. This holds for both the 40km-P and the 5km-E simulations. The improved conditions for convection lead to a northward extension of the monsoonal precipitation of about 4-5° (Fig. B.4). The results reveal that, on the one hand, increased vegetation cover yields higher latent heat fluxes over the Sahel and Sahara region, which increases the boundary-layer atmospheric moisture and generates more supportive thermodynamic conditions for convection to develop. On the other hand, the change in vegetation cover also alters the dynamics of the monsoon circulation by affecting the temperature and moisture gradient. The decrease in the temperature and moisture gradient results in a weakening and northward shift of the AEJ. These changes in the AEJ lead to moister conditions

over the Sahel in the whole troposphere, by both, enhanced upward transport (together with the TEJ) of boundary layer moisture and decreased, mid-level export of moisture from the African continent. The shift of precipitation from the coastal to the Sahel region indicates that the dynamic effects are of major importance as compared to the thermodynamic feedback.

B.3.2 *Positive land-atmosphere feedbacks but with different strength - differences between 40km-P and 5km-E simulations*

In the previous section, we analyzed the differences between the DS and the GS simulations, which are similar in parameterized and explicitly resolved convection simulations. Both representations of convection show a positive precipitation feedback if the vegetation cover increases. In the following section, we want to highlight the differences between parameterized and explicitly resolved convection simulations.

By comparing the change in latent heat flux (Fig. B.3c,d) and in precipitation Fig. B.4), we notice that both show a stronger increase over the Sahel and Sahara region in the 40km-P compared to the 5km-E simulations. Over the coastal region, however, latent heat flux and precipitation decrease more strongly in the 5km-E simulations. The mean increase in precipitation in the 40km-P GS simulation over the Sahel region is 2.1 mm day^{-1} while the mean increase in evapotranspiration is 1.1 mm day^{-1}. In contrast, in the 5km-E GS simulation, the mean increase in precipitation is 1.3 mm day^{-1} and the increase in evapotranspiration is 0.9 mm day^{-1}. Therefore, the increase in precipitation relative to the increase in evapotranspiration (Fig. B.3 c,d) is higher in the 40km-P GS simulation than in the 5km-E GS simulation, indicating a higher sensitivity of the atmosphere to changes in the land surface and evapotranspiration.

As a direct result of the stronger increase in latent heat flux relative humidity in the boundary layer also increases more strongly (Fig. B.5) in the 40km-P simulations. The higher boundary-layer relative humidity supports the triggering of convection and also the stability parameters (Fig. A.1) indicate a less stable atmosphere in the 40km-P simulations as compared to the 5km-E simulations. Over the coastal region, the GS simulations reveal small differences in the 40km-P simulation and a slightly stronger drying in the 5km-E simulation in agreement with the decrease in latent heat flux (Fig. B.3), precipitation (Fig. B.4) and vertical upward motion (Fig. B.7).

Consistently to the stronger change in latent heat flux, the temperature decreases more strongly over the Sahel and Sahara region in the 40km-P simulations. Hence, the temperature gradient between the Sahara and the coastal region in the 40km-P simulations decreases more strongly. (Because the temperature gradient was stronger in the 40km-P DS as compared to the 5km-P DS, the stronger decrease in the 40km-P GS simulations results in an approximately similar temperature gradient in the 5km-E and the 40km-P GS simulations.) As a result, the AEJ (Fig. B.6) weakens more strongly in the 40km-P as compared to the 5km-E simulations. However, in the end, the AEJ is equally strong in the GS simulations with a mean maximum wind speed of 8.4 m s^{-1} and 8.6 m s^{-1} in the 40km-P and the 5km-E simulations, respectively. Furthermore, in the GS simulations, the AEJ core is located further north in the 40km-P (at about 19°N) than in the 5km-E (at about 17°N) simulations.

The associated mean upward vertical motion (Fig. B.7) between the axes of the AEJ and the TEJ is generally stronger in the 40km-P simulations compared to the 5km-E simulations (not shown). Therefore, the moisture distribution from the lower into the upper troposphere levels is more effective in the 40km-P simulations, in addition to the stronger convective activity (indicated by higher precipitation rates) which also contributes to the vertical moisture distribution. Consequently, stronger vertical upward motion and higher relative humidity throughout the atmosphere are more supportive for the development of convection and precipitation. In turn, the higher convective activity positively feeds back on tropospheric relative humidity.

We notice that the responses of the latent heat flux, the thermodynamics, and dynamics of the atmosphere and, consequently, of precipitation to the change in land surface properties are weaker in the 5km-E simulation than in the 40km-P simulations. The smaller changes in atmospheric humidity, stability, and dynamics reveal a weaker land-atmosphere coupling in the explicitly resolved convection simulations as compared to parameterized convection simulations. Fig. B.8 reveals that, as shown in the DS simulations from Jungandreas et al. (2021), soil moisture content (in the four uppermost soil layers), as well as the increase in the GS simulation, is much lower in the 5km-E as compared to the 40m-P simulations. Over the Sahel, the maximum storage rate (not shown) is 2 mm day^{-1} in the 40km-P GS simulation, and only 0.5 mm day^{-1} in the 5km-E GS simulation. This indicates that hardly any of the surplus of precipitation in the 5km-E GS simulation is stored in the soil (especially in the Sahel and Sahara region) as compared to the 40km-E simulations. The lower soil moisture is a consequence of higher runoff in the 5km-E simulations which is caused by more local and intense precipitation events (not shown; compare to Jungandreas et al. (2021)). In the mean over the WA-domain, about 37% and 35% of precipitation become runoff in the 5km-E GS and the DS simulation, while in the 40km-P GS and DS simulations only about 21% and 20% of the precipitation leaves the system as runoff, respectively.

Our results suggest a similar precipitation-runoff-soil moisture mechanism in the GS simulations as introduced by Jungandreas et al. (2021) for the DS simulations. Here we argue that this precipitation-runoff-soil moisture mechanism damps the potential precipitation response to a vegetated Sahel-Sahara region in the 5km-E compared to the 40km-P simulations. We hypothesize that higher soil moisture values in the explicitly resolved convection simulations, comparable to the ones in the parameterized convection simulations, will enhance the land-atmosphere coupling and shift monsoonal precipitation further north.

B.3.3 *The influence of runoff-controlled soil moisture*

In the following, we test our hypothesis that the high amounts of runoff influence the precipitation response more strongly in the 5km-E GS simulation than in the 40km-P GS simulation via the control of the soil moisture. We eliminate the limiting influence of the runoff on soil moisture in both representations of convection. For this purpose, we perform a set of simulations where we prescribe the same soil moisture fields in the 40km-P and the 5km-E GS simulations and keep this soil moisture field constant for the whole simulation period (Sec.B.2.2.2). We refer to these simulations as GS-cSM ("Green Sahara with constant soil moisture) simulations.

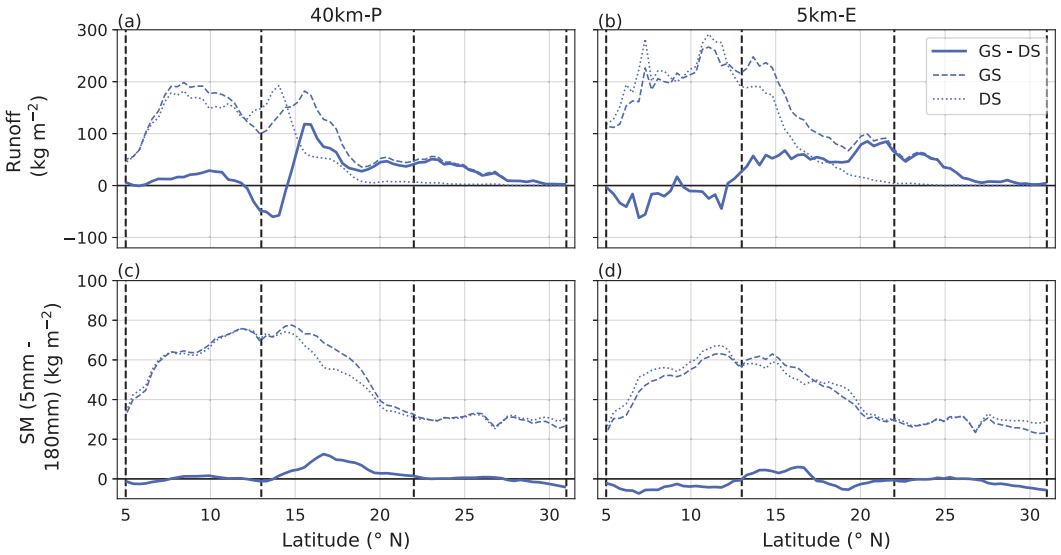

Figure B.8: JAS-mean-meridional distribution of the runoff (a,b), and the soil moisture content of the uppermost four soil layers (c,d). The longitudinal-mean is taken over the WA-Domain for the 40km-P (a,c) and the 5km-E (b,d) simulations, respectively. The lines indicate the distribution for the Desert Sahara simulations (DS, blue dotted line), for the Green Sahara simulations (GS, blue dashed line), and the difference between the GS and the DS simulations (blue solid line). The vertical black, dashed lines indicate the borders of the coastal, the Sahel, and the Sahara region outlined in Fig. B.1.

This means, both, the 40km-P GS-cSM and the 5km-E GS-cSM simulations, simulate with the same surface conditions.

Figure B.9 shows that the prescribed soil moisture strongly increases soil moisture in the 5km-E GS-cSM simulation while it remains mostly unchanged in the 40km-P GS-cSM simulation. As a result, evapotranspiration strongly increases in the 5km-E GS-cSM simulation, especially over the Sahel region. It demonstrates that the lower soil moisture in the 5km-E GS simulation strongly limits evapotranspiration as compare to the 40km-P GS simulation.

Over the coastal and southern Sahel region up to about 17°N, precipitation, however, does not show as a clear response to the increased soil moisture and evapotranspiration. This indicates that precipitation in this region is not soil moisture-controlled. This is because the coastal and southern Sahel regions are not moisture limited, hence, whether convection and precipitation can develop are determined by other processes, such as if vertical lifting is strong enough and how effective moisture in the atmosphere is transformed into precipitation. Over the northern Sahel however, precipitation shows a stronger increase of maximum 2 mm day^{-1} in the 5km-E GS-cSM simulations, while the increase in the 40km-P GS-cSM simulation is noticeably smaller. As a result, monsoonal precipitation extends equally far north in the 5km-E GS-cSM and the 40km-P GS-cSM simulation. We, therefore, argue that the soil moisture north of about 17°N becomes an important factor for the northward propagation of monsoonal precipitation in explicitly resolved convection simulations. Hence, in the 5km-E DS and GS simulations, the limited soil moisture hampers the northward extent of monsoonal precipitation as compared to the respective 40km-P simulations.

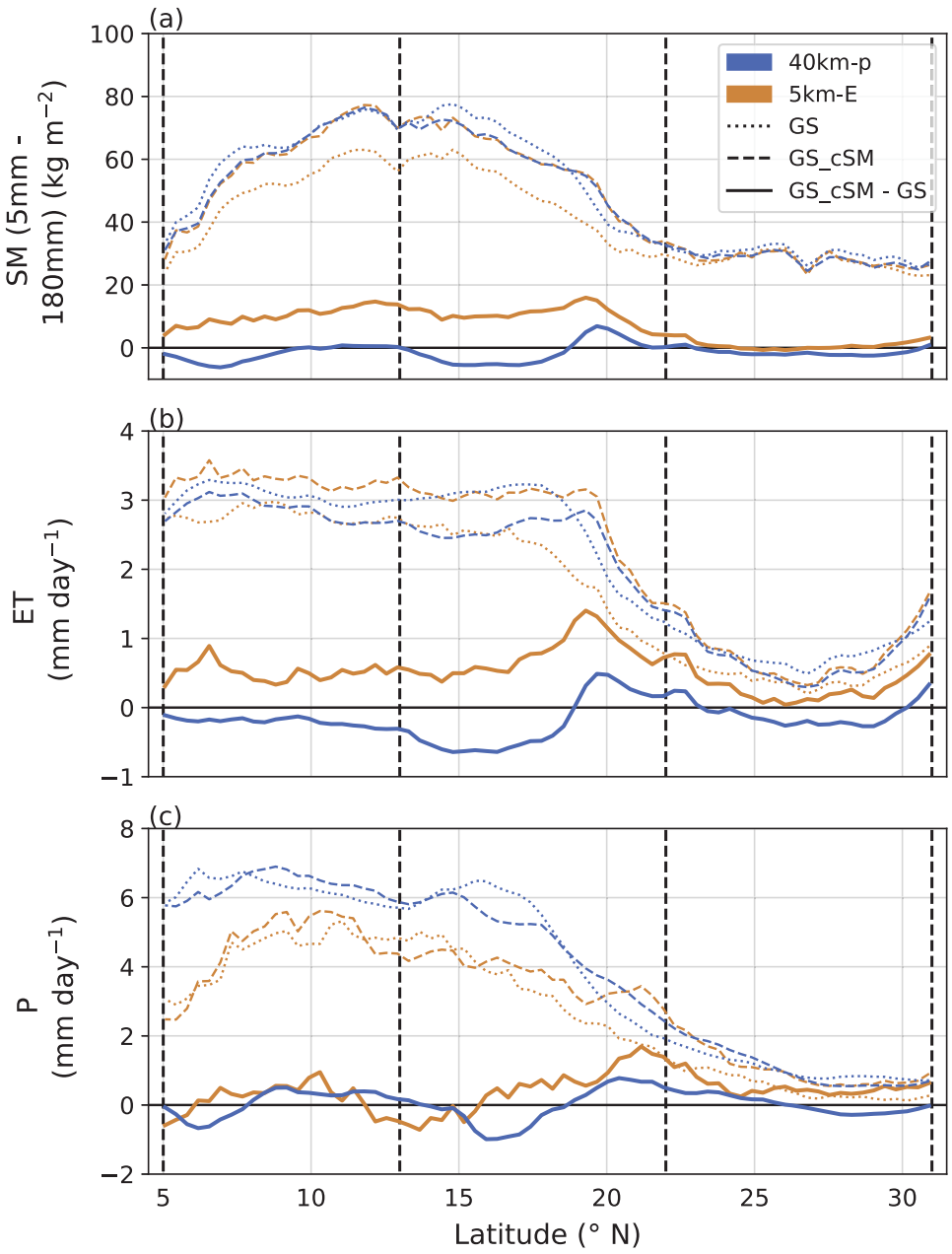

Figure B.9: JAS-mean meridional distributions of soil moisture content in the four uppermost soil layers (a), evapotranspiration (b) and precipitation (c) for the 5km-E GS-cSM simulation (dashed blue), the 40km-P GS-cSM simulation (dotted blue) and the difference between the GS-cSM and the GS simulation (solid blue), respectively.

B.3.4 *Influence on thermodynamic conditions*

We find that the lower tropospheric humidity increases more strongly in the 5km-E GS-cSM simulations, supporting the triggering of convection. Further, the stability of the atmosphere especially over the Sahel decreases, and conditions become more supportive in the 5km-E GS-cSM as compared to the GS simulation as indicated by higher CAPE, less negative CIN, and lowered LFC height (Table B.3). These changes are less pronounced between the 40km-P GS-cSM and GS simulations. This

indicates that increased soil moisture feeds back on the atmospheric thermodynamic conditions.

		40 km-P GS	40 km-P cSM	5 km-E GS	5 km-E cSM
coastal	CAPE ($J\,kg^{-1}$)	561.1	503.9	505.6	718.8
	CIN ($J\,kg^{-1}$)	-25.7	-22.6	-34.1	-18.6
	LFC (m)	652	683	1236	918
	cloud cover (%)	89	90	79	80
sahel	CAPE ($J\,kg^{-1}$)	500.7	474.1	220.6	498.8
	CIN ($J\,kg^{-1}$)	-232.8	-84.7	-211.5	-94.1
	LFC (m)	1482	1125	1940	1208
	cloud cover (%)	68	73	58	67
sahara	CAPE ($J\,kg^{-1}$)	12.1	25.5	2.1	6.0
	CIN ($J\,kg^{-1}$)	-106.1	-102.9	-28.2	-44.4
	LFC (m)	2804	2693	2973	2506
	cloud cover (%)	34	36	36	43

Table B.3: 12 UTC JAS-mean values of CAPE, CIN and JAS-mean values of the level of free convection (LFC) and total cloud cover for the coastal, Sahel and Sahara region (Fig. B.1) and for the 40 km-P GS and cSM simulation and for the 5 km-E GS and cSM simulation.

B.3.5 *Influence on dynamic conditions*

The increase in evapotranspiration further reduces the temperature gradient over the continent and strongly influences the AEJ strength and its location rather than the low-level southwesterly monsoon flow and the Harmattan winds. The temperature reduction between the 5km-E GS-cSM and GS simulation is stronger than in the 40km-P simulations, respectively (not shown). As a result, the AEJ weakens by $2\,m\,s^{-1}$ in the 5km-E GS-cSM simulation (compared to the GS simulation) and by $0.5\,m\,s^{-1}$ in the 40km-P GS-cSM simulations (Fig. B.10). In the end, the AEJ becomes weaker in the 5km-E GS-cSM ($6.6\,m\,s^{-1}$) than in the 40km-P GS-cSM simulation ($7.9\,m\,s^{-1}$). Moreover, the AEJ core displaces further north to about 20.8°N in the 5km-E GS-cSM simulation and about 20.4°N in the 40km-P GS-cSM simulation. Hence, the AEJ is located at about the same location in both the 5km-E and 40km-P GS-cSM simulations. This indicates that the location and strength of the AEJ are essential for the northward extent of monsoonal precipitation in our simulations. This result is consistent with the findings of (Cook, 1999; Grist and Nicholson, 2001; Nicholson and Grist, 2001).

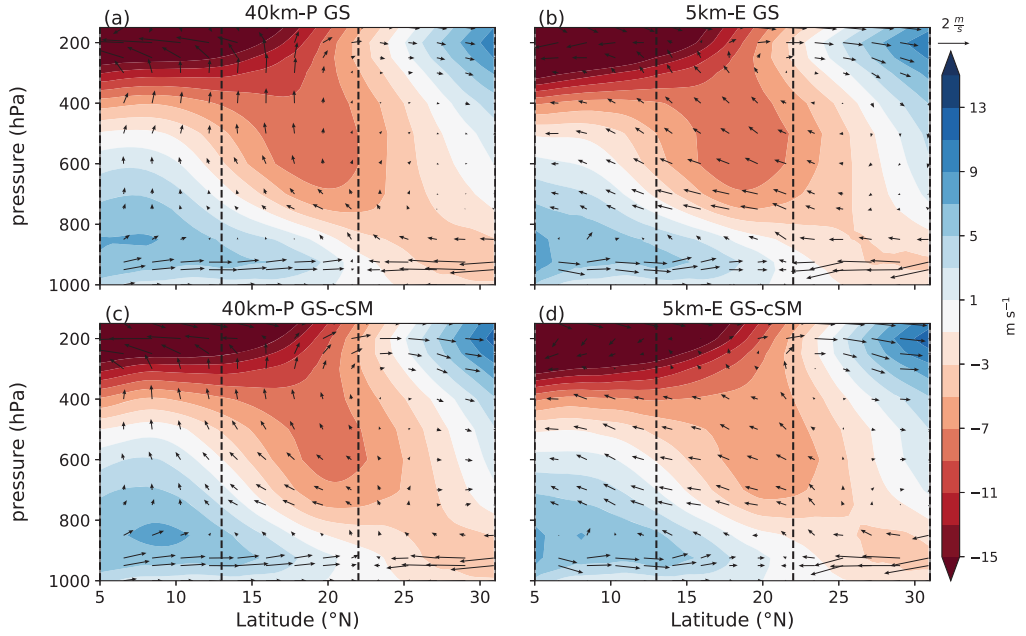

Figure B.10: The same as Fig. B.6 but for the GS simulation (a,b), the GS-cSM simulation (c,d) for the 40 km-P (a,c) and the 5 km-E simulation (b,d), respectively.

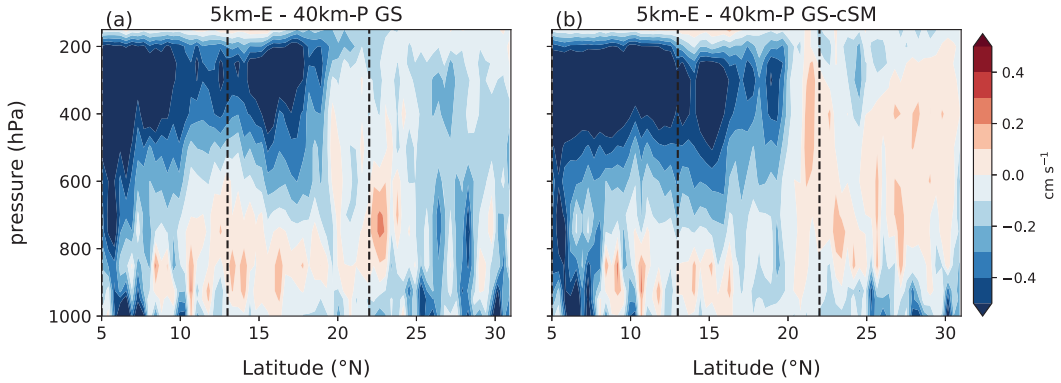

Figure B.11: The same as Fig. B.7 but displayed are the vertical cross sections of the vertical wind for the GS simulation (a,b), the GS-cSM simulation (c,d) and the difference between the GS-cSM and the GS simulation (e,f) for the 40 km-P (a,c,e) and the 5 km-E simulation (b,d,f).

The region over the Sahel-Sahara region between about 17-22°N, where precipitation strongly increases in the 5km-E GS-cSM simulation, is characterized by stronger upward vertical motion as compared to the 5km-E GS as well as compared to the 40km-P GS-cSM simulation. Moreover, the large-scale descending motion over the rest of the Sahara region weakens in the 5km-E GS-cSM simulation as compared to the 40km-P GS-cSM simulation. These changes in upward vertical motion could be either caused by the increased convection over the region itself, by the northward shift of the AEJ, or by both. To disentangle the respective contributions, sensitivity studies would be necessary.

However, the changes in the thermodynamic and dynamic state of the atmosphere in the 5km-E GS-cSM compared to the GS simulation shows the strong indirect effect of increased soil on the atmospheric state. We suggest that the effect of soil moisture on the AEJ dynamics is of major importance in our simulations.

Over the coastal and southern Sahel region, changes in precipitation are weaker and precipitation is generally much higher in the 40km-P as compared to the 5km-E simulations. The most striking difference between the 40km-P and the 5km-E simulations in these regions is the much higher mean vertical upward motion. Again, this could also be caused by the higher convective activity but we nevertheless suggest that the higher vertical upward motion is a result of the convective parameterization scheme as we see the same mechanisms in the 10km-P simulations (Sec. B.5.3). Again, to disentangle, whether this is the case, or if there is a strong positive feedback with the stronger convective activity, it needs sensitivity experiments which are out of the scope of this paper.

B.4 SUMMARY AND CONCLUSION

In this study we have performed parameterized (40km-P) and explicitly resolved convection simulations (5km-E) of vegetated, mid-Holocene North Africa to investigate the land-atmosphere feedbacks in response to a higher vegetation cover in both representations of convection. Regardless of the representation of convection, we have found a similar positive sign of land-atmosphere feedbacks between simulations with present-day surface cover (DS) and with a higher, more realistic mid-Holocene vegetation cover (GS). In response to the higher vegetation cover, precipitation shifts from the coastal towards the Sahel and Sahara region in the GS simulation. This leads to a northward shift of monsoonal precipitation of about 4-5° (regardless of the representations of convection). The main findings are:

- The increase in vegetation causes an increase in surface latent heat flux over the North African continent, especially over the Sahel. The increase in surface latent heat flux increases the moisture in the lower troposphere and decreases the thermodynamic stability by increasing the energy (CAPE) and lowering the height of the LFC. The decrease in atmospheric stability and the increase in humidity support the generation of more frequent and/or more intense convection and precipitation.

- The increase in the latent heat flux decreases the temperature gradient between the Sahara and the near-coastal regions of North Africa. This decrease in the temperature gradient weakens the AEJ and the AEJ core shifts further north. On the one hand, this reduces the mid-level export of moisture, hence more moisture remains over the continent. On the other hand, the region of strong vertical upward motion, which is confined between the axes of the AEJ and the TEJ, expands further north. These findings are consistent with previous results of Cook (1999) and Grist and Nicholson (2001) and Nicholson and Grist (2001) who associated a weaker and further northward located AEJ with more humid conditions over the Sahel.

Besides the, in principle, similar feedback mechanisms, we find important differences between the 40km-P and the 5km-E simulations. Similar to the findings in

Jungandreas et al. (2021), the representation of convection causes differences in precipitation intensity, frequency, and spatial distribution. As a result of these different precipitation characteristics, we show that the representation of convection influences the soil moisture-precipitation pathway and the strength of land-atmosphere coupling. The main results are:

- The 40km-P simulations reveal a higher sensitivity of precipitation to changes in the land surface compared to the 5km-E simulations. We show that this is because of a stronger soil moisture-precipitation feedback. So far, the focus in land-atmosphere coupling was, how strong precipitation changes due to a certain change in evapotranspiration/soil moisture. Here we emphasize that it is of higher importance how the land surface reacts to specific precipitation characteristics. Hence, the representation of convection can have substantial influence on the hydrological cycle.

- The elimination of the impact of runoff on soil moisture induces stronger changes in the 5km-E than in the 40km-P GS-cSM simulations, especially over the northern Sahel and Sahara region. In the GS-cSM simulations, the monsoonal precipitation extends equally strong north in both representations of convection. This is a result of stronger changes in evapotranspiration and precipitation over the northern Sahel and Sahara region in the 5km-E GS-cSM simulation as compared to the 40km-P GS-cSM simulation.

- However, we point out that over the coastal and southern Sahel region, precipitation is much weaker in the 5km-E than in the 40km-P simulations. We hypothesize that this is mainly caused by the convective parameterization scheme because a similar result is found in the 10km-P simulations. A more detailed process study is needed to clarify the mechanisms that cause these stronger mean vertical motions in the parameterized convection simulations.

Firstly, with this study, we emphasize the importance of both a higher vegetation cover and increased soil moisture for the northward extension of the mid-Holocene West African monsoon. Secondly, this study highlights the importance to consider both pathways of the soil moisture-precipitation feedback: not only the precipitation response to changes in soil moisture conditions is important but also the soil moisture response to different precipitation characteristics. The latter, on the one hand, suggests that the representation of the land surface in modeling studies, especially the soil hydrology (including runoff), is of major importance for an adequate representation of land-atmosphere interactions and other atmospheric processes. On the other hand, the representation of convection can have far-reaching consequences for the representation of the hydrological cycle. For mid-Holocene North Africa, the formation of lakes and wetlands might be of high importance. We hypothesize that the higher amounts of runoff in explicitly resolved convection simulations compared to parameterized convection simulations potentially support the formation of more extended lakes and wetlands. Lakes and wetlands over North Africa are very likely to strongly amplify the vegetation/land-precipitation feedback and further extends the monsoonal rainbelt north (Specht et al., in peer-review).

B.5 ANALYSIS OF 10 KM SIMULATIONS

We analyze the effect of the horizontal resolution on our findings and present the results for the 10km parameterized (10km-P) and explicitly resolved convection (10km-E) simulations in the following. We show that the main mechanisms described for the 40km-P and the 5km-E simulations are also valid for the 10 km-P, and 10 km-E simulations. The results between simulations with the same representation of convection are more similar to each other than simulations with the same horizontal resolution. However, the results show that differences between the 10km-E and the 10km-P simulations are not as strong as between the 5km-E and the 40km-P simulation. We do find the characteristic precipitation-runoff-soil moisture mechanism that limits the soil moisture-precipitation feedback in the 10km-E DS and GS simulations but the difference in this coupling strength is not as strong. We argue that this is because, in the 10km-P simulation, the grid spacing already allows partly for explicit calculations of precipitation as compared to the 40km-P simulations. Therefore, precipitation intensity and runoff are more similar in the 10km-E and 10km-P simulations than in the 40km-P and the 5km-E simulations.

B.5.1 *Changes in vegetation, evapotranspiration and temperature*

Fig. B.12 shows dominantly similar responses of the surface variables in the 10km-P and 10km-E simulations compared to the 40km-P and 5km-E simulations, respectively. The meridional vegetation gradient (indicated by the NDVI) is identical to the 40km-P and the 5km-E simulations because it is prescribed in the external parameters. The increased vegetation cover leads to an increase in latent heat flux in both representations of convection. This increase is strongest over the Sahel and coincides with the strongest increase in vegetation. The temperature maximum over the north African continent decreases and shifts northward. This decrease in the temperature yields a decrease in the temperature gradient between the Sahara and the coastal regions of North Africa. These results are similar to the ones found in the main paper.

B.5.2 *Changes in precipitation*

In agreement with the results of the main Paper (Sec. B.3.1.2), precipitation in the GS simulations decrease over the coastal and strongly increases over the Sahel region. The decrease over the coastal region is consistent with the decrease in latent heat flux. The strongest increase in precipitation (Fig. B.13) occurs over the Sahel region, coinciding with the region of the strongest increase in evapotranspiration (Fig. B.12 c,d).

B.5.2.1 *Changes in atmospheric thermodynamics*

Changes in relative humidity in the 10km-P and the 10km-E simulation are consistent with the changes in the 40km-P and the 5km-E simulation, respectively. Relative

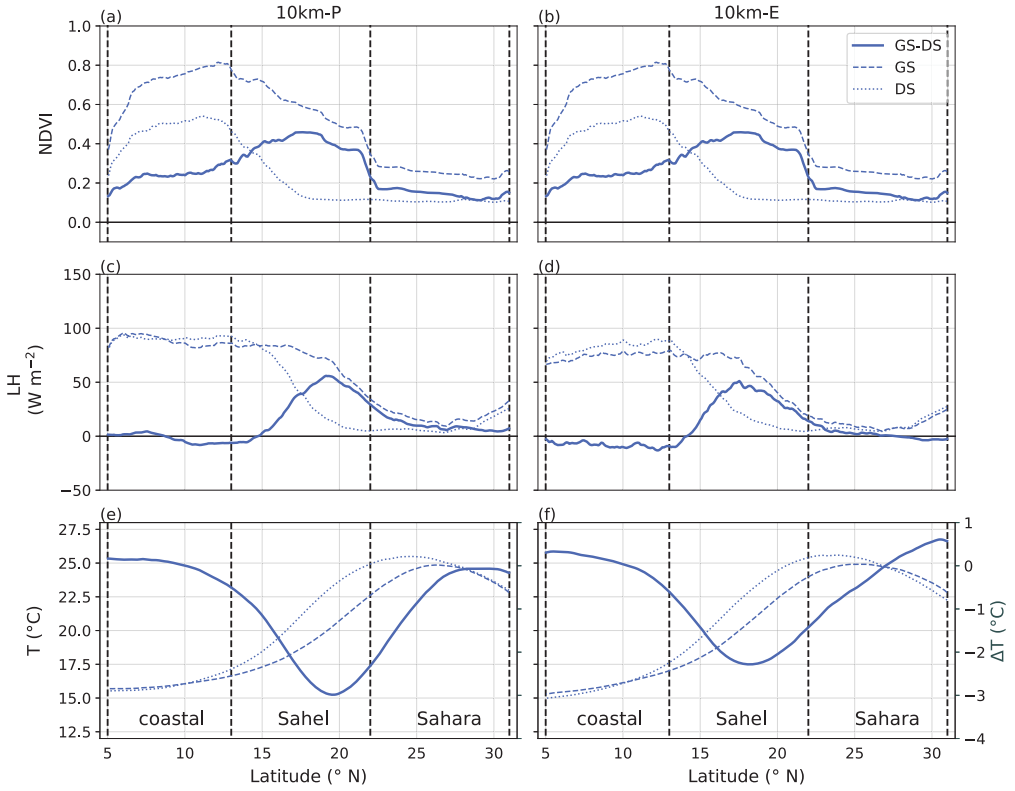

Figure B.12: The same as Fig. B.3 but for the 10km-P (a) and 10 km-E (b) simulations.

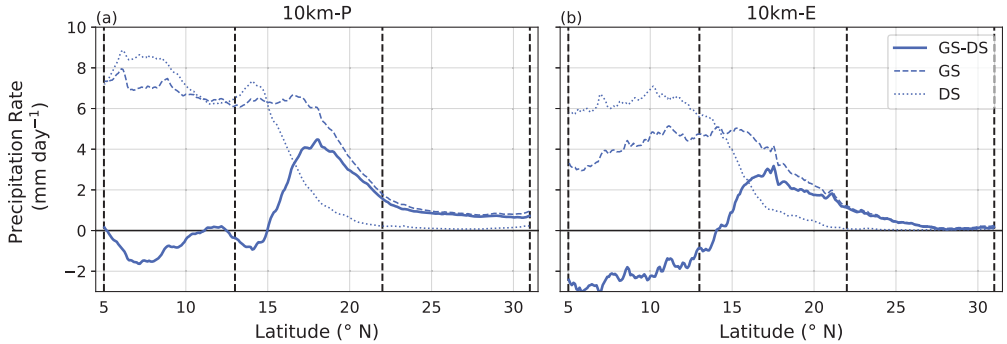

Figure B.13: The same as Fig. B.4 but for the 10km-P (a) and 10 km-E (b) simulations.

humidity reveals a strong increase over the Sahel and Sahara region, which is consistent with the changes in latent heat flux (Fig. B.12 c,d) and in precipitation (Fig. B.13). Again, it is likely that stronger convection in the GS simulations positively feeds back on the atmospheric humidity.

Table B.4 reveals that the stability of the atmosphere becomes more supportive for convection and precipitation in the GS compared to the DS simulations in both representations of convection. Over the coastal region, conditions for convection and precipitation are very supportive, with high CAPE and cloud cover and low (weak negative) CIN and LFC values. The decrease in CAPE over the coastal region in the GS simulations is consistent with the decrease in precipitation (Fig. B.13). Over the Sahel region, CAPE and cloud cover increase, resulting in higher precipitation rates over the region. Over the Sahara region, conditions for convection are unsupportive.

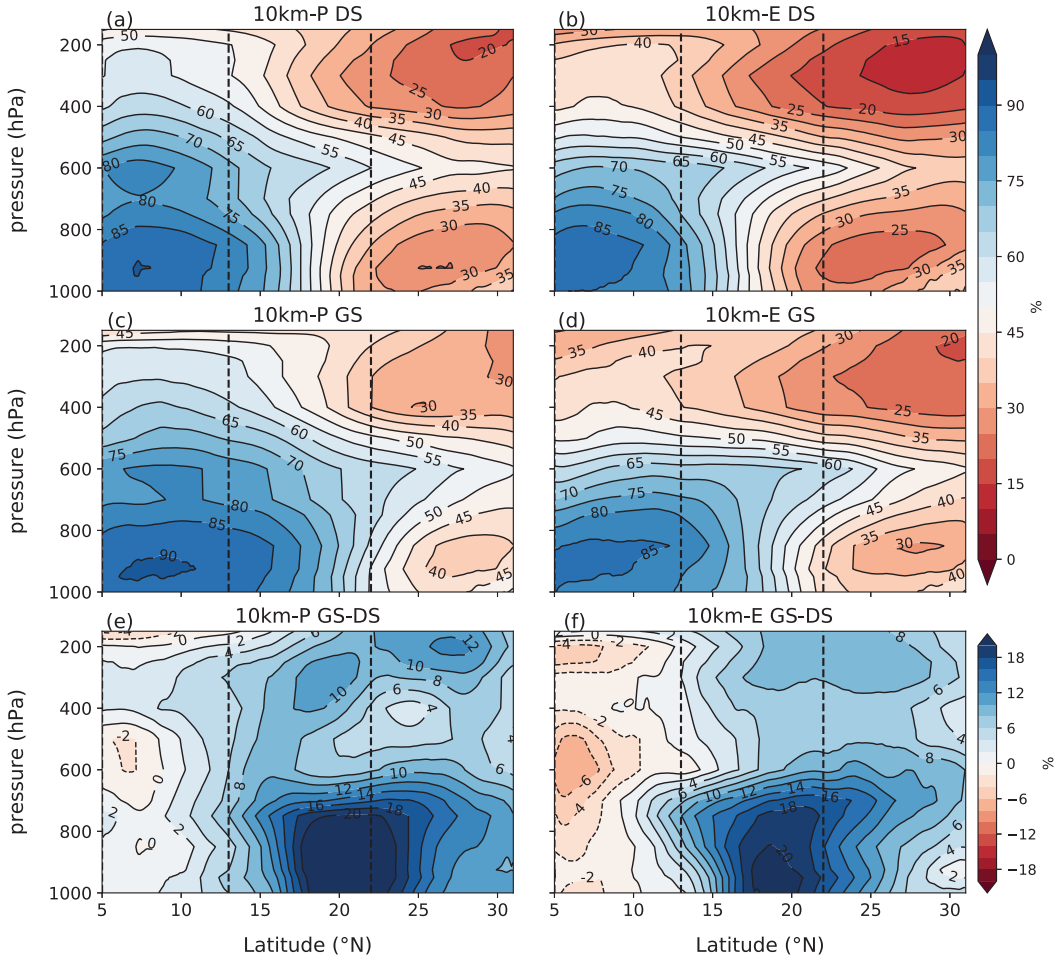

Figure B.14: JAS-mean meridional vertical crosssection of relative humidity for the 40km-P DS (a) and GS (c) simulation, the 5km-E DS (b) and GS (d) simulation and the difference between the GS and DS simulation for the 40km-P (e) and the 5km-E (f) simulations. The average is calculated over the WA-Domain outlined in Fig. B.1).

B.5.3 *Changes in atmospheric dynamics*

The AEJ (Fig. B.15) strongly weakens in the GS simulations and shift 3-4° northward. The weakening and northward shift of the AEJ are consistent with the higher rainfall rates over the Sahel-Sahara region in the GS simulations (Grist and Nicholson, 2001; Nicholson and Grist, 2001).

With the shift in the AEJ, the region of upward motion between the axes of the TEJ and the AEJ broaden/shift northward. In both representations of convection, the vertical upward motion decreases in the coastal and southern Sahel region and intensifies over the rest of the Sahel region. Furthermore, the descending motion over the Sahara decrease in the GS compared to the DS simulations. These results are consistent with the changes in relative humidity (Fig. B.14) and precipitation (Fig. B.13).

The low-level, southwesterly monsoon intensifies as a response to the increased vertical motion over the Sahel (due to increased energy at the surface and by the increase of vertical motion between the jet axes). With the strengthened monsoon

		10 km-P DS	10 km-P GS	10 km-E DS	10 km-E GS
coastal	CAPE ($J\,kg^{-1}$)	641.5	505.0	818.5	567.9
	CIN ($J\,kg^{-1}$)	-30.7	-22.8	-31.0	-31.2
	LFC (m)	738	654	945	1000
	cloud cover (%)	88	91	79	78
sahel	CAPE ($J\,kg^{-1}$)	309.6	390.6	162.6	300.2
	CIN ($J\,kg^{-1}$)	-257.6	-291.2	-128.1	-199.2
	LFC (m)	2253	1365	2648	1902
	cloud cover (%)	48	74	34	57
sahara	CAPE ($J\,kg^{-1}$)	0.8	13.01	0.0	0.7
	CIN ($J\,kg^{-1}$)	-43.7	-83.3	0.0	-4.3
	LFC (m)	3508	22692	3203	2907
	cloud cover (%)	18	37	17	33

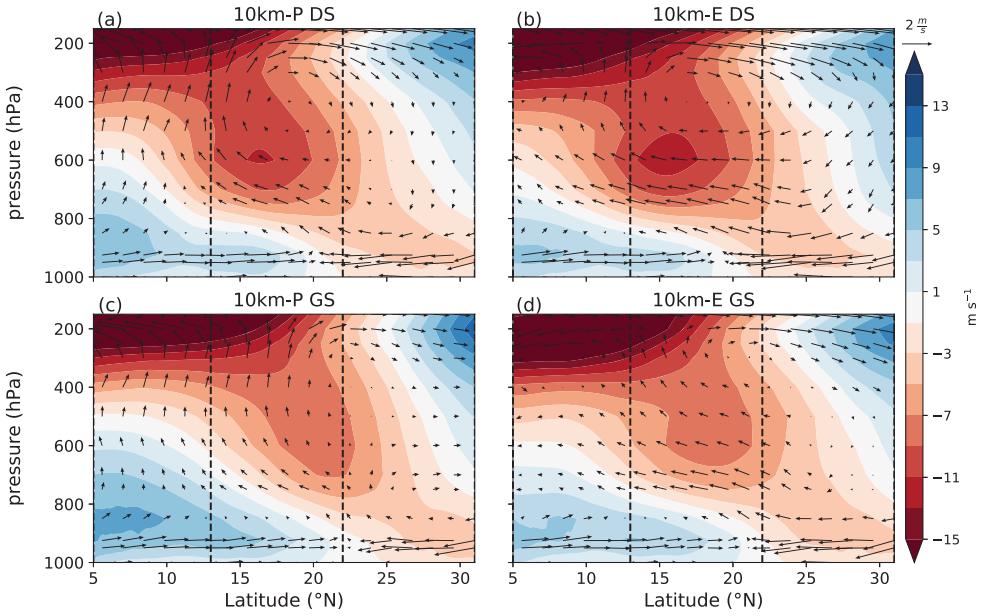

Figure B.15: The same as Fig. B.6 but for the 10km-P (a,c) and 10 km-E (b,d) simulations.

flow, the ITF shifts further north and thereby the region of dynamical uplifting that is associated with the ITF. Additionally, the descending motion over the Sahara strongly reduces.

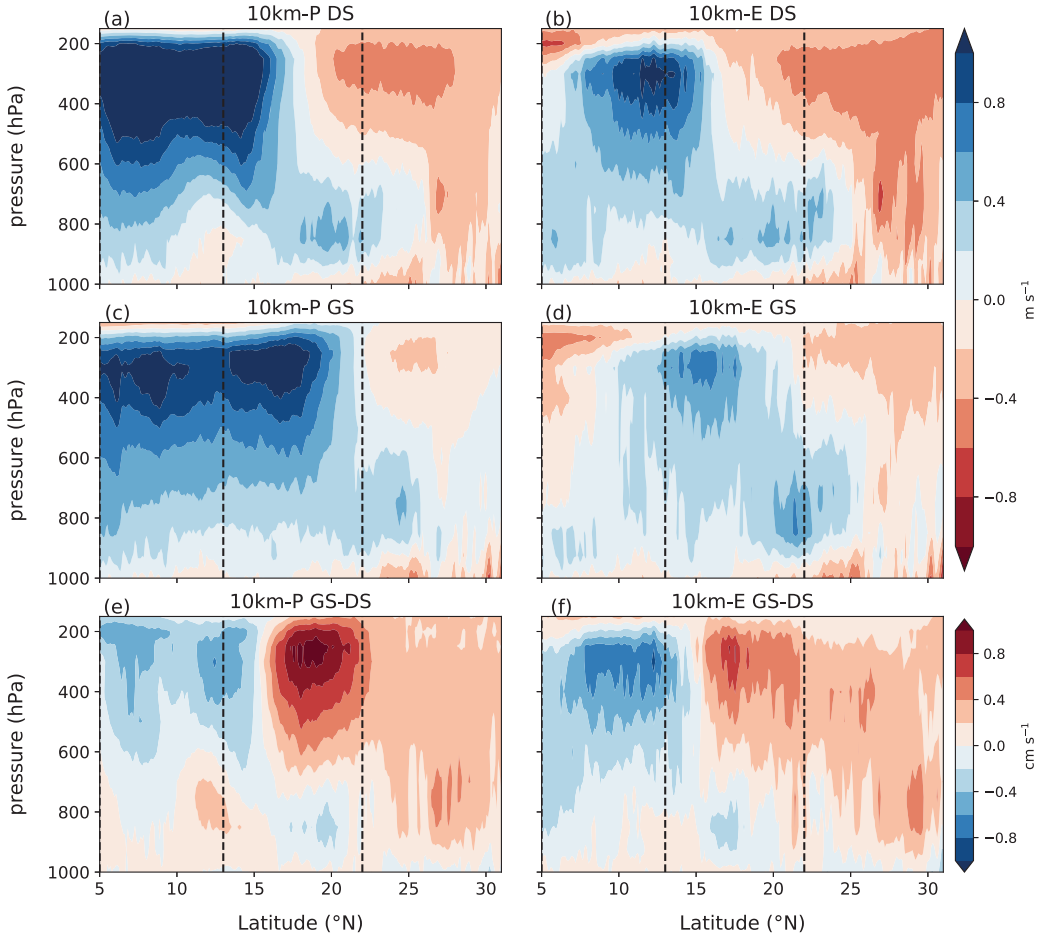

Figure B.16: JAS-mean meridional vertical crosssection of vertical velocity for the 10km-P DS (a) and GS (c) simulation, the 10km-E DS (b) and GS (d) simulation and the difference between the GS and DS simulation for the 10km-P (e) and the 10km-E (f) simulations. Positive values indicate upward motion. The average is calculated over the WA-Domain outlined in Fig. B.1). Note the different colorscale in panel e and f.

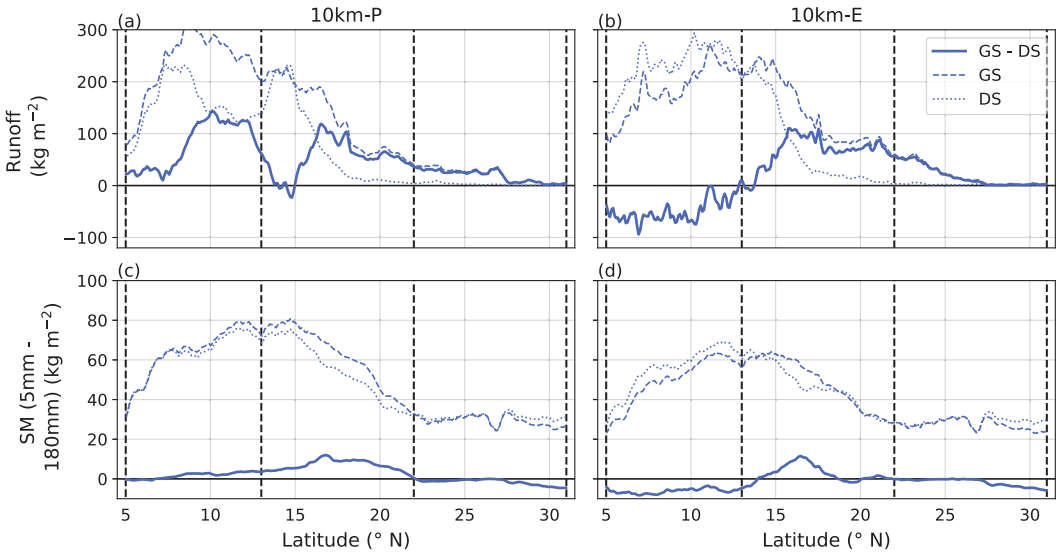

Figure B.17: The same as Fig. B.8 but for the 10km-P (a,c) and 10 km-E (b,d) simulations.

The increase in atmospheric moistening, the described changes in the thermodynamics and dynamics imply more supportive conditions for convection and precipitation to develop. However, similarly to the findings in the main paper, the shift of precipitation from the coastal to the Sahel region indicates higher importance of the dynamical rather than the thermodynamical feedbacks. The results reveal a positive land-atmosphere coupling and are consistent with the findings in the main paper.

B.5.4 *Positive land-atmosphere feedbacks but with different strength - differences between 10km-P and 10km-E simulations*

We now focus on the different strengths of the land-atmosphere coupling between the 10km-P and the 10km-E simulations.

Fig. B.12 and Fig. B.13 shows that changes in latent heat flux and precipitation are higher, especially north of about 17°N in the 10km-P GS compared to the 10km-E GS simulations, despite the same increase in vegetation cover. However, the difference in latent heat flux and precipitation between the 10km-P and the 10km-E simulations is less pronounced compared to the 40km-P and the 5km-E simulations.

Over the coastal region and up to about 20°N, precipitation is noticeably higher in the 10km-P than in the 10km-E simulations. However, north of 20°N differences between both representations of convection are smaller. We argue that this is because the precipitation intensity in this region (north of 20°N) is relatively equal between both representations of convection. This is potentially a result of the parametrization scheme, which, at 10km horizontal resolution, already generates some precipitation via the explicit calculations and slightly less via the parametrization scheme. Therefore, precipitation in the 10km-P simulations has more characteristics from the explicitly resolved convection simulations, than the 40km-P simulations.

Differences in the runoff between the 10km-P and the 10km-E simulations are smaller over the Sahel and Sahara region as compared to the 40km-P and the 5km-E simulations. However, over the coastal region, the runoff reveals stronger differences

in the 10km-P simulations compared to the 40km-P simulations. The 10km-P DS simulation shows a similar meridional runoff distribution as the 40km-P DS simulation with a double peak in the coastal and Sahel region and a sharp decrease in runoff north of about 13°N. In the GS simulations, however, the parameterized convection simulations show different behavior. The 40km-P GS simulation displays similar amounts of runoff as in the 40km-P DS simulation with only slightly modified meridional runoff distribution. In contrast, the 10km-P GS simulation shows a strong increase in runoff in the coastal region compared to the 10km-DS simulation. We argue that this strong increase in runoff can be attributed to the fact, that water infiltration is an extremely non-linear function of soil moisture. The soil moisture content in the 10km-P GS simulations is very high, especially over the coastal region (Fig. B.17 c,d). Water infiltration strongly increases the wetter the soil and goes into groundwater runoff. This causes the runoff to increase, although precipitation does not increase as strongly.

The 10km-E DS and GS simulations behave similarly to the 5km-E DS and GS simulations. Both show generally high amounts of runoff over the coastal region and a slight decrease in the GS compared to the DS simulation. Over the Sahel and Sahara region runoff increases in the 10km-E GS simulations, similar to the results from the 5km-E GS simulations.

Based on these results, we argue that the precipitation-runoff-soil moisture mechanisms also exist in the 10km-E simulations but is less pronounced as compared to the 5km-E simulations.

Generally, the 10km-P simulations show higher relative humidity values throughout the troposphere and overall latitudes as well as a stronger upward transport of moisture compared to the 10km-E simulations. The increase in relative humidity over the Sahel-Sahara region between the GS and the DS simulation is more pronounced in the 10km-P GS than in the 10km-E GS simulation. Conditions for convection and precipitation are overall more supportive in the 10km-P simulations. However, differences in CAPE between the 10km-P GS and the 10km-E GS simulation are smaller than between the 40km-P GS and the 5km-E GS simulation.

The AEJ in the 10km-P and the 10km-E GS simulations is similarly strong with about $8.2\,\mathrm{m\,s^{-1}}$. However, the AEJ is located further north in the 10km-P GS compared to the 10km-E GS simulations. The associated upward vertical motion between axes of the AEJ and the Tropical easterly jet is generally stronger in the 10km-P than in the 10km-E simulations (Fig. B.16).

Similar to the 40km-P simulations, the southwesterly monsoon flow is stronger and the monsoon layer is deeper in the 10km-P compared to the 10km-E simulations. Therefore, the ITF is located further north and more cool, moist air is transported further north into the African continent.

Consistently with the findings in the main paper, both representations of convection simulate a positive land-atmosphere coupling. This land-atmosphere coupling is stronger in the 10km-P simulations compared to the 10km-E simulations. However, differences tend to be smaller (e.g. in latent heat flux, precipitation, AEJ strength, runoff). We suggest that this is because the differences in the precipitation intensity between the 10km-P and the 10km-E simulations are smaller and thereby differences in runoff are smaller. Consequently, the precipitation-runoff-soil moisture mechanism is not as pronounced in the 10km-E compared to the 10km-P simulations.

B.5.5 *The influence of runoff-controlled soil moisture*

We now analyze the differences between the 10km GS and GS-cSM simulations.

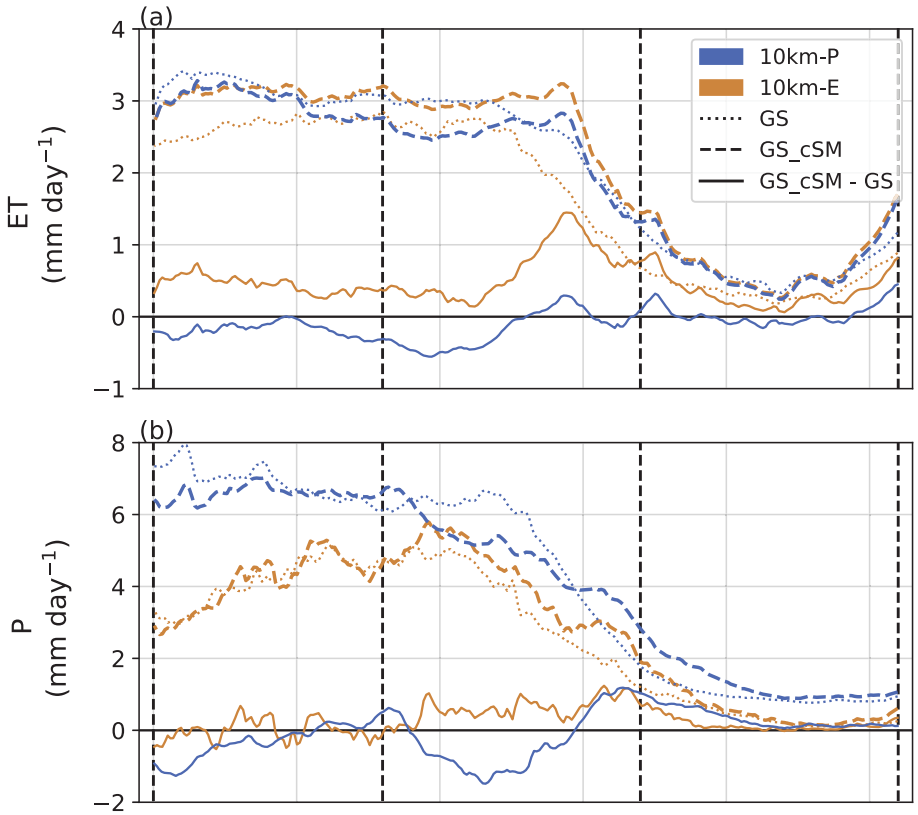

Figure B.18: JAS-mean meridional distribution of evapotranspiration (a) and precipitation (b) for the 10km-P (blue lines) and the 10km-E (orange lines) and for the GS simulations (dotted lines), the GS-cSM simulations (dashed lines) and the difference between the GS-cSM and the GS simulations (solid lines), respectively. The average is taken over the WA-Domain outlined in Fig. B.1.

The differences in soil moisture, evapotranspiration, and precipitation between the 10km-E and the 10km-E simulations are not as pronounced as between the 5km-E and the 40km-P simulations. Monsoonal precipitation in the 10km-P GS-cSM simulations remains higher in the whole WA-Domain compared to the 10km-E GS-cSM simulation in contrast to the results in the main paper. Fig. B.18 nevertheless demonstrates that changes in the 10km-E GS-cSM compared to the GS simulation are more pronounced. Especially the strong increase in evapotranspiration over the whole WA-Domain and increased precipitation over the Sahel and southern Sahara region is stronger in the 10km-E GS-cSM than in the 10km-P GS-cSM simulation.

However, despite only weak increases in evapotranspiration, precipitation shows a similarly strong increase over the northern Sahel and the southern Sahara region in the 10km-P GS-cSM as in the 10km-E GS-cSM simulations.

B.5.5.1 *Influence on atmospheric thermodynamics*

The strongest increase in relative humidity (not shown) in the 10km-E GS-cSM simulation occurs over the Sahel-Sahara region. This increase coincides with the

increase in evapotranspiration and is more pronounced than in the 10km-P GS-cSM simulation.

		40 km-P GS	40 km-P cSM	5 km-E GS	5 km-E cSM
coastal	CAPE ($J\,kg^{-1}$)	505.0	423.8	567.9	792.4
	CIN ($J\,kg^{-1}$)	-22.8	-24.1	-31.2	-17.3
	LFC (m)	654	748	1000	781
	cloud cover (%)	91	90	78	79
sahel	CAPE ($J\,kg^{-1}$)	390.6	349.7	300.2	721.3
	CIN ($J\,kg^{-1}$)	-128.1	-92.27	-199.23	-84.72
	LFC (m)	1365	1076	1902	1269
	cloud cover (%)	74	76	57	66
sahara	CAPE ($J\,kg^{-1}$)	13.0	16.0	0.74	5.49
	CIN ($J\,kg^{-1}$)	-83.3	-119.52	-4.26	-77.35
	LFC (m)	2692	2448	2907	2730
	cloud cover (%)	37	41	33	38

Table B.5: The same as Table **??** but for the 10km-P and 10km-E simulations.

The changes in CAPE, CIN, LFC height, and cloud cover between the GS-cSM and the GS simulations are stronger in the 10km-E than in the 10km-P simulations and further support the increase in precipitation in the 10km-E GS-cSM simulation. In the 10km-P GS-cSM simulation, CAPE decreases slightly over the Sahel region, but CIN values, LFC height, and cloud cover support the still higher precipitation rates in the 10km-P GS-cSM compared to the 10km-E GS-cSM simulations. Differences in the thermodynamics of the atmosphere between the 10km-P and the 10km-E simulations are weaker as between the 40km-P and the 5km-E simulations. Nevertheless, they reflect a noticeable influence of soil moisture on the atmosphere.

B.5.5.2 *Influence on atmospheric dynamics*

The AEJ strength (Fig. B.19 c,d) is equally strong in both the 10km-E and the 10km-P GS-cSM simulation. However, the AEJ core again shifts about 1° further north in the 10km-E GS-cSM simulation to about the same location as in the 10km-P GS-cSM simulation. Generally, dynamic changes in the 10km-E GS-cSM to the GS simulation are more pronounced as compared to no remarkable changes in the 10km-P simulations.

South of about 20°N the differences in vertical upward motion between the 10km-E GS-cSM and the 10km-P GS-cSM simulation are similar to those in the 40km-P GS-cSM and the 5km-E GS-cSM simulation, respectively. Vertical upward motion is substantially stronger in the 10km-P GS-cSM simulation than in the 10km-E GS-cSM simulation.

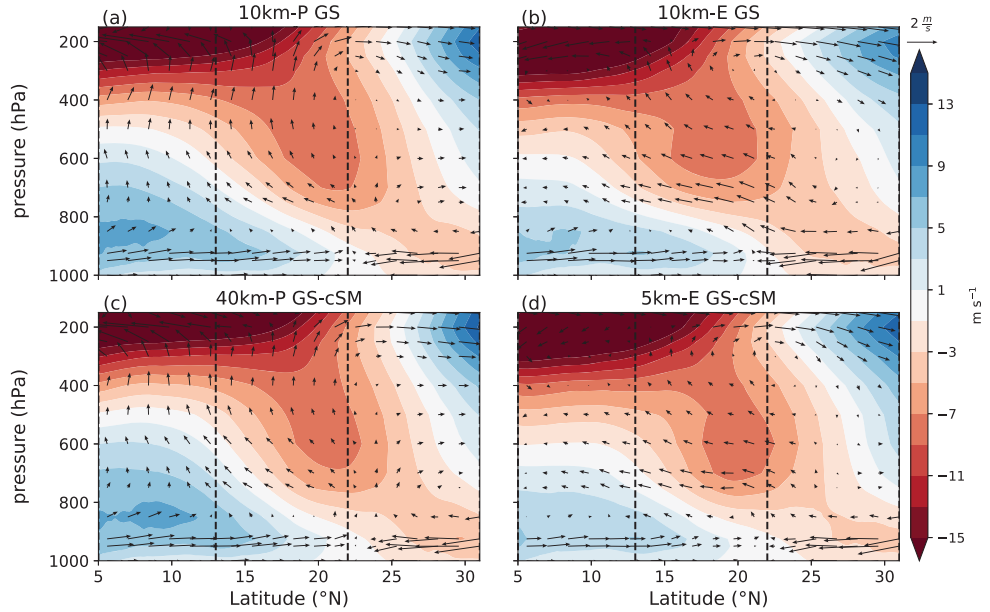

Figure B.19: The same as Fig. B.6 but for the 10km-P (a,c) and 10 km-E (b,d) simulations.

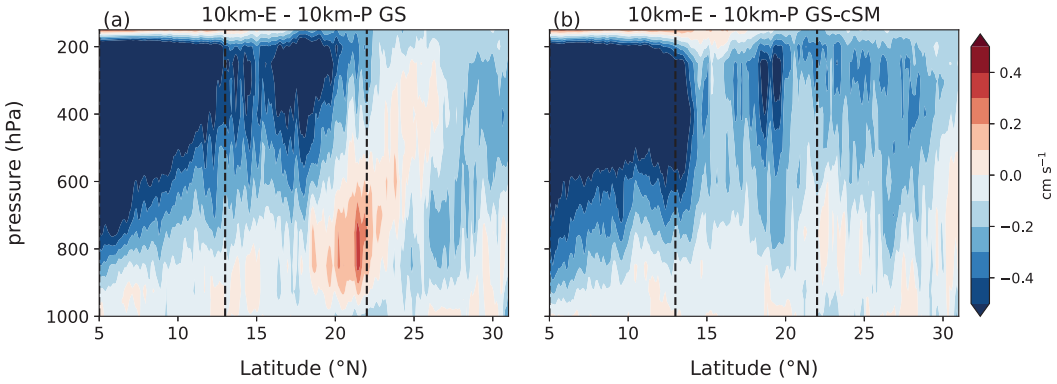

Figure B.20: The same as Fig. B.11 but for the 10km-P (a) and 10 km-E (b) simulations.

North of 20°N, the difference in vertical upward motion between the 10km-P GS-cSM and 10km-E GS-cSM simulation becomes apparent and is contrasting to the difference between the 40km-P GS-cSM and the 5km-E GS-cSM simulation. Vertically upward motion remains stronger in the 10km-P GS-cSM simulations over the whole WA-Domain. Additionally, the descending motion over the Sahara region (north of about 25°N and above 800hPa) is weaker in the 10km-P GS-cSM than in the 10km-E GS-cSM simulation. This could be a result of the higher convective activity in the 10km-P simulations.

In summary, the 10km-P and 10km-E simulations also show positive land-atmosphere feedbacks. However, the differences in coupling strength are not as pronounced as between the 40km-P and the 5km-E simulations. We argue that this is

because the horizontal resolution in the 10km-P simulations already allows for partly explicit calculations of convective processes. Thus, the precipitation characteristics and therefore the runoff in the 10km-P simulations are more similar to the 10km-E simulations than in simulations between the 40km-P and the 5km-E simulations. However, the comparison between the GS and the GS-cSM simulations reveals a considerable influence of the runoff (i.e of soil moisture) on the atmospheric state, hence on precipitation.

Fig. B.21 additionally shows estimates of JAS-mean precipitation reconstructions of mid-Holocene North Africa based on Bartlein et al. (2011). This gives an impression on the model performance compared to proxy data. We use the dataset of Bartlein et al. (2011) which provides mean annual precipitation anomalies between the mid-Holocene and pre-industrial period. To compare the reconstructions to our analysis, we need to estimate the JAS-mean precipitation from the reconstructions. To estimate absolute mid-Holocene daily-mean JAS precipitation rates we use the CRU (Climatic Research Unit) dataset spanning the period from 1961 to 1990. Firstly, from the CRU dataset, we calculate the mean ratio of the JAS precipitation to the annual precipitation. Secondly, we scale the reconstructed, annual mean precipitation anomalies with the JAS-ratio. Thirdly, we sum the scaled JAS precipitation from the reconstructions with the JAS precipitation from the CRU dataset to obtain an estimate of the JAS-mean, mid-Holocene precipitation rate.

The estimation of reconstructed precipitation (Sec. **??**) indicates that the 40km-P GS simulation shows good agreement in terms of the mean meridional precipitation distribution over the coastal and Sahel region. The 5km-E GS simulation seems to underestimate mid-Holocene precipitation rates. However, the comparison to these reconstructions should be considered only as a rough estimate and taken with care. First, we just estimated the JAS-mean precipitation from the reconstructions based on pre-industrial ratios, which could have been different during the mid-Holocene. Secondly, the reconstruction sides that are available and which match our analysis domain are very few (16 sites). Therefore, the comparison of our model data with the meridional mean of only 16 reconstruction sites can only serve as an estimation rather than a robust statement about the performance of our mid-Holocene simulations. In Appendix **??** Fig. B.22 we provide a geographical map of our modeled precipitation and the JAS-mean estimated precipitation at the reconstruction sites. In this map, the 5km-E GS simulations indicate a higher agreement with the reconstruction data as compared to the meridional mean distribution.

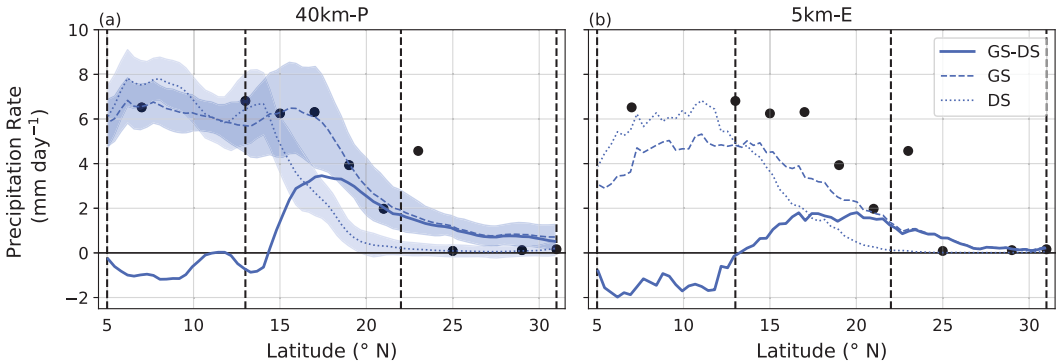

Figure B.21: The same as Fig. B.4 but included are estimates from JAS daily-mean precipitation precipitation reconstructions (black dots) based on Bartlein et al. (2011).

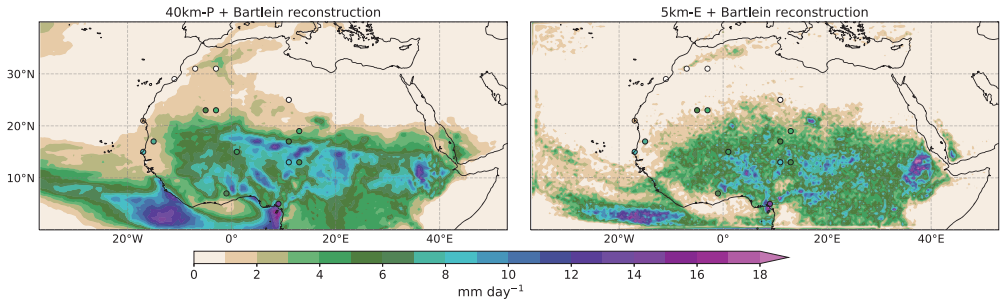

Figure B.22: Map of JAS-mean precipitation rate (shading) for the 40km-P GS (a) and the 5km-E GS (b) simulation, respectively. The dots display the location of the reconstructions sites (Bartlein et al., 2011). The dots color indicate the estimated, reconstructed JAS-mean precipitation rate (see Sec. B.3.1.2 for exact explanation.

BIBLIOGRAPHY

Burpee, Robert W (1972). "The origin and structure of easterly waves in the lower troposphere of North Africa." *Journal of the Atmospheric Sciences* 29.1, pp. 77–90.

Charney, Jule, Peter H Stone, and William J Quirk (1975). "Drought in the Sahara: a biogeophysical feedback mechanism." *Science* 187.4175, pp. 434–435.

Charney, Jule G (1975). "Dynamics of deserts and drought in the Sahel." *Quarterly Journal of the Royal Meteorological Society* 101.428, pp. 193–202.

Rennick, Mary Alice (1976). "The generation of African waves." *Journal of Atmospheric Sciences* 33.10, pp. 1955–1969.

Ripley, EA, Jule Charney, Peter H Stone, and William J Quirk (1976). "Drought in the Sahara: Insufficient biogeophysical feedback?" *Science* 191.4222, pp. 100–102.

Simmons, AJ (1977). "A note on the instability of the African easterly jet." *Journal of Atmospheric Sciences* 34.10, pp. 1670–1674.

Berger, AndréL (1978). "Long-term variations of daily insolation and Quaternary climatic changes." *Journal of Atmospheric Sciences* 35.12, pp. 2362–2367.

Kutzbach, John E (1981). "Monsoon climate of the early Holocene: climate experiment with the earth's orbital parameters for 9000 years ago." *Science* 214.4516, pp. 59–61.

Kutzbach, JE and BL Otto-Bliesner (1982). "The sensitivity of the African-Asian monsoonal climate to orbital parameter changes for 9000 years BP in a low-resolution general circulation model." *Journal of the Atmospheric Sciences* 39.6, pp. 1177–1188.

Cunnington, WM and PR Rowntree (1986). "Simulations of the Saharan atmosphere—dependence on moisture and albedo." *Quarterly Journal of the Royal Meteorological Society* 112.474, pp. 971–999.

Kutzbach, John E and Peter J Guetter (1986). "The influence of changing orbital parameters and surface boundary conditions on climate simulations for the past 18 000 years." *Journal of atmospheric sciences* 43.16, pp. 1726–1759.

Sud, YC and A Molod (1988). "A GCM simulation study of the influence of Saharan evapotranspiration and surface-albedo anomalies on July circulation and rainfall." *Monthly Weather Review* 116.11, pp. 2388–2400.

Druyan, Leonard M and Randal D Koster (1989). "Sources of Sahel precipitation for simulated drought and rainy seasons." *Journal of Climate* 2.12, pp. 1438–1446.

Kwon, H Joe (1989). "A reexamination of the genesis of African waves." *Journal of Atmospheric Sciences* 46.24, pp. 3621–3631.

Tiedtke, MICHAEL (1989). "A comprehensive mass flux scheme for cumulus parameterization in large-scale models." *Monthly weather review* 117.8, pp. 1779–1800.

Rowell, DP and C Blondin (1990). "The influence of soil wetness distribution on short-range rainfall forecasting in the West African Sahel." *Quarterly Journal of the Royal Meteorological Society* 116.496, pp. 1471–1485.

Street-Perrott, FA, JFB Mitchell, DS Marchand, and JS Brunner (1990). "Milankovitch and albedo forcing of the tropical monsoons: a comparison of geological evi-

dence and numerical simulations for 9000 yBP." *Earth and Environmental Science Transactions of The Royal Society of Edinburgh* 81.4, pp. 407–427.
Moncrieff, Mitchell W (1992). "Organized convective systems: Archetypal dynamical models, mass and momentum flux theory, and parametrization." *Quarterly Journal of the Royal Meteorological Society* 118.507, pp. 819–850.
Houze, R (1993). *Cloud Dynamics*.
Xue, Yongkang and Jagadish Shukla (1993). "The influence of land surface properties on Sahel climate. Part 1: desertification." *Journal of climate* 6.12, pp. 2232–2245.
Lare, AR and SE Nicholson (1994). "Contrasting conditions of surface water balance in wet years and dry years as a possible land surface-atmosphere feedback mechanism in the West African Sahel." *Journal of Climate* 7.5, pp. 653–668.
Thorncroft, CD and BJ Hoskins (1994a). "An idealized study of African easterly waves. I: A linear view." *Quarterly Journal of the Royal Meteorological Society* 120.518, pp. 953–982.
Thorncroft, CD and BJ Hoskins (1994b). "An idealized study of African easterly waves. II: A nonlinear view." *Quarterly Journal of the Royal Meteorological Society* 120.518, pp. 983–1015.
Kutzbach, J, G Bonan, J Foley, and SP Harrison (1996). "Vegetation and soil feedbacks on the response of the African monsoon to orbital forcing in the early to middle Holocene." *Nature* 384.6610, pp. 623–626.
Savenije, Hubert HG (1996). "The runoff coefficient as the key to moisture recycling." *Journal of Hydrology* 176.1-4, pp. 219–225.
Xue, Yongkang and Jagadish Shukla (1996). "The influence of land surface properties on Sahel climate. Part II. Afforestation." *Journal of Climate* 9.12, pp. 3260–3275.
Yu, G and SP Harrison (1996). "An evaluation of the simulated water balance of Eurasia and northern Africa at 6000 y BP using lake status data." *Climate Dynamics* 12.11, pp. 723–735.
Claussen, Martin and Veronika Gayler (1997). "The greening of the Sahara during the mid-Holocene: results of an interactive atmosphere-biome model." *Global Ecology and Biogeography Letters*, pp. 369–377.
Hall, Nicholas MJ and Paul J Valdes (1997). "A GCM simulation of the climate 6000 years ago." *Journal of Climate* 10.1, pp. 3–17.
Kutzbach, John E and Z Liu (1997). "Response of the African monsoon to orbital forcing and ocean feedbacks in the middle Holocene." *Science* 278.5337, pp. 440–443.
Texier, D, N De Noblet, SP Harrison, A Haxeltine, D Jolly, S Joussaume, F Laarif, IC Prentice, and P Tarasov (1997). "Quantifying the role of biosphere-atmosphere feedbacks in climate change: coupled model simulations for 6000 years BP and comparison with palaeodata for northern Eurasia and northern Africa." *Climate Dynamics* 13.12, pp. 865–881.
Broström, Anna, Michael Coe, Sandy P Harrison, Robert Gallimore, JE Kutzbach, John Foley, IC Prentice, and Pat Behling (1998). "Land surface feedbacks and palaeomonsoons in northern Africa." *Geophysical Research Letters* 25.19, pp. 3615–3618.
Ganopolski, Andrey, Claudia Kubatzki, Martin Claussen, Victor Brovkin, and Vladimir Petoukhov (1998). "The influence of vegetation-atmosphere-ocean interaction on climate during the mid-Holocene." *Science* 280.5371, pp. 1916–1919.

Harrison, SP, D Jolly, F Laarif, A Abe-Ouchi, B Dong, K Herterich, C Hewitt, S Joussaume, JE Kutzbach, J Mitchell, et al. (1998). "Intercomparison of simulated global vegetation distributions in response to 6 kyr BP orbital forcing." *Journal of Climate* 11.11, pp. 2721–2742.

Hewitt, Chris D and John FB Mitchell (1998). "A fully coupled GCM simulation of the climate of the mid-Holocene." *Geophysical Research Letters* 25.3, pp. 361–364.

Jolly, Dominique, I Colin Prentice, Raymonde Bonnefille, Aziz Ballouche, Martin Bengo, Patrice Brenac, Guillaume Buchet, David Burney, Jean-Pierre Cazet, Rachid Cheddadi, et al. (1998). "Biome reconstruction from pollen and plant macrofossil data for Africa and the Arabian peninsula at 0 and 6000 years." *Journal of Biogeography* 25.6, pp. 1007–1027.

Braconnot, P, S Joussaume, O Marti, and N De Noblet (1999). "Synergistic feedbacks from ocean and vegetation on the African monsoon response to mid-Holocene insolation." *Geophysical Research Letters* 26.16, pp. 2481–2484.

Cook, Kerry H (1999). "Generation of the African easterly jet and its role in determining West African precipitation." *Journal of climate* 12.5, pp. 1165–1184.

Joussaume, S, KE Taylor, PJFB Braconnot, JFB Mitchell, JE Kutzbach, SP Harrison, IC Prentice, AJ Broccoli, A Abe-Ouchi, PJ Bartlein, et al. (1999). "Monsoon changes for 6000 years ago: results of 18 simulations from the Paleoclimate Modeling Intercomparison Project (PMIP)." *Geophysical Research Letters* 26.7, pp. 859–862.

Schär, Christoph, Daniel Lüthi, Urs Beyerle, and Erdmann Heise (1999). "The soil–precipitation feedback: A process study with a regional climate model." *Journal of Climate* 12.3, pp. 722–741.

Thorncroft, CD and M Blackburn (1999). "Maintenance of the African easterly jet." *Quarterly Journal of the Royal Meteorological Society* 125.555, pp. 763–786.

Braconnot, P, S Joussaume, N De Noblet, and G Ramstein (2000). "Mid-Holocene and last glacial maximum African monsoon changes as simulated within the paleoclimate modelling intercomparison project." *Global and planetary change* 26.1-3, pp. 51–66.

Doherty, Ruth, J Kutzbach, J Foley, and D Pollard (2000). "Fully coupled climate/-dynamical vegetation model simulations over Northern Africa during the mid-Holocene." *Climate Dynamics* 16.8, pp. 561–573.

Prentice, I Colin, Dominique Jolly, and Biome 6000 Participants (2000). "Mid-Holocene and glacial-maximum vegetation geography of the northern continents and Africa." *Journal of biogeography* 27.3, pp. 507–519.

Grist, Jeremy P and Sharon E Nicholson (2001). "A study of the dynamic factors influencing the rainfall variability in the West African Sahel." *Journal of climate* 14.7, pp. 1337–1359.

Nicholson, Sharon E and JP Grist (2001). "A conceptual model for understanding rainfall variability in the West African Sahel on interannual and interdecadal timescales." *International Journal of Climatology: A Journal of the Royal Meteorological Society* 21.14, pp. 1733–1757.

Yang, Gui-Ying and Julia Slingo (2001). "The diurnal cycle in the tropics." *Monthly Weather Review* 129.4, pp. 784–801.

Diongue, A, J-P Lafore, J-L Redelsperger, and R Roca (2002). "Numerical study of a Sahelian synoptic weather system: Initiation and mature stages of convection and its interactions with the large-scale dynamics." *Quarterly Journal of the Royal*

Meteorological Society: A journal of the atmospheric sciences, applied meteorology and physical oceanography 128.584, pp. 1899–1927.

Grist, Jeremy P (2002). "Easterly waves over Africa. Part I: The seasonal cycle and contrasts between wet and dry years." *Monthly Weather Review* 130.2, pp. 197–211.

Mass, Clifford F, David Ovens, Ken Westrick, and Brian A Colle (2002). "Does increasing horizontal resolution produce more skillful forecasts?: The Results of Two Years of real-Time Numerical Weather Prediction over the Pacific Northwest." *Bulletin of the American Meteorological Society* 83.3, pp. 407–430.

Mathon, Vincent, Henri Laurent, and Thierry Lebel (2002). "Mesoscale convective system rainfall in the Sahel." *Journal of applied meteorology* 41.11, pp. 1081–1092.

Redelsperger, J-L, A Diongue, A Diedhiou, J-P Ceron, M Diop, J-F Gueremy, and J-P Lafore (2002). "Multi-scale description of a Sahelian synoptic weather system representative of the West African monsoon." *Quarterly Journal of the Royal Meteorological Society: A journal of the atmospheric sciences, applied meteorology and physical oceanography* 128.582, pp. 1229–1257.

Bader, Jürgen and Mojib Latif (2003). "The impact of decadal-scale Indian Ocean sea surface temperature anomalies on Sahelian rainfall and the North Atlantic Oscillation." *Geophysical Research Letters* 30.22.

Giannini, Alessandra, R Saravanan, and Ping Chang (2003). "Oceanic forcing of Sahel rainfall on interannual to interdecadal time scales." *Science* 302.5647, pp. 1027–1030.

Nicholson, Sharon E and Jeremy P Grist (2003). "The seasonal evolution of the atmospheric circulation over West Africa and equatorial Africa." *Journal of climate* 16.7, pp. 1013–1030.

Randall, David, Marat Khairoutdinov, Akio Arakawa, and Wojciech Grabowski (2003). "Breaking the cloud parameterization deadlock." *Bulletin of the American Meteorological Society* 84.11, pp. 1547–1564.

Sultan, Benjamin, Serge Janicot, and Arona Diedhiou (2003). "The West African monsoon dynamics. Part I: Documentation of intraseasonal variability." *Journal of Climate* 16.21, pp. 3389–3406.

Braconnot, Pascale, Sandy P Harrison, Sylvie Joussaume, Chris D Hewitt, Akio Kitoch, John E Kutzbach, Zhengyu Liu, Bette Otto-Bliesner, Jozef Syktus, and SL Weber (2004). "Evaluation of PMIP coupled ocean-atmosphere simulations of the Mid-Holocene." In: *Past climate variability through Europe and Africa*. Springer, pp. 515–533.

Holton, James R (2004). "An introduction to dynamic meteorology Fourth edition." *Department of Atmo*.

Levis, Samuel, Gordon B Bonan, and Céline Bonfils (2004). "Soil feedback drives the mid-Holocene North African monsoon northward in fully coupled CCSM2 simulations with a dynamic vegetation model." *Climate Dynamics* 23.7-8, pp. 791–802.

Liu, Z, SP Harrison, J Kutzbach, and B Otto-Bliesner (2004). "Global monsoons in the mid-Holocene and oceanic feedback." *Climate Dynamics* 22.2-3, pp. 157–182.

Colle, Brian A, Justin B Wolfe, W James Steenburgh, David E Kingsmill, Justin AW Cox, and Jason C Shafer (2005). "High-resolution simulations and microphysical validation of an orographic precipitation event over the Wasatch Mountains during IPEX IOP3." *Monthly weather review* 133.10, pp. 2947–2971.

Giannini, Alessandra, R Saravanan, and Ping Chang (2005). "Dynamics of the boreal summer African monsoon in the NSIPP1 atmospheric model." *Climate Dynamics* 25.5, pp. 517–535.

Held, Isaac M, Thomas L Delworth, Jian Lu, KL u Findell, and TR Knutson (2005). "Simulation of Sahel drought in the 20th and 21st centuries." *Proceedings of the National Academy of Sciences* 102.50, pp. 17891–17896.

Jankov, Isidora, William A Gallus, Moti Segal, Brent Shaw, and Steven E Koch (2005). "The impact of different WRF model physical parameterizations and their interactions on warm season MCS rainfall." *Weather and forecasting* 20.6, pp. 1048–1060.

Parker, DJ, RR Burton, A Diongue-Niang, RJ Ellis, M Felton, CM Taylor, CD Thorncroft, P Bessemoulin, and AM Tompkins (2005). "The diurnal cycle of the West African monsoon circulation." *Quarterly Journal of the Royal Meteorological Society: A journal of the atmospheric sciences, applied meteorology and physical oceanography* 131.611, pp. 2839–2860.

Zhao, Y, Pascale Braconnot, O Marti, SP Harrison, C Hewitt, A Kitoh, Z Liu, Uwe Mikolajewicz, B Otto-Bliesner, and SL Weber (2005). "A multi-model analysis of the role of the ocean on the African and Indian monsoon during the mid-Holocene." *Climate Dynamics* 25.7-8, pp. 777–800.

Guo, Zhichang, Paul A Dirmeyer, Randal D Koster, YC Sud, Gordon Bonan, Keith W Oleson, Edmond Chan, Diana Verseghy, Peter Cox, CT Gordon, et al. (2006). "GLACE: the global land–atmosphere coupling experiment. Part II: analysis." *Journal of Hydrometeorology* 7.4, pp. 611–625.

Hall, Nicholas MJ and Philippe Peyrillé (2006). "Dynamics of the West African monsoon." In: *Journal de Physique IV (Proceedings)*. Vol. 139. EDP sciences, pp. 81–99.

Koster, Randal D, YC Sud, Zhichang Guo, Paul A Dirmeyer, Gordon Bonan, Keith W Oleson, Edmond Chan, Diana Verseghy, Peter Cox, Harvey Davies, et al. (2006). "GLACE: the global land–atmosphere coupling experiment. Part I: overview." *Journal of Hydrometeorology* 7.4, pp. 590–610.

Peyron, Odile, Dominique Jolly, Pascale Braconnot, Raymonde Bonnefille, Joël Guiot, Denis Wirrmann, and Françoise Chalié (2006). "Quantitative reconstructions of annual rainfall in Africa 6000 years ago: Model-data comparison." *Journal of Geophysical Research: Atmospheres* 111.D24.

Taylor, Christopher M and Richard J Ellis (2006). "Satellite detection of soil moisture impacts on convection at the mesoscale." *Geophysical Research Letters* 33.3.

Braconnot, P, B Otto-Bliesner, S Harrison, S Joussaume, J-Y Peterchmitt, Ayako Abe-Ouchi, Michel Crucifix, Emmanuelle Driesschaert, Th Fichefet, CD Hewitt, et al. (2007). "Results of PMIP2 coupled simulations of the Mid-Holocene and Last Glacial Maximum–Part 1: experiments and large-scale features." *Climate of the Past* 3.2, pp. 261–277.

Hohenegger, Cathy and Christoph Schar (2007). "Atmospheric predictability at synoptic versus cloud-resolving scales." *Bulletin of the American Meteorological Society* 88.11, pp. 1783–1794.

Nicholson, SE, AI Barcilon, M Challa, and J Baum (2007). "Wave activity on the tropical easterly jet." *Journal of the Atmospheric Sciences* 64.7, pp. 2756–2763.

Patricola, Christina M and Kerry H Cook (2007). "Dynamics of the West African monsoon under mid-Holocene precessional forcing: Regional climate model simulations." *Journal of Climate* 20.4, pp. 694–716.
Richard, Evelyne, Andrea Buzzi, and Günther Zängl (2007). "Quantitative precipitation forecasting in the Alps: The advances achieved by the Mesoscale Alpine Programme." *Quarterly Journal of the Royal Meteorological Society: A journal of the atmospheric sciences, applied meteorology and physical oceanography* 133.625, pp. 831–846.
Taylor, Christopher M, Douglas J Parker, and Phil P Harris (2007). "An observational case study of mesoscale atmospheric circulations induced by soil moisture." *Geophysical Research Letters* 34.15.
Yeshanew, A and MR Jury (2007). "North African climate variability. Part 2: Tropical circulation systems." *Theoretical and applied climatology* 89.1, pp. 37–49.
Biasutti, Michela, Isaac M Held, Adam H Sobel, and Alessandra Giannini (2008). "SST forcings and Sahel rainfall variability in simulations of the twentieth and twenty-first centuries." *Journal of Climate* 21.14, pp. 3471–3486.
Cook, Kerry H (2008). "The mysteries of Sahel droughts." *Nature Geoscience* 1.10, pp. 647–648.
Zhang, Chidong, David S Nolan, Christopher D Thorncroft, and Hanh Nguyen (2008). "Shallow meridional circulations in the tropical atmosphere." *Journal of Climate* 21.14, pp. 3453–3470.
Dirmeyer, Paul A, C Adam Schlosser, and Kaye L Brubaker (2009). "Precipitation, recycling, and land memory: An integrated analysis." *Journal of Hydrometeorology* 10.1, pp. 278–288.
Hohenegger, Cathy, Peter Brockhaus, Christopher S Bretherton, and Christoph Schär (2009). "The soil moisture–precipitation feedback in simulations with explicit and parameterized convection." *Journal of Climate* 22.19, pp. 5003–5020.
Nicholson, Sharon E (2009a). "A revised picture of the structure of the "monsoon" and land ITCZ over West Africa." *Climate Dynamics* 32.7, pp. 1155–1171.
Nicholson, Sharon E (Jan. 2009b). "A revised picture of the structure of the "monsoon" and land ITCZ over West Africa." *Climate Dynamics* 32.7-8, pp. 1155–1171.
Nicholson, Sharon E (2009c). "On the factors modulating the intensity of the tropical rainbelt over West Africa." *International Journal of Climatology: A Journal of the Royal Meteorological Society* 29.5, pp. 673–689.
Wu, Man-Li C, Oreste Reale, Siegfried D Schubert, Max J Suarez, Randy D Koster, and Philip J Pegion (2009). "African easterly jet: Structure and maintenance." *Journal of Climate* 22.17, pp. 4459–4480.
Pu, Bing and Kerry H Cook (2010). "Dynamics of the West African westerly jet." *Journal of Climate* 23.23, pp. 6263–6276.
Stephens, Graeme L, Tristan L'Ecuyer, Richard Forbes, Andrew Gettelmen, Jean-Christophe Golaz, Alejandro Bodas-Salcedo, Kentaroh Suzuki, Philip Gabriel, and John Haynes (2010). "Dreary state of precipitation in global models." *Journal of Geophysical Research: Atmospheres* 115.D24.
Vamborg, FSE, V Brovkin, and M Claussen (2010). "The effect of a dynamic background albedo scheme on Sahel/Sahara precipitation during the mid-holocene." *CliPD* 6.5, pp. 2335–2370.
Bartlein, Patrick J, SP Harrison, Sandra Brewer, Simon Connor, BAS Davis, K Gajewski, Joel Guiot, TI Harrison-Prentice, A Henderson, Odile Peyron, et al.

(2011). "Pollen-based continental climate reconstructions at 6 and 21 ka: a global synthesis." *Climate Dynamics* 37.3-4, pp. 775–802.

Bock, Olivier, F Guichard, Remi Meynadier, Sébastien Gervois, A Agustı-Panareda, A Beljaars, A Boone, M Nuret, J-L Redelsperger, and P Roucou (2011). "The large-scale water cycle of the West African monsoon." *Atmospheric Science Letters* 12.1, pp. 51–57.

Dirmeyer, Paul A (2011). "The terrestrial segment of soil moisture–climate coupling." *Geophysical Research Letters* 38.16.

Pohl, Benjamin and Hervé Douville (2011). "Diagnosing GCM errors over West Africa using relaxation experiments. Part I: Summer monsoon climatology and interannual variability." *Climate dynamics* 37.7, pp. 1293–1312.

Thorncroft, Chris D, Hanh Nguyen, Chidong Zhang, and Philippe Peyrillé (2011). "Annual cycle of the West African monsoon: regional circulations and associated water vapour transport." *Quarterly Journal of the Royal Meteorological Society* 137.654, pp. 129–147.

Vamborg, FSE, V Brovkin, and M Claussen (2011). "The effect of a dynamic background albedo scheme on Sahel/Sahara precipitation during the mid-Holocene." *Climate of the Past* 7.1, pp. 117–131.

Braconnot, Pascale, Sandy P Harrison, Masa Kageyama, Patrick J Bartlein, Valerie Masson-Delmotte, Ayako Abe-Ouchi, Bette Otto-Bliesner, and Yan Zhao (2012). "Evaluation of climate models using palaeoclimatic data." *Nature Climate Change* 2.6, pp. 417–424.

Dirmeyer, Paul A, Benjamin A Cash, James L Kinter, Thomas Jung, Lawrence Marx, Masaki Satoh, Cristiana Stan, Hirofumi Tomita, Peter Towers, Nils Wedi, et al. (2012). "Simulating the diurnal cycle of rainfall in global climate models: Resolution versus parameterization." *Climate Dynamics* 39.1-2, pp. 399–418.

Krinner, Gerhard, A-M Lézine, Pascale Braconnot, Pierre Sepulchre, Gilles Ramstein, Christophe Grenier, and I Gouttevin (2012). "A reassessment of lake and wetland feedbacks on the North African Holocene climate." *Geophysical Research Letters* 39.7.

Taylor, Christopher M, Richard AM de Jeu, Françoise Guichard, Phil P Harris, and Wouter A Dorigo (2012). "Afternoon rain more likely over drier soils." *Nature* 489.7416, pp. 423–426.

Larrasoaña, Juan C, Andrew P Roberts, and Eelco J Rohling (2013). "Dynamics of green Sahara periods and their role in hominin evolution." *PloS one* 8.10.

Marsham, John H, Nick S Dixon, Luis Garcia-Carreras, Grenville MS Lister, Douglas J Parker, Peter Knippertz, and Cathryn E Birch (2013). "The role of moist convection in the West African monsoon system: Insights from continental-scale convection-permitting simulations." *Geophysical Research Letters* 40.9, pp. 1843–1849.

Nicholson, Sharon E (2013). "The West African Sahel: A review of recent studies on the rainfall regime and its interannual variability." *ISRN Meteorology* 2013.

Taylor, Christopher M, Cathryn E Birch, Douglas J Parker, Nick Dixon, Françoise Guichard, Grigory Nikulin, and Grenville MS Lister (2013). "Modeling soil moisture-precipitation feedback in the Sahel: Importance of spatial scale versus convective parameterization." *Geophysical Research Letters* 40.23, pp. 6213–6218.

Bechtold, Peter, Noureddine Semane, Philippe Lopez, Jean-Pierre Chaboureau, Anton Beljaars, and Niels Bormann (2014). "Representing equilibrium and nonequilibrium convection in large-scale models." *Journal of the Atmospheric Sciences* 71.2, pp. 734–753.

Pearson, KJ, GMS Lister, CE Birch, RP Allan, RJ Hogan, and SJ Woolnough (2014). "Modelling the diurnal cycle of tropical convection across the 'grey zone'." *Quarterly Journal of the Royal Meteorological Society* 140.679, pp. 491–499.

Harrison, Sandy P, PJ Bartlein, K Izumi, Guangqi Li, J Annan, J Hargreaves, P Braconnot, and M Kageyama (2015). "Evaluation of CMIP5 palaeo-simulations to improve climate projections." *Nature Climate Change* 5.8, pp. 735–743.

Lélé, M Issa, Lance M Leslie, and Peter J Lamb (2015). "Analysis of low-level atmospheric moisture transport associated with the West African Monsoon." *Journal of Climate* 28.11, pp. 4414–4430.

Park, Jong-Yeon, Jürgen Bader, and Daniela Matei (2015). "Northern-hemispheric differential warming is the key to understanding the discrepancies in the projected Sahel rainfall." *Nature communications* 6.1, pp. 1–8.

Rachmayani, R, Matthias Prange, and Michael Schulz (2015). "North African vegetation–precipitation feedback in early and mid-Holocene climate simulations with CCSM3-DGVM." *Climate of the Past* 11.2, pp. 175–185.

Zängl, Günther, Daniel Reinert, Pilar Rıpodas, and Michael Baldauf (2015). "The ICON (ICOsahedral Non-hydrostatic) modelling framework of DWD and MPI-M: Description of the non-hydrostatic dynamical core." *Quarterly Journal of the Royal Meteorological Society* 141.687, pp. 563–579.

Pausata, Francesco SR, Gabriele Messori, and Qiong Zhang (2016). "Impacts of dust reduction on the northward expansion of the African monsoon during the Green Sahara period." *Earth and Planetary Science Letters* 434, pp. 298–307.

Claussen, Martin, Anne Dallmeyer, and Jürgen Bader (2017). "Theory and modeling of the African humid period and the green Sahara." In: *Oxford Research Encyclopedia of Climate Science*.

Gaetani, Marco, Gabriele Messori, Qiong Zhang, Cyrille Flamant, and Francesco SR Pausata (2017). "Understanding the mechanisms behind the northward extension of the West African Monsoon during the Mid-Holocene." *Journal of Climate* 30.19, pp. 7621–7642.

Hopcroft, Peter O, Paul J Valdes, Anna B Harper, and David J Beerling (2017). "Multi vegetation model evaluation of the Green Sahara climate regime." *Geophysical Research Letters* 44.13, pp. 6804–6813.

Klocke, Daniel, Matthias Brueck, Cathy Hohenegger, and Bjorn Stevens (2017). "Rediscovery of the doldrums in storm-resolving simulations over the tropical Atlantic." *Nature Geoscience* 10.12, pp. 891–896.

Tierney, Jessica E, Francesco SR Pausata, and Peter B deMenocal (2017). "Rainfall regimes of the Green Sahara." *Science advances* 3.1, e1601503.

Dixit, Vishal, Steven Sherwood, Olivier Geoffroy, and Damianos Mantsis (2018). "The role of nonlinear drying above the boundary layer in the mid-holocene African monsoon." *Journal of Climate* 31.1, pp. 233–249.

Berthou, Ségolène, David P Rowell, Elizabeth J Kendon, Malcolm J Roberts, Rachel A Stratton, Julia A Crook, and Catherine Wilcox (2019). "Improved climatological precipitation characteristics over West Africa at convection-permitting scales." *Climate Dynamics* 53.3-4, pp. 1991–2011.

Lemburg, Alexander, Jürgen Bader, and Martin Claussen (2019). "Sahel rainfall–tropical easterly jet relationship on synoptic to intraseasonal time scales." *Monthly Weather Review* 147.5, pp. 1733–1752.

Rio, Catherine, Anthony D Del Genio, and Frédéric Hourdin (2019). "Ongoing breakthroughs in convective parameterization." *Current Climate Change Reports* 5.2, pp. 95–111.

Stevens, Bjorn, Masaki Satoh, Ludovic Auger, Joachim Biercamp, Christopher S Bretherton, Xi Chen, Peter Düben, Falko Judt, Marat Khairoutdinov, Daniel Klocke, et al. (2019). "DYAMOND: The DYnamics of the atmospheric general circulation modeled on non-hydrostatic domains." *Progress in Earth and Planetary Science* 6.1, p. 61.

Thompson, Alexander J, Christopher B Skinner, Christopher J Poulsen, and Jiang Zhu (2019). "Modulation of mid-Holocene African rainfall by dust aerosol direct and indirect effects." *Geophysical Research Letters* 46.7, pp. 3917–3926.

Brierley, Chris (2020). "Large-scale features and evaluation of the PMIP4-CMIP6 midHolocene simulations." *Climate of the Past Discussions*.

Dallmeyer, Anne, Martin Claussen, Stephan Lorenz, and Timothy Shanahan (2020). "The end of the African humid period as seen by transient comprehensive Earth system model simulation of the last 8000 years." *Climate of the Past*.

Fiedler, Stephanie, Traute Crueger, Roberta D'Agostino, Karsten Peters, Tobias Becker, David Leutwyler, Laura Paccini, Jörg Burdanowitz, Stefan A Buehler, Alejandro Uribe Cortes, et al. (2020). "Simulated Tropical Precipitation Assessed across Three Major Phases of the Coupled Model Intercomparison Project (CMIP)." *Monthly Weather Review* 148.9, pp. 3653–3680.

Hohenegger, Cathy, Luis Kornblueh, Daniel Klocke, Tobias Becker, Guido Cioni, Jan Frederik Engels, Uwe Schulzweida, and Bjorn Stevens (2020). "Climate statistics in global simulations of the atmosphere, from 80 to 2.5 km grid spacing." *Journal of the Meteorological Society of Japan. Ser. II*.

Hopcroft, Peter O, Paul J Valdes, and William Ingram (2021). "Using the Mid-Holocene "Greening" of the Sahara to Narrow Acceptable Ranges on Climate Model Parameters." *Geophysical Research Letters* 48.6, e2020GL092043.

Jungandreas, Leonore, Cathy Hohenegger, and Martin Claussen (2021). "Influence of the representation of convection on the mid-Holocene West African Monsoon." *Climate of the Past* 17, pp. 1665–1684.

Leutwyler, David, Adel Imamovic, and Christoph Schär (2021). "The Continental-Scale Soil-Moisture Precipitation Feedback in Europe with Parameterized and Explicit Convection." *Journal of Climate*, pp. 1–56.

Nicholson, Sharon E and Douglas Klotter (2021). "The Tropical Easterly Jet over Africa, its representation in six reanalysis products, and its association with Sahel rainfall." *International Journal of Climatology* 41.1, pp. 328–347.

DECLARATION

Versicherung an Eides statt
Declaration of oath

Hiermit erkläre ich an Eides statt, dass ich die vorliegende Dissertationsschrift selbst verfasst und keine anderen als die angegebenen Quellen und Hilfsmittel benutzt habe.

I hereby declare upon oath that I have written the present dissertation independently and have not used further resources and aids than those stated.

Hamburg, 12th October 2021

Leonore Jungandreas